

TEMPERATURE EFFECT IN MULTIPHASE FLOW METER USING
SLOTTED ORIFICE PLATE

A Thesis

by

DOHAR JONO SIHOMBING

Submitted to the Office of Graduate and Professional Studies of
Texas A&M University
in partial fulfillment of the requirements for the degree of

MASTER OF SCIENCE

Chair of Committee, Gerald L. Morrison
Committee Members, Debjyoti Banerjee
Robert Randall
Head of Department, Andreas A. Polycarpou

May 2015

Major Subject: Mechanical Engineering

Copyright 2015 Dohar Jono Sihombing

ABSTRACT

Multiphase flow metering is one of the major focuses to develop in oil and gas industries. A combination of slotted orifice plate and electrical impedance technique was investigated in order to provide further development of a new type of multiphase flow meter. Flow visualization was conducted in this study to show the performance of the slotted orifice plate to homogenize the mixture flow and continued with the pattern flow discussion.

The visualization studied showed that the slotted orifice plate can be applied as a flow conditioner for two-phase flow in the pipe in many patterns flow. An existing pattern flow map based on the velocity of the each component in the mixture showed that the flow regime is a volumetric flow rate and gas volume fraction (GVF) dependant.

Temperature affected the measurement results based on the mixture conductivity behavior. Using a combination of linearization technique and curve fit method, the effect of the temperature to the measurement results can be eliminated for GVF range from 2.5% to 97.5%. The slotted orifice characteristics were then investigated with using the calibration factor, Euler number, and Morrison number with respect to differential pressure and pressure of the mixture flow.

DEDICATION

This work is dedicated to my lovely wife, Sunny Simangunsong, and my kids, Jonathan Sihombing, Joan Sihombing, and Jovani Sihombing. Thank you for all of your support and prayer together in this moment. I also dedicated to my mother, T. br. Purba, and my parent in law, P. Simangunsong and J. br. Silitonga. Thank you for your continuous prayer for my study success.

The fear of the LORD *is* the beginning of knowledge: *but* fools despise wisdom and instruction.
(Proverbs 1:7)

ACKNOWLEDGEMENTS

I would like to thank my advisor, Dr. G. L. Morrison, for his time, guidance, and support throughout this project research. I also would like to thank to my committee members, Dr. D. Banerjee and Dr. R. Randall, for their support in this research.

I would like to thank my colleagues at Turbomachinery Lab. especially Dr. Sahand Pirouzpanah and Dr. Chien Scott for their willingness to give advice during my research process and completion. Thanks to Chokote Kamdeu for his helping during rig installation and measurement process. I also thanks to Sujan Reddy, Wen Fei, and Peng Liu for their support in this research.

I would like to thank Pertamina for financial support throughout my master program in Texas A&M University.

Finally, I would like to thank my big families in Indonesia for their support and prayer on my study success.

NOMENCLATURE

A	Cross-section area
ACFM	Actual cubic feet per minute
	Beta ratio
CD	Coefficient of Discharge
C _f	Feedback capacitance
C _s	Stray capacitance
C _x	Electrical mixture capacitance
d	Plate width
D	Diameter
DP	Differential Pressure
Eu	Euler number
f	frequency
G	Gain
GPM	Gallon per minute
GVF	Gas Volume Fraction
KY	Calibration factor
\dot{m}_{air}	Air mass flow rate
\dot{m}_{mix}	Mixture mass flow rate
\dot{m}_w	Water mass flow rate
Mo	Morrison number

P	Pressure
ρ_{air}	Air density
ρ_{mix}	Mixture density
ρ_w	Water density
\dot{Q}	Volumetric flow rate
R_f	Feedback resistance
R_x	Mixture flow resistance
T	Temperature
μ_{air}	Air viscosity
μ_{mix}	Mixture viscosity
μ_w	Water viscosity
X	Quality of the mixture flow
V_i	Excitation voltage
V_{mix}	Mixture superficial velocity
V_{sg}	Gas or air superficial velocity
V_{sl}	Liquid or water superficial velocity
V_o	Output voltage
Z_x	Impedance of the mixture flow

TABLE OF CONTENTS

	Page
ABSTRACT	ii
DEDICATION	iii
ACKNOWLEDGEMENTS.....	iv
NOMENCLATURE.....	v
TABLE OF CONTENTS.....	vii
LIST OF FIGURES	ix
LIST OF TABLES	xv
1. INTRODUCTION	1
2. LITERATURE REVIEW	3
2.1 Standard Orifice Plate.....	3
2.2 Slotted Orifice Plate.....	4
2.3 Electrical Impedance	7
2.4 Flow Regimes.....	9
3. OBJECTIVES	13
4. EXPERIMENTAL FACILITIES AND METHODS.....	15
4.1 Experimental Facility	15
4.1.1 Water Supply System.....	16
4.1.2 Air Supply System.....	17
4.1.3 Measurement System	18
4.2 Experimental Methods.....	23
4.2.1 Measurement Procedure and Visualization.....	23
4.2.2 Data Acquisition	25
4.2.3 Data Processing and Calculation	25

	Page
5. RESULTS AND DISCUSSION	29
5.1 Flow Visualization Results	29
5.2 Temperature Effect upon the Measurement Result	35
5.3 The Slotted Orifice Characteristics	46
6. CONCLUSION AND RECOMMENDATIONS	53
6.1 Conclusions	53
6.2 Recommendations.....	55
REFERENCES	56
APPENDIX A	61
APPENDIX B	99
APPENDIX C	100

LIST OF FIGURES

	Page
Figure 2.1 Operational Amplifier (op-amp) Circuit	8
Figure 2.2 Flow regimes in horizontal gas-liquid flows	11
Figure 2.3 Flow pattern map	12
Figure 4.1 PFD Multiphase Flow Measurement	15
Figure 4.2 Water Supply System	17
Figure 4.3 Air Supply System	18
Figure 4.4 Multiphase Flow System	19
Figure 4.5 Test Section	20
Figure 4.6 Slotted Orifice Plate with $\beta=0.467$	20
Figure 4.7 Pressure and DP Transducer	21
Figure 4.8 Electrode Probe	22
Figure 4.9 Op-amp Configuration	22
Figure 4.10 Experimental box	23
Figure 4.11 LabView Interface	24
Figure 5.1 Visual flow at the low liquid flow rate (20 GPM)	31
Figure 5.2 Visual flow at the low liquid flow rate (30 GPM)	32
Figure 5.3 Visual flow at the high liquid flow rate (80 GPM)	33
Figure 5.4 Horizontal flow regime map of the experimental data	34
Figure 5.5 Gain variation with GVF for different frequencies @30GPM & 40psi	36

	Page
Figure 5.6 Gain vs GVF for different operation range @ Freq. 1 MHz.....	37
Figure 5.7 Surface curve GVF @ 1 MHz	38
Figure 5.8 Surface curve GVF after temperature isolation process @ 1 MHz	41
Figure 5.9 Measured GVF vs Gain" @ 1 MHz.....	41
Figure 5.10 Calculated GVF as the function of Measured GVF at various frequencies	43
Figure 5.11 The differences of the calculated GVF and measured GVF as the function of measured GVF at various frequencies.....	45
Figure 5.12 Calibration surface fit	47
Figure 5.13 The differences between calculated and measured total mass flow rate as a function measured total mass flow rate	48
Figure 5.14 Surface fit the Euler number	49
Figure 5.15 Differences between calculated and measured mixture density as a function of measured mixture density	49
Figure 5.16 Surface fit the Morrison number	50
Figure 5.17 Differences between calculated and measured dynamic viscosity as a function of measured dynamic viscosity	51
Figure 5.18 Euler number as a function of Morrison number at various liquid volumetric flow rate	52
Figure 5.19 Modify Euler number to liquid volumetric flow rate as a function of Morrison number	52
Figure A.1 Gain variation with GVF for different frequencies @10GPM & 40psi	61
Figure A.2 Gain variation with GVF for different frequencies @10GPM & 60psi.....	61

	Page
Figure A.3 Gain variation with GVF for different frequencies @10GPM & 80psi	62
Figure A.4 Gain variation with GVF for different frequencies @20GPM & 20psi	62
Figure A.5 Gain variation with GVF for different frequencies @20GPM & 40psi	63
Figure A.6 Gain variation with GVF for different frequencies @20GPM & 60psi	63
Figure A.7 Gain variation with GVF for different frequencies @20GPM & 80psi	64
Figure A.8 Gain variation with GVF for different frequencies @30GPM & 20psi	64
Figure A.9 Gain variation with GVF for different frequencies @30GPM & 60psi.....	65
Figure A.10 Gain variation with GVF for different frequencies @30GPM & 80psi	65
Figure A.11 Gain variation with GVF for different frequencies @40GPM & 20psi	66
Figure A.12 Gain variation with GVF for different frequencies @40GPM & 40psi	66
Figure A. 13 Gain variation with GVF for different frequencies @40GPM & 60 psi	67
Figure A.14 Gain variation with GVF for different frequencies @40GPM & 80 psi	67
Figure A.15 Gain variation with GVF for different frequencies @50GPM & 20psi	68
Figure A.16 Gain variation with GVF for different frequencies @50GPM & 40psi	68

	Page
Figure A.17 Gain variation with GVF for different frequencies @50GPM & 60psi	69
Figure A.18 Gain variation with GVF for different frequencies @50GPM & 80psi	69
Figure A.19 Gain variation with GVF for different frequencies @60GPM & 20psi	70
Figure A.20 Gain variation with GVF for different frequencies @60GPM & 40psi	70
Figure A.21 Gain variation with GVF for different frequencies @60GPM & 60psi	71
Figure A.22 Gain variation with GVF for different frequencies @70GPM & 20psi	71
Figure A.23 Gain variation with GVF for different frequencies @70GPM & 40psi	72
Figure A.24 Gain variation with GVF for different frequencies @70GPM & 60psi	72
Figure A.25 Gain variation with GVF for different frequencies @80GPM & 20psi	73
Figure A.26 Gain variation with GVF for different frequencies @80GPM & 40psi.....	73
Figure A.27 Gain vs GVF for different operation range @ Freq. 200 kHz.....	74
Figure A.28 Gain vs GVF for different operation range @ Freq. 600 kHz.....	75
Figure A.29 Gain vs GVF for different operation range @ Freq. 1.28 MHz.....	76
Figure A.30 Gain vs GVF for different operation range @ Freq. 2.37 MHz.....	77
Figure A.31 Gain vs GVF for different operation range @ Freq. 3.46 MHz.....	78
Figure A.32 Gain vs GVF for different operation range @ Freq. 4.55 MHz.....	79

	Page
Figure A.33 Gain vs GVF for different operation range @ Freq. 5.64 MHz.....	80
Figure A.34 Gain vs GVF for different operation range @ Freq. 6.73 MHz.....	81
Figure A.35 Gain vs GVF for different operation range @ Freq. 7.82 MHz.....	82
Figure A.36 Gain vs GVF for different operation range @ Freq. 8.91 MHz.....	83
Figure A.37 Gain vs GVF for different operation range @ Freq. 10 MHz.....	84
Figure A.38 Measured GVF vs Gain" @ 200 kHz	85
Figure A.39 Measured GVF vs Gain" @ 600 kHz	85
Figure A.40 Measured GVF vs Gain" @ 1.28 MHz	86
Figure A.41 Measured GVF vs Gain" @ 2.37 MHz	86
Figure A.42 Measured GVF vs Gain" @ 3.46 MHz	87
Figure A.43 Measured GVF vs Gain" @ 4.55 MHz	87
Figure A.44 Measured GVF vs Gain" @ 5.64 MHz	88
Figure A.45 Measured GVF vs Gain" @ 6.73 MHz	88
Figure A.46 Measured GVF vs Gain" @ 7.82 MHz	89
Figure A.47 Measured GVF vs Gain" @ 8.91 MHz.....	89
Figure A.48 Measured GVF vs Gain" @ 10 MHz	90
Figure A.49 Calculated GVF as the function of Measured GVF for high frequencies	91
Figure A.50 The differences of the calculated GVF and measured GVF as the function of measured GVF at high frequencies	92
Figure A.51 Surface curve GVF @ 200 kHz	93
Figure A.52 Surface curve GVF @ 600 kHz	93

	Page
Figure A.53 Surface curve GVF @ 1.28 MHz	94
Figure A.54 Surface curve GVF @ 2.37 MHz	94
Figure A.55 Surface curve GVF @ 3.46 MHz	95
Figure A.56 Surface curve GVF @ 4.55 MHz	95
Figure A.57 Surface curve GVF @ 5.64 MHz	96
Figure A.58 Surface curve GVF @ 6.73 MHz	96
Figure A.59 Surface curve GVF @ 7.82 MHz	97
Figure A.60 Surface curve GVF @ 8.91 MHz	97
Figure A.61 Surface curve GVF @ 10 MHz	98

LIST OF TABLES

	Page
Table 5.1 Linearization equation for each GVF @ 1 MHz	40
Table 5.2 Curve fitting equation for all frequency	43
Table B.1 Linearization equation for each GVF and all frequencies	99

1. INTRODUCTION

Multiphase flow is a common flow for producing oil and gas wells, and when processing and transporting hydrocarbon products. The most well-known method to measure multiphase flow is using a separator system. The multiphase flow is separated into single-phase components then each component is measured with conventional single-phase flow meters such as orifice plate flow meters, Coriolis flow meters, or turbine flow meters. These conventional multiphase flow measurement systems have some weaknesses such as large size, high cost, stabilization time for better accuracy, and have difficulties being use in limited space areas [1].

Research has been conducted to overcome the disadvantages of the conventional multiphase flow measurement systems particularly in the oil and gas industry. The driving forces to develop multiphase flow measurement were the declined production from offshore fields and increasing gas and water fractions in the mature production area [2].

Multiphase flow meters provide a prospective alternative to conventional systems. They offer a compact design, adequate accuracy without stabilization time, and operate continuously in all types of flow regimes. These flow meters do not require a separator in the system, which consequently reduces measurement size and cost [1] [2].

The multiphase flow meter development has been directed by some researchers and manufacturers recently. They developed the multiphase flow metering in terms of production facilities, well testing, reservoir management, production monitoring, and fiscal metering or custody transfer application. There are three main accuracy ranges required for multiphase metering: for reservoir management approximately 5-10%, for production application approximately 2-5%, and for fiscal metering or custody transfer approximately 0.25-1% [2].

One of the multiphase phase flowmeter developments is the slotted orifice flow meter which was developed in the Turbomachinery Laboratory at Texas A&M University over 20 years ago [3]. The slotted orifice flow meter is based on the differential pressure downstream and upstream of the flow meter, as a standard orifice flow meter [4]. It uses an orifice plate that has arranged radial slots instead of a single central hole as in a standard orifice flow meter.

The goal of this research is to continue the experimental investigation of the slotted orifice plate using air and water as the working fluids from 0% to 100% Gas Volume Fraction (GVF) over a range of total mass flow rate. This covers several types of flow regimes. The effect of the temperature on the measurement results will be studied. Flow visualization will be included to show the incoming flows and how they are altered by the slotted orifice plate.

2. LITERATURE REVIEW

The literature review is important to investigate the previous research of the slotted orifice flowmeter from the early development until the last work. The investigation provides the information needed for this research and how the flow meter can be better developed. The general information of standard orifice plate, the basic working principles of the standard orifice plate, electrical impedance, and flow regimes also will be discussed in this section.

2.1 Standard Orifice Plate

The orifice plate flowmeter is the most common of the differential pressure (DP) flowmeter family for industrial application. It has a simple construction and installation, having a circular hole at its center to create pressure drop across it [5] [6].

The standard orifice plate has installation constraints to maintain 0.5% uncertainty due to its sensitivity to upstream flow conditions. The constraints are based on the beta ratio (β), bends distance, and fittings that induce swirl. The standard of the upstream and downstream pipe lengths is set up in ISO 5167-1. For instance, at $\beta=0.5$, 14D clear pipe upstream and 6D clear pipe downstream are needed to reach 0.5% uncertainty [5].

The other disadvantages are the nonlinear characteristic of the meter due to its coefficient of discharge (CD) and high pressure loss due to the poor pressure recovery after the plate [5] [7].

2.2 Slotted Orifice Plate

The slotted orifice plate initial function was to produce differential pressure for gas sampling purpose and return it to the pipeline without using a pump or compressor. Ihfe [8], along with Dr. Morrison, began research of the slotted orifice plate using it as a flow conditioner to obtain a fully developed turbulent flow. The research result showed that the plate was not acceptable as a conditioner because it produced higher head loss compared to other flow conditioners. Then, the plate development changed from flow conditioner to flow meter.

Macek [9], under the supervision of Dr. Morrison, was the first one to investigate the plate as a flow meter in a single-phase flow. He found that the plate is independent of upstream flow conditions and has consistent and well-distributed pipe-wall pressure. He also concluded that the slotted orifice plate has better performance due to its ability to reduce head loss, and faster pressure recovery compared to standard orifice plate.

Terracina [10] and Dr. Morrison performed further numerical and experimental investigations to study the effects of velocity profile distortions, mass flow rate, line pressure, tube bundle location, and pipe size scaling in the single-

phase measurement. He reported that the slotted orifice plate has more accurate performance than the standard orifice plate when the slot width to thickness ratio was maintained at 0.25. The slotted orifice plate has less sensitivity to upstream flow velocity and lower head loss than the standard orifice plate with the same effective β [6] [10] [12]. Using $\beta = 0.5$ and swirl free flow condition, the standard orifice plate produced discharge coefficient variation -1% to +6% while the slotted orifice plate had only $\pm 0.25\%$ [6].

Brewer [13], under the direction of Dr. Morrison, studied the performance of the slotted orifice plate in two-phase flow in the beta ratio range 0.43 and 0.5 and flow qualities varied from 100% (pure air) to 20% (slug flow). He also investigated the locations of pressure taps in order to measure the differential pressure. The flange tap can be placed 2.5 pipe diameter from upstream and downstream of the slotted orifice plate. Compare to standard orifice plate, which is needed 3.5 pipe diameter, the slotted orifice plate has better pressure recovery [11] [13].

Flores [14] evaluated the slotted orifice plate in the horizontal two-phase flow with repeatability data for water and steam as the working fluids, and reproducibility data for beta ratio 0.43, 0.467, and 0.5. For repeatability data, the same trends were shown as the previous results with using water and air as the working fluids. For reproducibility data, the uncertainty in the calibration coefficient of the slotted orifice plate was dominated by the beta ratio.

Sparks [15] observed the performance of the slotted orifice to produce homogenized flow compare to the standard orifice plate and V-cone. The slotted orifice plate showed superior performance for homogenizing flow.

The slotted orifice plate has shown its superior capabilities to characterized two phase flow easily where KY is only a function of the mixture quality [11]. Morrison [3] proposed the total length of slotted orifice flow meter is $10D$ without flow conditioner and low swirl flow present. The meter requires only $5D$ clear pipe upstream, due to its insensitivity to upstream flow, and $5D$ clear pipe downstream regarding to its capabilities to have fast pressure recovery.

Cevik [16] evaluated two different non-nuclear multiphase flow meters with wide GVF range to determine the accurate mixture mass flow measurement and optimum operating conditions. He used ten different frequencies and six impedance electrode probe sensors (10 inches, 11 inches, and 12 inches distance from the downstream of the slotted orifice plate) to obtain the optimum operation position. Two sensors were applied at the same distance and placed in the different side (left side and right side). The slotted orifice plate produces well-homogenized downstream flow due to its independent of upstream flow conditions and good response in two-phase flow. The optimum position of the sensor is the combination of the left 12 inches and right 10 inches.

2.3 Electrical Impedance

Electrical impedance is a commonly used technique in multiphase flow measurement. It is applied to measure the electromagnetic properties of fluids by defining the correlation between voltage and current for non-steady state behavior. This technique quantifies the capacitance and resistance of a mixture which is represented by a parallel capacitance and resistance and known as the function of primarily GVF [17].

The impedance technique relies on flow regime since changing the flow regime will consequently change the correlation between measured impedance and phase fraction [1]. Fossa [18] investigated the performance of a conductance probe for measuring the liquid fraction in the two-phase flow. He compared the performance of ring-shaped and plate electrodes for different experimental set ups then he evaluated the experimental results with the theory available in the literature. The electrodes were conditioned with annular, stratified, and bubble flow patterns. Considered the effect of the probes geometry, the results showed that the ring-shaped electrodes provided better performance than the plate electrodes.

Andreussi [19] evaluated the impedance method for the measurement of liquid hold-up in a multiphase flow. The method used two ring electrodes mounted to the pipe wall and the impedance measurement was affected by the distance between the electrodes and on the liquid hold-up. The results showed that the

distance between 1.5-2.5D delivered good results and the measurement were independent of the flow patterns.

DaSilva [17] studied the variation of the impedance methods for fast multiphase flow measurement. He proposed the auto-balancing bridge using an operational amplifier (op-amp) to measure the impedance. This method produced low output resistance from high input resistance and suitable for high speed measurement because of its quick response. The circuit measures capacitive impedances in the form of parallel circuit of a capacitor and a resistor.

Figure 2.1 shows a practical circuit for the measurement of capacitive impedances, where V_i is the excitation voltage, V_o is the output voltage, C_{s1} and C_{s2} are the stray capacitances due to the effect of the cables, R_f (as the inverse of G_f) and C_f are the feedback resistance and capacitance, R_x (as the inverse of G_x) and C_x are the resistance and capacitance of the mixture flow, and Z_x represents the impedance of the flow.

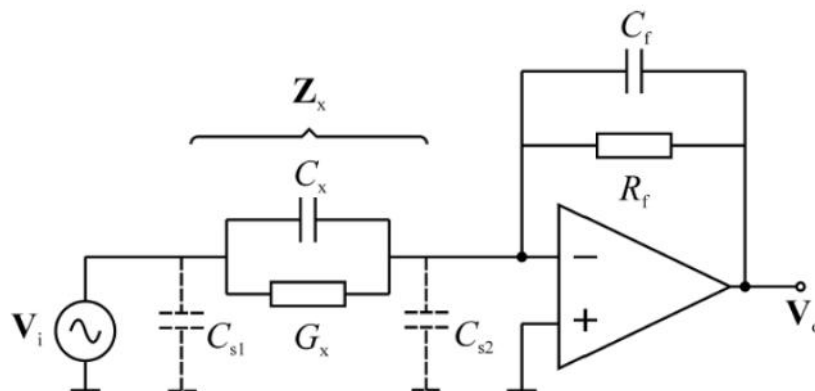


Figure 2.1 Operational Amplifier (op-amp) Circuit

The response of the circuit is obtained by the following equation. If the gain and phase of the single frequency signal are known, R_x and C_x can be calculated by [17]

$$\frac{V_o}{V_i} = - \left(\frac{G_x + j\omega C_x}{G_f + j\omega C_f} \right) \quad (2.1)$$

where $\omega = 2\pi f$, and f is the frequency of the excitation signal.

The other approach is to obtain these unknowns from gains calculated from two different frequencies [17].

$$\left| \frac{V_i}{V_o} \right| = \frac{\sqrt{G_x^2 + (2\pi f)^2 C_x^2}}{\sqrt{G_f^2 + (2\pi f)^2 C_f^2}} \quad (2.2)$$

2.4 Flow Regimes

Flow regimes or flow patterns are one of the most difficult aspects to understand, predict, and model in multiphase flow due to the behavior and shape of the interfaces between phases in a mixture flow. The regimes vary based on operation pressure and temperature, flow rates, fluid properties, types of flow (steady state, transient, pseudo steady state), and geometry of the pipe (size, shape, roughness, and inclination) in which fluid flows inside [20] [21].

Many studies have been conducted to predict the flow patterns of two-phase gas-liquid flows in pipes. Experimental methods are the most widely used to observe the flow regimes in two-phase flow in pipes by using the high speed cameras and transparent pipes [21] [22]. In horizontal pipes, the major flow regimes from top to bottom with increasing the gas flow rate are shown in Figure 2.2 [17] [23].

- Bubbly flow: this flow occurs when the gas flow is laminar and small bubbles are driven by buoyancy forces and flow in the upper part of the pipe
- Plug flow: the gas flow is increased, the bubbles size is bigger and a thin film of liquid coats and surrounds the plug. This flow is also called elongated bubble flow.
- Stratified flow: the liquid and gas phases are completely separate with smooth interface.
- Wavy flow: increasing the gas flow rate forms instabilities at the gas-liquid interface due to interfacial velocity differential. This flow is characterized by small interfacial waves.
- Slug flow: gas velocity is increased, the disturbance waves amplify along the liquid surface and the flow pattern becomes slug at the tube wall. Some portion of the amplified waves break in to smaller bubbles.

- Annular flow: when the gas flow is high enough, the gas momentum increased and pushed up the liquid around the circumference of the tube wall. Liquid also falls downward the tube wall due to effect of the gravity.

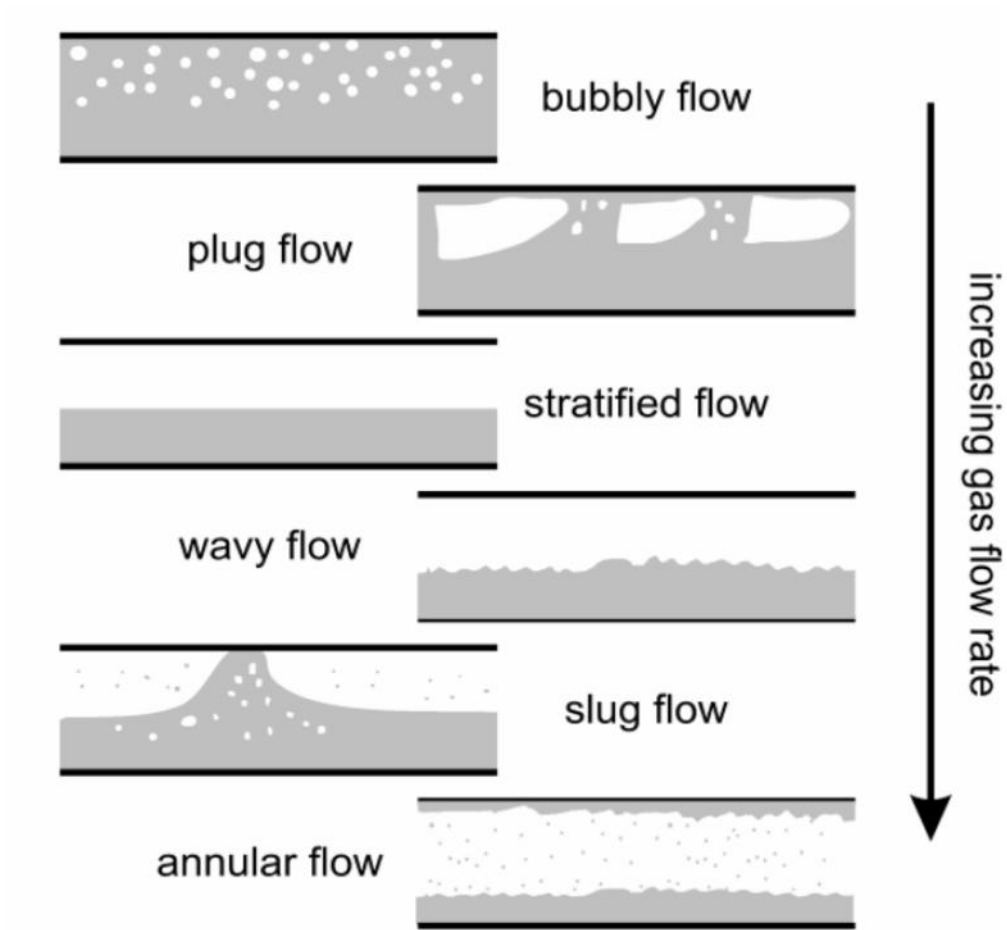


Figure 2.2. Flow regimes in horizontal gas-liquid flows

The flow regimes and transitions are simply defined in a flow pattern map. The map was constructed based upon the superficial liquid velocity as the function

of the superficial gas velocity. Mandhane [22] studied a flow pattern map for the gas-liquid flow in horizontal pipes (inside diameter from 0.5-6.5 inch) with using some range parameters. Air and water were used as the working fluids. He compared many flow pattern maps from the previous experiment which cover a wide range physical properties and flow parameters. A new flow pattern map was proposed which is suited for all available data (Figure 2.3).

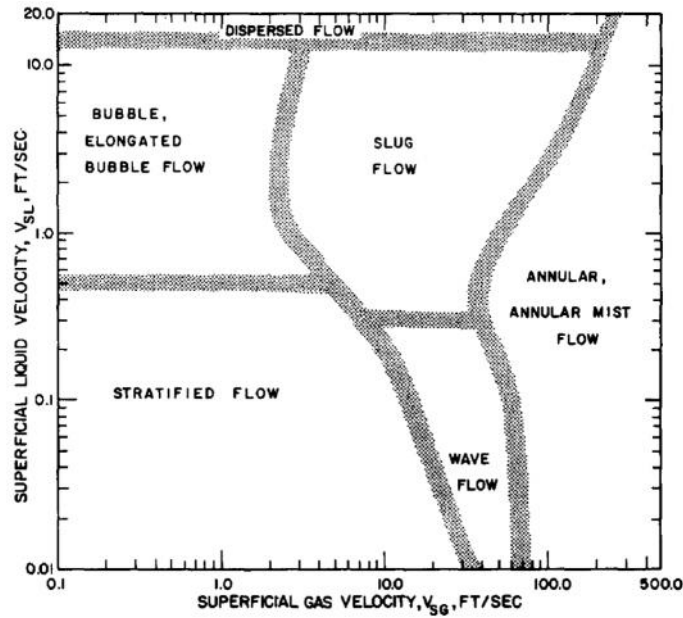


Figure 2.3 Flow pattern map

3. OBJECTIVES

One of the most challenging problems that needs to be solved is the accuracy and the reliability of the multiphase flow rate measurement in a flow line or pipe line particularly when the temperature is changing while measuring. In two-phase flow, as the simplest form of multiphase flow, the temperature changing will affect the measurement result regarding to the fluid properties response to it.

The objectives of this research:

- To analyze the flow alteration after the slotted orifice plate based on the flow visualization results.
- To evaluate the pattern flow in the measurement and the factors which affect to the flow regimes
- To obtain GVF as the function of Gain (electrical properties) in two-phase flow.
- To determine the mass flow rate of each fluid component in two-phase flow
- To determine the temperature effect correction in the GVF calculation of the two-phase flow
- To obtain the accuracy of the slotted orifice plate while using the temperature effect correction regarding to GVF.

- To evaluate the characteristics of the slotted orifice plate in order to calculate the mass flow rate and dynamic viscosity. The evaluation is based on the calibration factor, the Euler number and the Morrison number with respect to the differential pressure and pressure.

4. EXPERIMENTAL FACILITY AND METHODS

This chapter provides all the information about the experimental facility which was used in the two-phase flow measurement. Data acquisition, data processing and calculation also will be discussed.

4.1 Experimental Facility

The experimental work was conducted in Turbomachinery Laboratory at Texas A&M University. The experimental facility flow diagram can be seen in Figure 4.1. The facility is divided into three main systems: water supply system, air supply system, and measurement system.

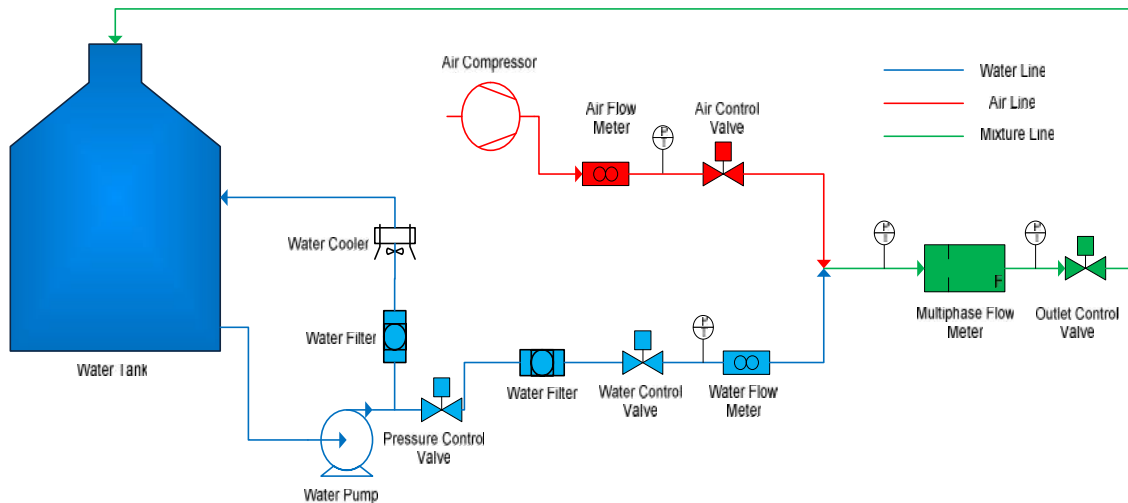


Figure 4.1 PFD Multiphase Flow Measurement

4.1.1 Water Supply System

Figure 4.2 shows the water supply system. The water supply system used a 5000 gallon tank for the water storage. A centrifugal pump with 100 Gallon per minute (GPM) capacity is installed to pump water in the system. In the discharge line, a pressure control valve, and a volume control are applied to control working pressure and flow rate of the water flow in the system. PID controllers in LabView are applied to adjust the valves. For safety reason, the system is also equipped with by-pass water pipes. In the by-pass pipe, water is returned to the storage tank and cooled by a water cooler to minimize temperature increase in the flow system. Water filters are installed to reduce impurities in the water which can affect the measurement results. Water is flowed inside two inch inner diameter PVC pipe and mixed with air in a two-inch mixing pipe.

Two turbine flow meters are calibrated with water to measure the water volume flow rate in GPM. For medium rate flow, an Omega FTB-1425 meter within range 5-50 GPM and accuracy of reading $\pm 1\%$ is used. An Omega FTB-1441 within range 15-180 GPM and accuracy of reading $\pm 1\%$ is applied for high rate flow. The turbine flow meters were installed in 10D clear pipe in upstream and 5D clear pipe in downstream to obtain accurate measurement.

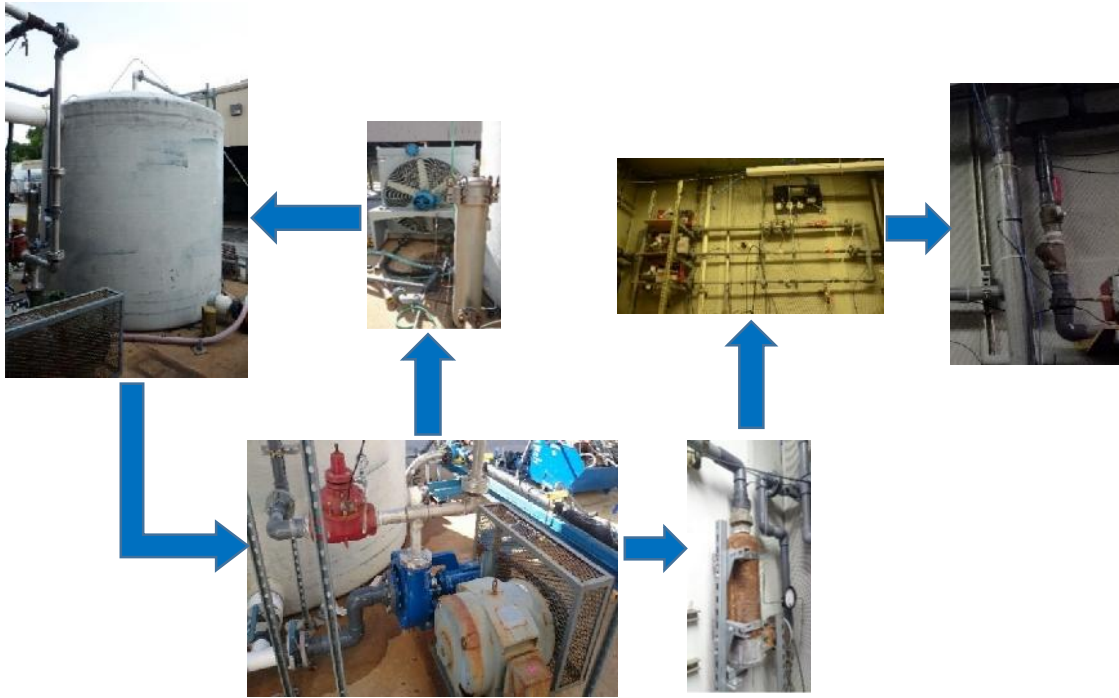


Figure 4.2 Water Supply System

4.1.2 Air Supply System

The air supply system is shown in Figure 4.3. The air system used a 110-psig oil free compressor for air supply. The air brought to the system through a four-inch pipe. The air flow rate is adjusted by using a pneumatic control valve. A PID controller in LabView is used to control the valve.

Two turbine flow meters and a Coriolis flow meter are calibrated with air to measure the air flow rate in ACFM. For low rate flow, a Micro Motion CMFS015M Coriolis flow meter within range 0.05-2.5 ACFM with accuracy

$\pm 0.25\%$ (for 2.5 ACFM) and $\pm 1.17\%$ (for 0.05 ACFM) is used. An Omega FTB-933 turbine flow meter within range 1-10 ACFM and accuracy of reading $\pm 1\%$ is applied for medium rate flow and an Omega FTB-938 turbine flow meter within range 8-130 ACFM and accuracy of reading $\pm 1\%$ is installed for high rate flow. The meters were installed 10D clear pipe in upstream and 5D clear pipe in downstream to produce accurate measurement.

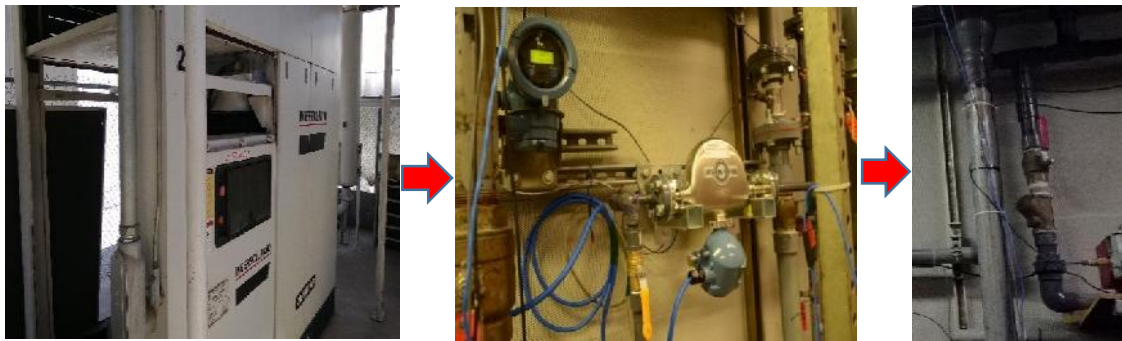


Figure 4.3 Air Supply System

4.1.3 Measurement System

The measurement system is presented in Figure 4.4. Water and air are mixed in a two-inch supply pipe then the mixture flows to the two-phase flow meter system which consists of PVC pipe with two inch inner diameter, the test section, two pressure transmitters, a temperature meter, and a box of experimental circuits. After measured, the mixture is flowed back to the water tank and air is released to atmosphere.

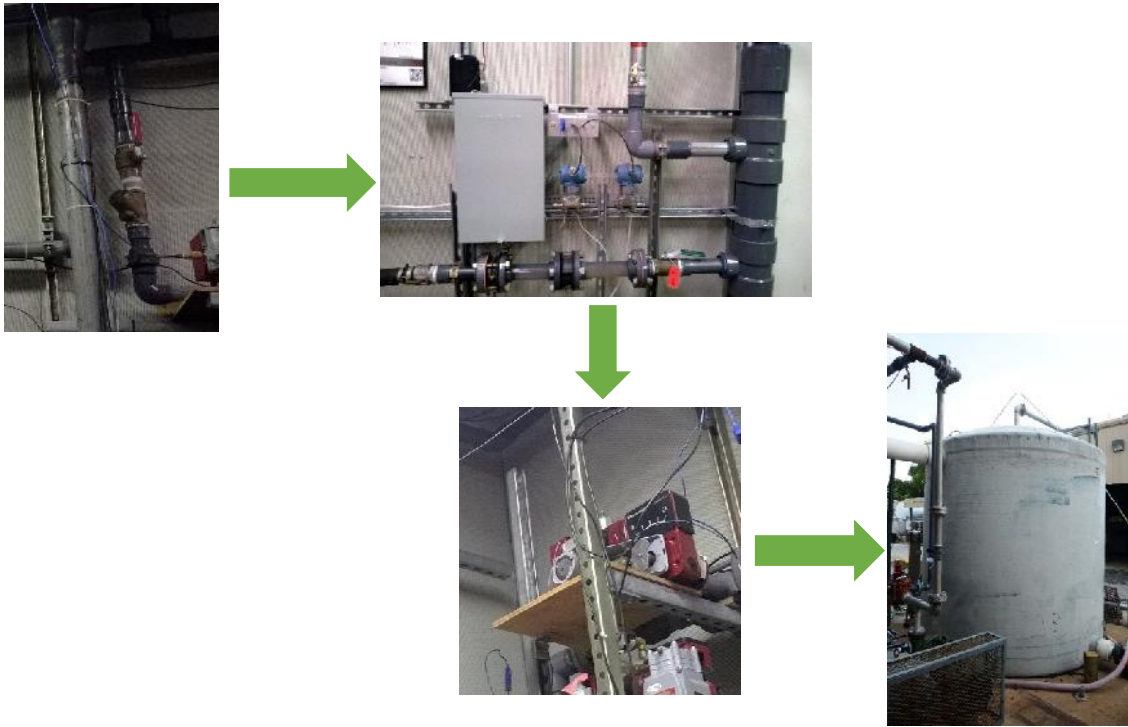


Figure 4.4 Multiphase Flow System

For more detail, the test section is aligned with transparent PVC pipe schedule 80 with two inch inner diameter, the slotted orifice plate, one temperature probe, pressure taps, and two ultra-machinable brass impedance electrodes which were mounted to the pipe across each other (Figure 4.5). The total length of the test section is 24 inches (12D) include the sandwich section. The upstream length is 10 inches (5D) and the remaining is the downstream section.

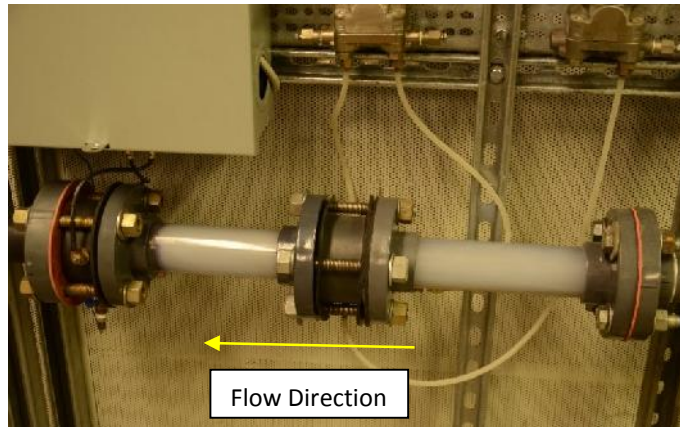


Figure 4.5 Test Section

This research uses a slotted orifice plate with a beta ratio of 0.467 and thickness of 0.25" (Figure 4.6).

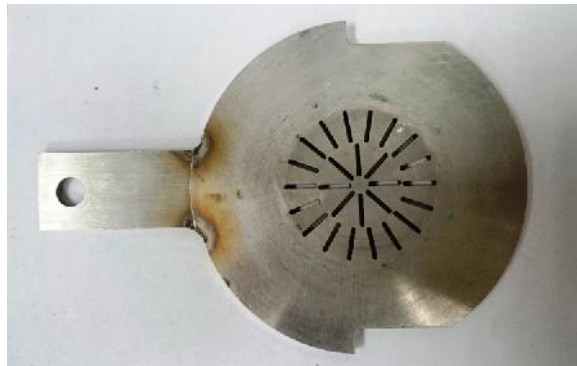


Figure 4.6 Slotted Orifice Plate with $\beta = 0.467$

Pressure taps were placed one inch ($\frac{1}{2} D$) away from downstream and upstream slotted orifice plate. A Rosemount 3051 differential pressure transducer

is used to measure the differential pressure of the flow mixture across the plate and a Rosemount 2088 pressure transducer is installed to measure the downstream pressure. The differential pressure transducer has range pressure 0-36 psi with uncertainty 0.065%. The pressure transducer has maximum working pressure 136 psi with error 0.075%. The differential pressure transducer and the pressure transducer can be seen in Figure 4.7.



Figure 4.7 Pressure and DP Transducer

Two ultra-machinable brass impedance electrodes were placed 12 inches or 6D (left and right side) from the downstream of the slotted orifice plate. The geometry of the electrodes for this experiment are round shaped probe. Sensors are applied at the tip of the electrodes and contacted with the mixture flow. The ultra-machinable brass impedance electrode is shown in Figure 4.8.



Figure 4.8 Electrode Probe

One Omega T-Type thermocouple, which is used to measure the mixture temperature, is mounted at the same distance (12 inches or 6D) from the downstream of the plate with rotated 90° from the electrode probes. The uncertainty of the thermocouple is $\pm 0.5\%$.

The electrodes are connected with the experimental circuit which used Texas Instrument LM-7171 op-amp configuration (Figure 4.9). The configuration is supplied with 15 VDC.

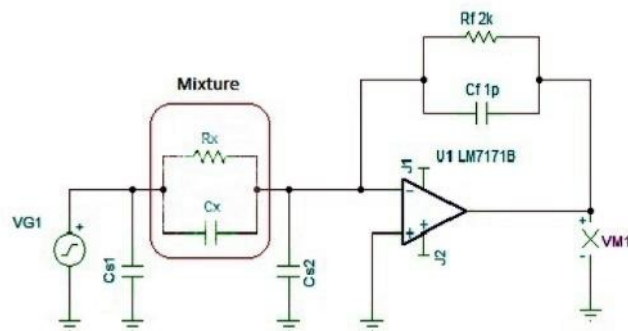


Figure 4.9 Op-amp Configuration

An experimental box, which is shown in Figure 4.10, is used as a bridge of data from the test section to the LabView program. The box configures with an op-am circuit, a picoscope, an IO-Gear and two power supplies. A Picoscope-5242, which has two input channels and one output channel, is installed as a signal generator and data acquisition system. An output signal from the op-am circuit is generated and processed in the picoscope and sent by using IO-Gear to the LabView program.



Figure 4.10 Experimental box

4.2 Experimental Methods

4.2.1 Measurement Procedure and Visualization

The measurement started from June to August 2014. The ambient temperature in College Station was reported from 67° F up to 99° F [24]. The operation range of the measurement are:

- Water volumetric flow rate (\dot{Q}_{water}) (GPM): 10, 20, 30, 40, 50, 60, 70, and 80.
- Pressure (P) (Psig): 20, 40, 60, and 80.
- GVF (%): 0-100

For the measurement process, a LabView program and interface are used to display input setting and output result (Figure 4.11). Input settings in this measurement are working pressure (psig), water flow volumetric rate (GPM), and GVF (%). The display results are the air volumetric flow rate (ACFM) and differential pressure (psig).

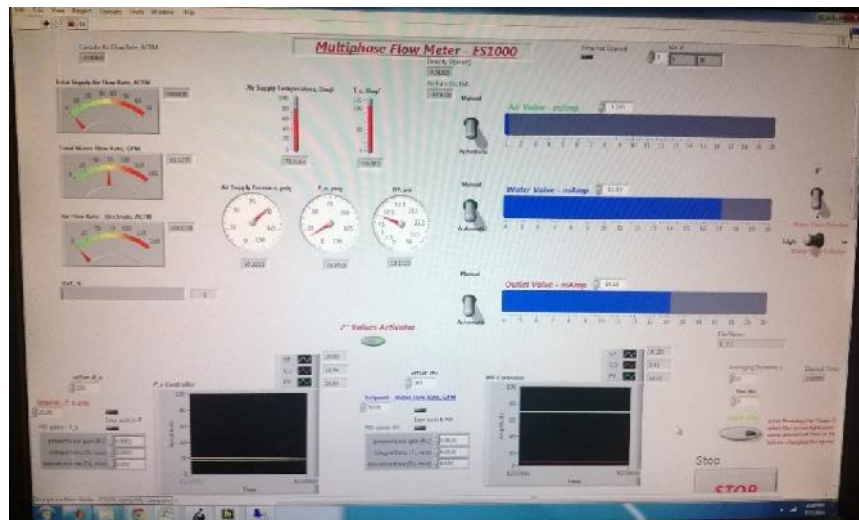


Figure 4.11 Labview Interface

A Sony type HDR-CX560V video camcorder is set up to visualize the mixture motion in the test section. Duration for each capture is 11 seconds.

4.2.2 Data Acquisition

This research uses twelve sinusoidal signals with different frequencies, ranging from 0.2 MHz to 10 MHz with similar amplitude applied as the input of the experimental circuit. The output channel of the circuit is connected with the input channel of a Data Acquisition (DAQ) system. The input voltage, output voltage, and phase shift are measured in the DAQ system. The gain and phases are calculated from the output voltage divided by input voltage for each specific frequency.

The output saves data given the measured and calculated data such as input voltage, output voltage, and phase shift. They can be saved as '.csv' file and using a Matlab program, the data is opened and processed in MS Excel.

4.3 Data Processing and Calculation

This section provides the procedure of data processing and calculation such as density, quality, mass flow rate, velocity, etc. Once data is collected and converted to spreadsheet, the data is analyzed with using these assumption:

- steady state flow
- ideal gas for air flow
- incompressible flow for water

The air mass flow rate (\dot{m}_{air}) and air density (ρ_{air}) are calculated based on the ideal gas equation:

$$P_{air} = \rho_{air} R T_{air} \quad (4.1)$$

$$\rho_{air} = \frac{P_{air}}{R T_{air}} \quad (4.2)$$

$$\dot{m}_{air} = \rho_{air} \dot{Q}_{air} \quad (4.3)$$

Quality of the mixture flow (X) is a function of air and water mass flow rate as shown below

$$\dot{m}_{mix} = \dot{m}_{air} + \dot{m}_{liq} \quad (4.4)$$

$$X = \frac{\dot{m}_{air}}{\dot{m}_{mix}} \quad (4.5)$$

The GVF is defined by

$$GVF = \frac{\dot{Q}_{air}}{\dot{Q}_{liq} + \dot{Q}_{air}} \quad (4.6)$$

Knowing the quality of the flow, the mixture density (ρ_{mix}) can be described with the following equation

$$\rho_{mix} = \frac{\rho_{air}}{X + (1-X) \rho_{air} / \rho_{liq}} \quad (4.7)$$

Superficial velocity of individual flows is used to evaluate mapping the flow regimes. The velocity is the function of mass flow rate and density and is defined as

$$V_{sa} = \frac{\dot{m}_{air}}{\rho_{air} A_{pipe}} \quad (4.8)$$

$$V_{sl} = \frac{\dot{m}_{liq}}{\rho_{liq} A_{pipe}} \quad (4.9)$$

where V_{sa} is the air superficial velocity and V_{sl} is the water superficial velocity.

The calibration factor (KY) is calculated to evaluate the slotted orifice plate performance in the mass flow rate measurement which is characterized with the differential pressure (P).

$$KY = \frac{4 \dot{m}}{\pi (D_{pipe} \beta)^2} \frac{1}{\sqrt{2 \rho \Delta P}} \quad (4.10)$$

where beta ratio (β) is defined as

$$\beta = \sqrt{\frac{A_{slots}}{A_{pipe}}} = \frac{D_{slots}}{D_{pipe}} \quad (4.11)$$

The Euler number (Eu) is used to characterize the slotted orifice plate to the differential pressure. This number is also as a function of density and velocity of the mixtures and is defined as follow

$$Eu = \frac{\Delta P}{\frac{1}{2} \rho_{mix} V_{mix}^2} \quad (4.12)$$

where mixture superficial velocity (V_{mix}) is defined as

$$V_{mix} = \frac{\dot{m}_{mix}}{\rho_{mix} A_{pipe}} \quad (4.13)$$

Morrison number (Mo) is another non-dimensional variable to evaluate the slotted orifice characteristics. The variable is the function of the mixture density, plate width (d), differential pressure, and mixture viscosity (μ_{mix})

$$Mo = \frac{\rho_{mix} d^2 \Delta P}{\mu_{mix}^2} \quad (4.14)$$

where mixture viscosity can be calculated as

$$\mu_{mix} = \mu_{air} X + (1 - X)\mu_{liq} \quad (4.15)$$

5. RESULTS AND DISCUSSION

In this section, the performance of the slotted orifice plate meter will be presented. The flow visualizations show the capability of the slotted orifice plate to homogenize the mixture flow. The pattern flow description is also included in this discussion. Existing pattern flow map based on the each component velocity of the mixture is provided to verify the visual flow description.

Evaluation of the slotted orifice plate performance is performed based on the fluid properties and the resistivity of the mixture. The temperature effect is defined to calculate the uncertainty of the slotted orifice plate.

5.1 Flow Visualization Results

The test section used transparent PVC pipes, thus the visual flow can be recorded. Selected flow was captured to represent liquid the segment of the flow rate such as 20 GPM (low rate), 30 GPM (medium rate), and 80 GPM (high rate) for various GVF. The mixture flow is shown before the plate (upstream) and after the plate (downstream) to visualize the effect of the plate to the mixture flow. The visualization video can be seen in the supplemental files of this report.

The flow pattern description based on the visual flow is very challenging due to the capability of the video recorder to capture the flow. It is difficult to

determine the exact flow regime because the transition between regimes is not really clear in the flow.

At the low rate (20GPM, 20 psi and 40 psi), the mixture is bubbly flow until 5% GVF. The bubbly flow occurs in the upstream and downstream sections of the pipe. From 7.5% to 30% GVF, the mixture flow regime is wavy flow in the upstream and homogenized flow with combination of plug flow and bubbly flow in the downstream. The wavy flow is present in the flow due to the different density of the components in the mixture flow which changed abruptly and formed an interface between air and water. Water, which has higher density, tends to flow on the bottom of the pipe flow. When the mixture flow is passed through an obstacle, in this case the slotted orifice plate, vorticity is generated due to the interaction of the pressure and the density field. The density varies from point to point in the fluid with the gradient of the density is everywhere normal to the stream line while the pressure drop occurs in the flow. This gives a well-mixed flow taking place downstream of the plate.

From 40% to 50% GVF, the upstream flow is in combination of the wavy flow and plug flow in the upstream and homogenized flow of plug flow and wavy flow in the downstream. From 60% to 70% GVF, a combination of wavy flow, plug flow, and slug flow is formed in the upstream and well-mixed flow of wavy flow, plug flow, and slug flow in the downstream. From 80% GVF and above, slug flow is present in the pipe in the upstream and well homogenized slug flow in downstream. At 98% GVF (20 GPM, 20 psi), combination of annular and slug flow

occurs in the upstream and it is well-homogenized in the downstream. The visual low liquid flow rate is shown in the Figure 5.1. The videos available at the supplemental files.

	20 GPM, 40 psi, 5% GVF
	20 GPM, 40 psi, 7.5% GVF
	20 GPM, 40 psi, 30% GVF
	20 GPM, 40 psi, 50% GVF
	20 GPM, 40 psi, 70% GVF
	20 GPM, 20 psi, 98% GVF

Figure 5.1 Visual flow at the low liquid flow rate (20 GPM)

At the medium liquid flow rate (30GPM, 80 psi), a mixture bubbly flow is formed until 10% GVF. From 20% to 30% GVF, a combination of bubbly flow and slug flow is present in the upstream and a well-homogenized flow is present in the downstream. In the range of 40% to 50% GVF, the combination of plug flow and slug dominated the mixture flow. At 60% GVF until 95% GVF, the mixture flow is in the slug flow form. And for all of them, once the mixture leave the plate, the mixture flow is well-homogenized state. The visual medium liquid flow rate is shown in the Figure 5.2. The videos available at the supplemental files.



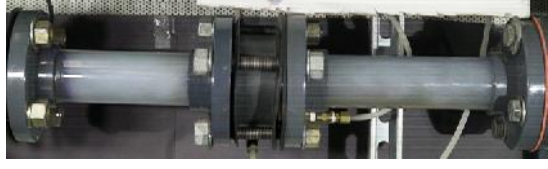

	30 GPM, 80 psi, 10% GVF
	30 GPM, 80 psi, 30% GVF
	30 GPM, 80 psi, 40% GVF
	30 GPM, 80 psi, 60% GVF

Figure 5.2 Visual flow at the low liquid flow rate (30 GPM)

The high liquid flow rate (80 GPM, 20 psi) only can reach 40% GVF maximum due to the pump operation and capacity limitation. Up to 10% GVF, the flow is in the bubbly flow form. Increasing GVF until 20%, plug flow is a dominant flow in the mixture. At 30% GVF, slug flow is occurred in the mixture. The mixture flow is well-mixed after the plate. The visual high liquid flow rate can be seen in the Figure 5.3. The videos available at the supplemental files

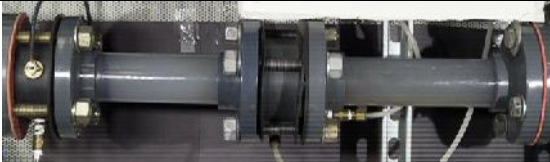


	<p>80 GPM, 20 psi, 10% GVF</p>
	<p>80 GPM, 20 psi, 20% GVF</p>
	<p>80 GPM, 20 psi, 30% GVF</p>

Figure 5.3 Visual flow at the high liquid flow rate (80 GPM)

Based on the visual flow description, the slotted orifice plate has capability to be a conditioner flow in all of the flow regimes. The flow in the downstream is in the well-mixed form because the turbulence blended the mixture flow after the plate.

According to the flow velocity, the flow regime map is drawn to verify the flow type of the mixture. The flow pattern map can be seen in the figure 5.4. The

mixture flow is considered to be bubbly flow, plug flow, and slug flow. The pattern of the mixture flow is dependent of the volumetric flow rate and GVF. For very low liquid flow rate (10 GPM), the bubbly and plug flow dominated the pattern flow, the slug flow occurred at 80% GVF, and transition of slug flow and annular flow can be seen at 98% GVF. The similar condition is applied for low liquid flow rate (20 GPM), the slug flow is formed at 70% GVF. For 30 GPM, slug flow begins at 60% GVF. Increasing the volumetric flow rate, slug flow pattern occurs at the lower GVF. For 40 GPM, slug flow occurs at 50% GVF and formed at 40% GVF when the volumetric flow rate reaches 50 and 60 GPM. For high liquid flow rate (70 GPM and 80 GPM), slug flow begins at 30% GVF.

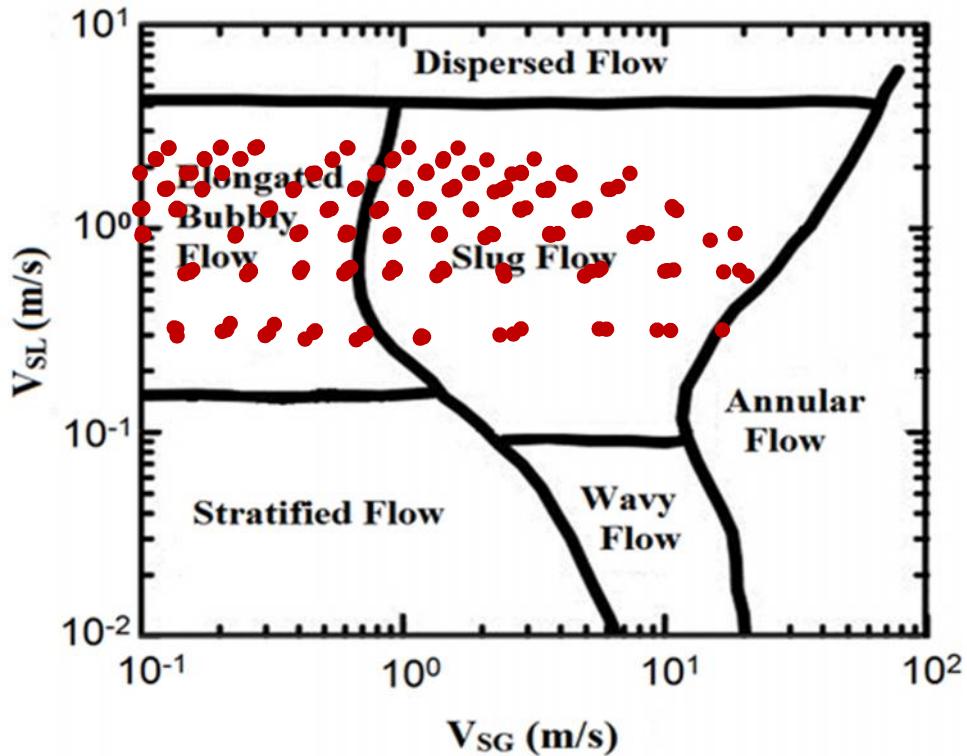


Figure 5.4 Horizontal flow regime map of the experimental data

Comparing the flow pattern from visualization and existing flow regime map showed some differences particularly at the low liquid flow rate. The wavy flow is formed at low rate while wavy flow is not stated in the flow regime map. The transition of the each pattern is not clear from the visual work.

5.2 Temperature Effect upon the Measurement Results

One of the results obtained from the electrical impedance device is gain. The gain is derived directly from the calculation of the unknown parameters C_x and R_x of the circuit from two different frequencies. Once all of the data results were tabulated for all of the flow conditions considered in this research, these data were then processed. The data were categorized based on the specific water volumetric flow rate (GPM) and pressure. The effect of the frequency to the gain can be evaluated by using the correlation between Gain and GVF as shown in Figure 5.5. The gain magnitude increased with the raising of the frequency. This result is consistent with the equation 2.2., since C_f and R_f are constant, increasing frequency will increase the gain. The mixtures' gain decreased as the GVF is raised. This is due to water having a higher conductivity and permittivity than air.

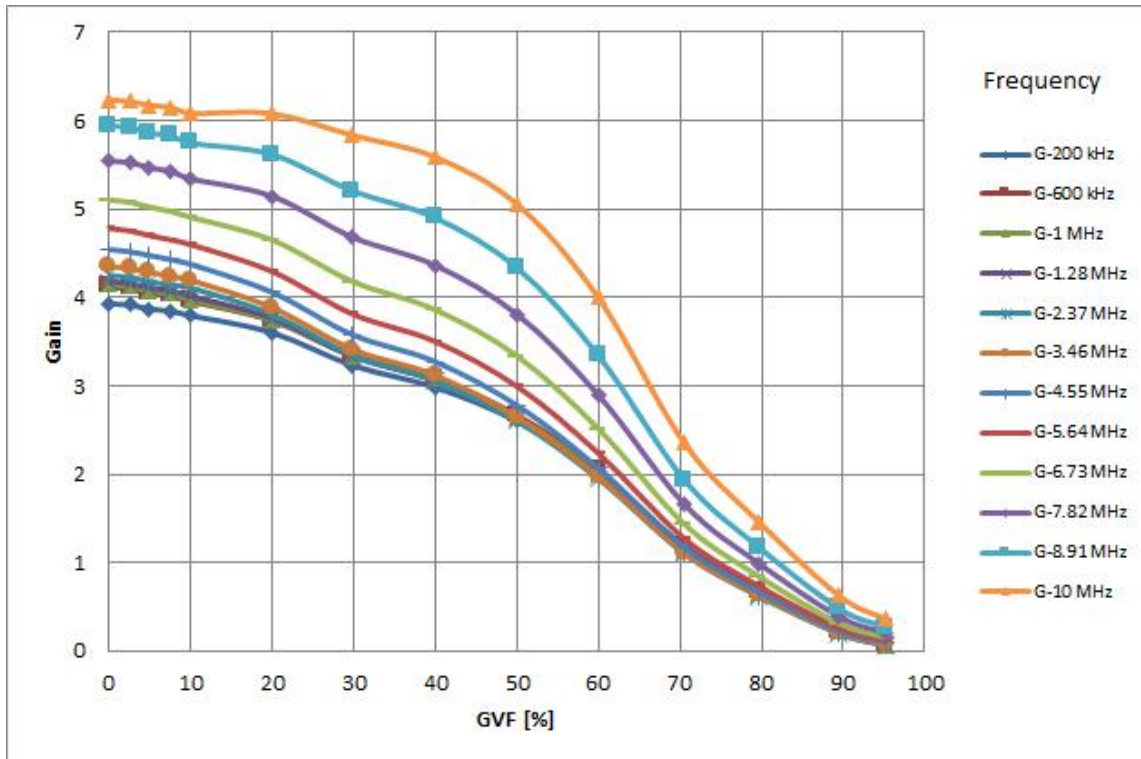


Figure 5.5 Gain variation with GVF for different frequencies @30GPM & 40psi

Figure 5.6 shows the gain magnitude as a function of GVF for all flow conditions considered at specific frequencies. Ideal result would be the gain magnitude being a function of only in a specific GVF and frequency. However, the graph indicates that the gain magnitude varied at the same GVF and frequency. For an example, at a frequency 1 MHz and 10% GVF, the gain magnitude spread from 3.1 to 4.1. The gain magnitude variation is relatively steady from 0% GVF to 60% GVF then decline while the GVF reach 70% and above, where air dominated the mixture. At very high GVF (above 90% GVF), the gain magnitude has less significant changing in all of the operation conditions.

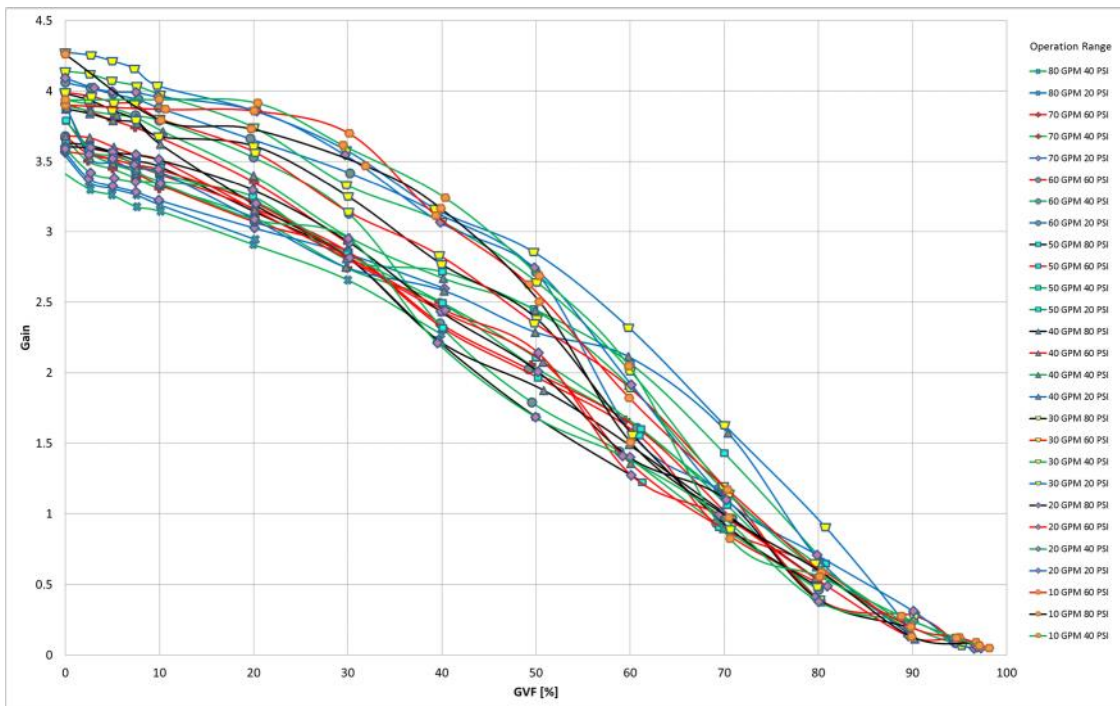


Figure 5.6 Gain vs GVF for different operation range @ Freq. 1 MHz

In order to determine the source of the gain magnitude variation, a surface curve was drawn where GVF is defined based on gain and temperature for a frequency 1 MHz. The frequency 1 MHz is chosen because it showed the best standard deviation for the further calculation. Figure 5.7 shows that the gain magnitude varied with the temperature changing where the higher temperature leads the higher gain magnitude. This is in line with the nature of the material conductivity. The temperature effect must be included in order to obtain more accurate the measurement results of GVF.

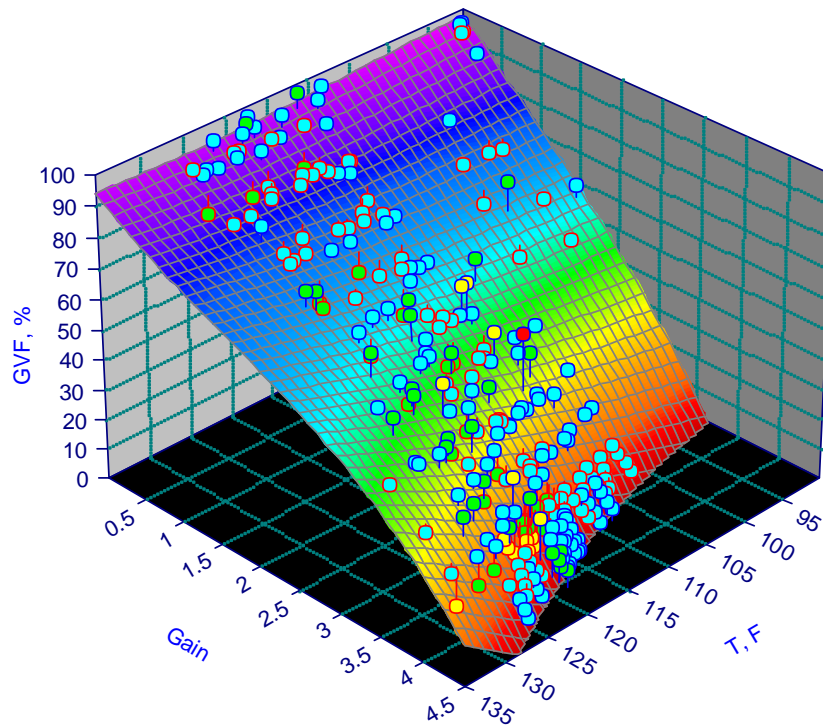


Figure 5.7 Surface curve GVF @ 1 MHz

Pumping liquid in a centrifugal pump continuously for a certain time will increase the temperature of the liquid. This rising temperature in the pump occurred due to energy imparted to the flow by the pump. The difference between energy consumed and energy needed to pump the water developed energy loss in the pump. The energy loss in the friction and hydraulic flow is also converted into heat, transferred to the liquid passing through the pump, and raised the liquid temperature. The temperature rise depends upon the total head and efficiency of the pump and the specific heat of the liquid [25].

The heat added to the liquid can be transmitted through the pump casing with differential temperature between liquid inside the pump and the surrounding air. However, if the energy loss is very high and the differential temperature is low, the liquid temperature increases transient with time. An air forced water cooler and by-pass system was applied to reduce the temperature rise rate.

Transferred heat to the liquid directly raised the mixture flow temperature. The temperature range of the mixture flow in this research varied from 91°F to 131°F. The data were then grouped based on the GVF, which ranged from 2.5% to 97.5% GVF, and evaluated based on the relation between the gain magnitude and the mixture temperature at the specific frequency.

To simplify this evaluation, a linear relation of the gain magnitude and the mixture temperature was applied. The linearization equation of the temperature corrected gain magnitude ($Gain'$) as a function of the mixture temperature (T) is given in the equation 5.1. Table 5.1 shows the complete lists of the equation for each GVF at a frequency 1 MHz. The complete equation for all frequencies can be seen at appendix.

$$Gain' = aT + b \quad (5.1)$$

GVF	Linearization Equation
2.5%	$y = 0.0371644x - 0.5373462$
5.0%	$y = 0.0376648x - 0.6436697$
7.5%	$y = 0.0399190x - 0.9547646$
10.0%	$y = 0.0335012x - 0.2954764$
20.0%	$y = 0.0414241x - 1.4395658$
30.0%	$y = 0.0423107x - 1.8737800$
40.0%	$y = 0.0415326x - 2.1794396$
50.0%	$y = 0.0308517x - 1.2917974$
60.0%	$y = 0.0132532x + 0.1871218$
70.0%	$y = 0.0084202x + 0.1489764$
80.0%	$y = -0.0001423x + 0.5720773$
90.0%	$y = -0.0039175x + 0.6580840$
95.0%	$y = 0.0003713x + 0.0587519$
97.5%	$y = 0.0005856x - 0.0039448$

Table 5.1 Linearization equation for each GVF @ 1 MHz

With the linearization approach, Gain' rises with temperature increase. A new parameter was introduced to minimize effect of the temperature to the new gain. The parameter is defined as modified Gain (Gain'') and is the function of the mixture temperature and Gain'. Equation 5.2. is used to determine the Gain''.

$$Gain'' = \frac{Gain'}{0.002 T^{1.3}} \quad (5.2)$$

Figure 5.8 presents the surface curve after temperature isolation process is applied. Gain'' is used in the y-coordinate instead of gain magnitude at the previous curve. The curve shows that the temperature effect has been removed from the gain magnitude.

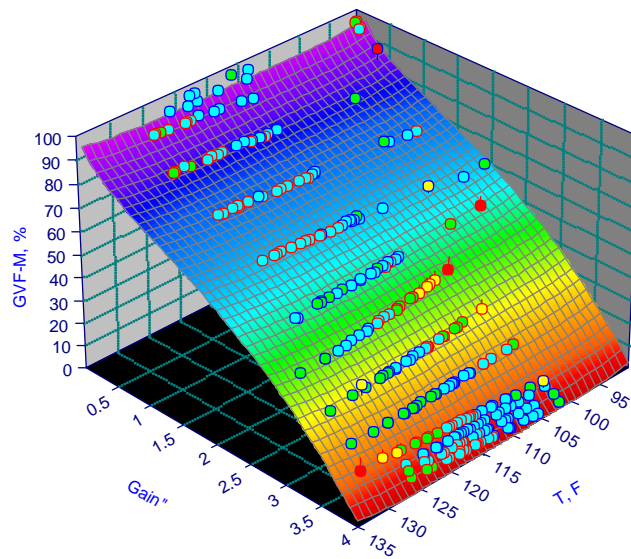


Figure 5.8 Surface curve GVF after temperature isolation process @ 1 MHz

Equation 5.2 is applied for the range of GVF within 2.5% to 97.5% for all frequencies. To predict a new GVF, a curve fitting method is applied which draws a correlation between measured GVF and Gain''. An example graph shows in Figure 5.9 for 1 MHz frequency.

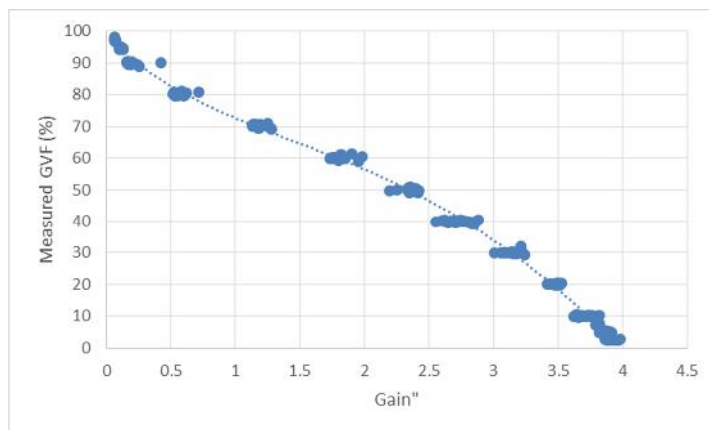


Figure 5.9 Measured GVF vs Gain'' @ 1 MHz

The correlation result from the curve fitting is formulated in the equation 5.3 to calculate temperature corrected value of GVF (Calculated GVF) from Gain".

$$\text{Calculated GVF (\%)} = a(\text{Gain}^n)^4 + b(\text{Gain}^n)^3 + c(\text{Gain}^n)^2 + d(\text{Gain}^n) + e \quad (5.3)$$

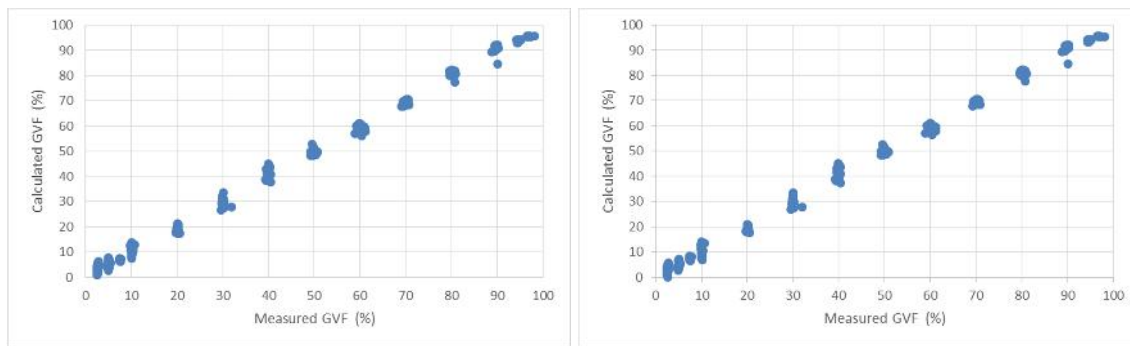
To verify the deviation of these approaches, equation 5.2 and equation 5.3 are used to calculate the calculated GVF for all frequencies. For low and medium frequency (from 0.2 MHz to 5.64 MHz), these equation produce high regression values and low standard deviations. The best result comes from 1 MHz frequency which produced the regression value 0.9976 and the standard deviation 1.47%.

For the higher frequencies (from 6.73 MHz to 10 MHz), the results produced unacceptable regression values and standard deviations. The worst frequency is 10 MHz which produced the regression value 0.942 and the standard deviation 7.22%. The curve fitting equation, the regression value of the curve (r^2) and the standard deviation are presented in Table 5.2.

Frequency	Curve Fitting Equation		R ²	Std. Dev (%)
	y = Calculated GVF (%)	x = Gain"		
200 kHz	$y = 0.40166x^4 - 5.26997x^3 + 17.55838x^2 - 38.52512x + 99.28175$		0.9974	1.52
600 kHz	$y = 0.4264x^4 - 5.1748x^3 + 17.065x^2 - 37.417x + 98.267$		0.9975	1.48
1 MHz	$y = 0.4167x^4 - 5.0558x^3 + 16.769x^2 - 37.316x + 97.781$		0.9976	1.47
1.28 MHz	$y = 0.2884x^4 - 4.0444x^3 + 14.404x^2 - 35.69x + 97.351$		0.9975	1.48
2.37 MHz	$y = 0.30869x^4 - 4.12867x^3 + 14.68772x^2 - 36.34810x + 97.37483$		0.9972	1.59
3.46 MHz	$y = 0.3021x^4 - 3.9972x^3 + 14.433x^2 - 36.255x + 97.598$		0.9972	1.59
4.55 MHz	$y = 0.33147x^4 - 4.15286x^3 + 14.98945x^2 - 36.43160x + 98.23907$		0.9973	1.55
5.64 MHz	$y = 0.41572x^4 - 4.87451x^3 + 17.36749x^2 - 38.26175x + 99.54331$		0.9965	1.76
6.73 MHz	$y = 0.50993x^4 - 5.92796x^3 + 21.46304x^2 - 42.28723x + 102.01380$		0.9935	2.42
7.82 MHz	$y = 0.44088x^4 - 5.55896x^3 + 21.96353x^2 - 43.79124x + 104.56915$		0.9885	3.20
8.91 MHz	$y = 0.33219x^4 - 4.56796x^3 + 19.63750x^2 - 41.56534x + 106.24166$		0.9761	4.62
10 MHz	$y = 0.19307x^4 - 2.89242x^3 + 13.33619x^2 - 32.24165x + 105.63652$		0.9416	7.22

Table 5.2 Curve fitting equation for all frequency

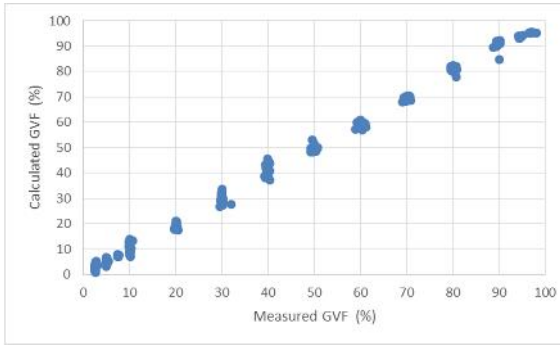
Figure 5.10 and Figure 5.11 were drawn to examine the calculated GVF and the measured GVF. The calculated GVF has a linear correlation with the measured GVF. The best uncertainty is in the range of $\pm 5.5\%$ which produced at 1 MHz frequency.



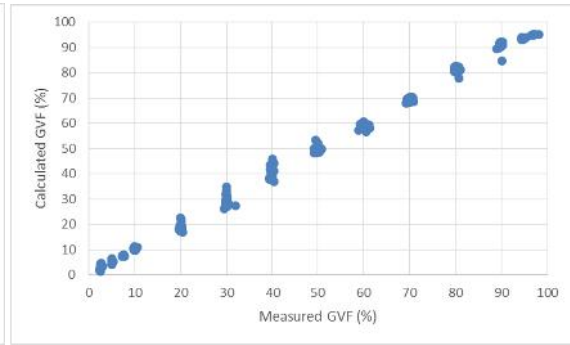
(a)200 kHz

(b)600 kHz

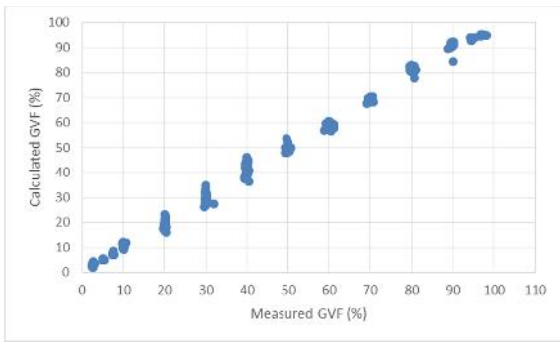
Figure 5.10 Calculated GVF as the function of Measured GVF at various frequencies



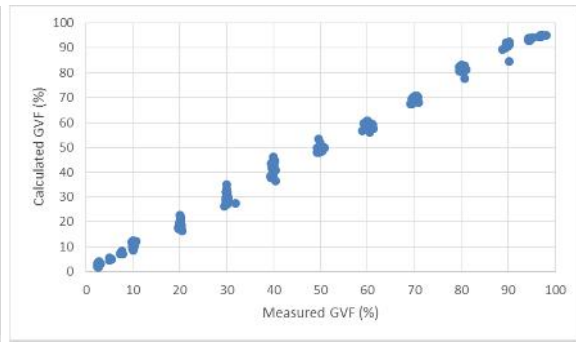
(c) 1 MHz



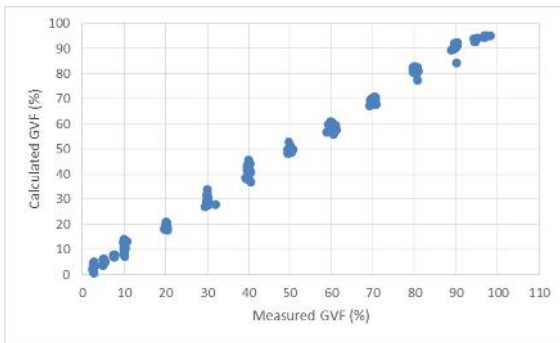
(d) 1.28 MHz



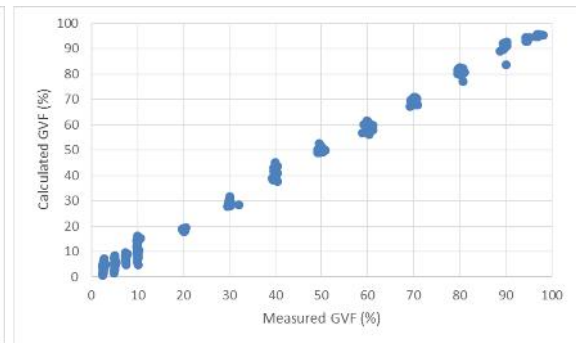
(e) 2.37 MHz



(f) 3.46 MHz

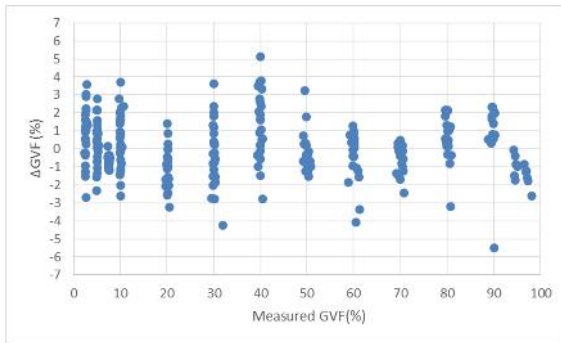


(g) 4.55 MHz

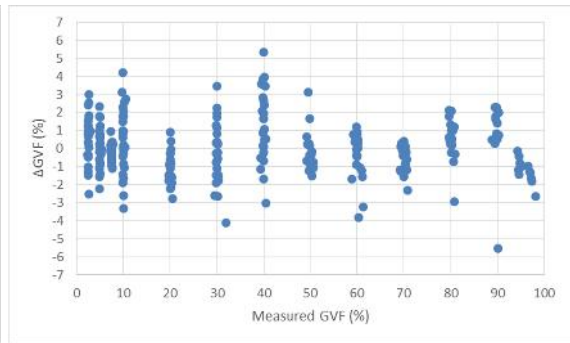


(h) 5.64 MHz

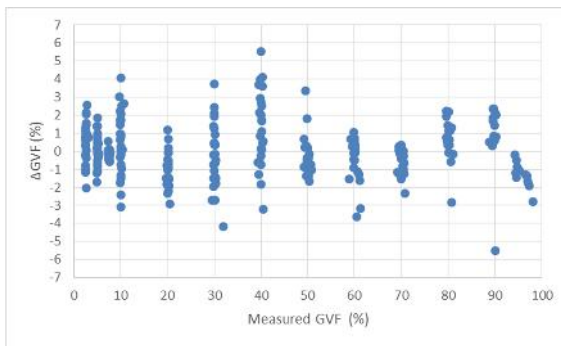
Figure 5.10 Continued



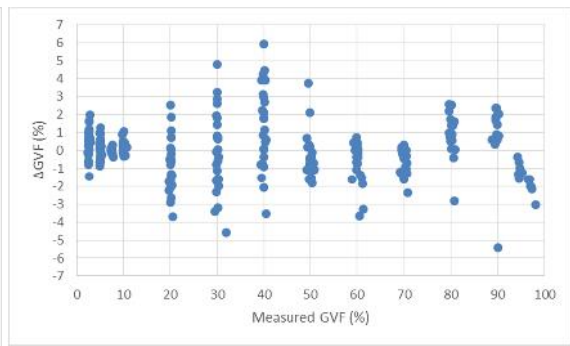
(a) 200 kHz



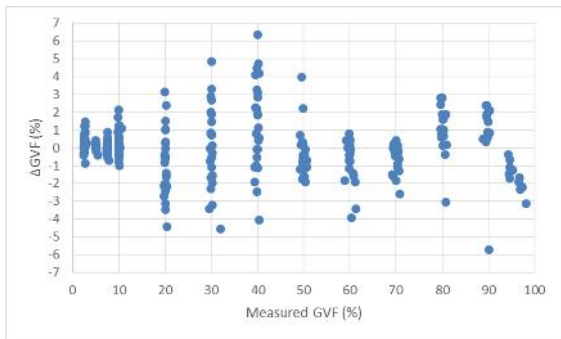
(b) 600 kHz



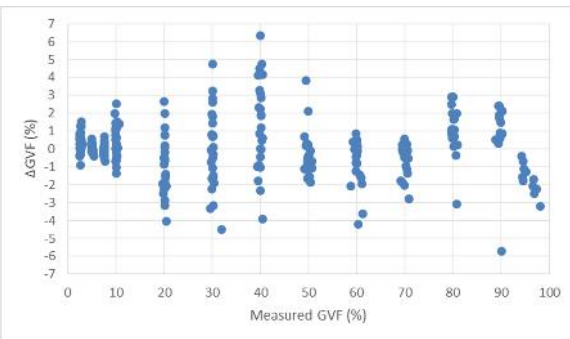
(c) 1 MHz



(d) 1.28 MHz

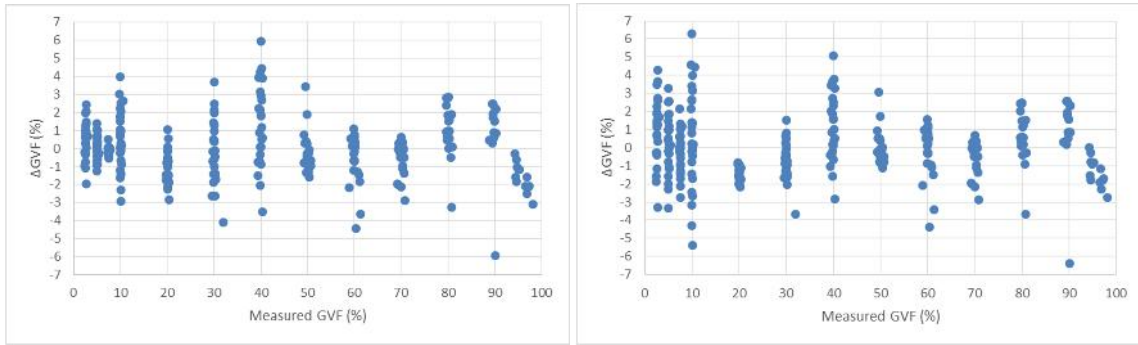


(e) 2.37 MHz



(f) 3.46 MHz

Figure 5.11 The differences of the calculated GVF and measured GVF as the function of measured GVF at various frequencies



(g)4.55 MHz

(h)5.64 MHz

Figure 5.11 Continued

The results show that the method can be used for frequencies from 0.2 MHz to 5.64 MHz for accurate GVF measurement. Regarding to the uncertainty and the standard deviation that produced in this experiment, the slotted orifice plate has capability to measure multiphase flow for reservoir management and production application. Further research needs to conduct in order to produce better accuracy for custody transfer application.

5.3 The Slotted Orifice Characteristics

The calibration factor (KY), Euler number (Eu), and Morrison number (Mo) were used to determine the slotted orifice characteristics with respect to the differential pressure (DP) and pressure (P) at the inlet of the plate. KY and Eu were applied to evaluate the mixture mass flow rate, while Mo was the parameter to examine the mixture dynamic viscosity.

Air density and the mixture mass flow rate were applied to calculate the measured KY. The measured GVF, in the range of 2.5% to 97.5%, is used to determine the mixture quality (X) for the further calculation. To predict the calculated KY, surface fit method was used to find the correlation between KY, X, and P as showed in Figure 5.12. The regression value of the surface curve is 0.955.

The calculated KY, which is obtained from the correlation, was applied to recalculate the mixture mass flow rate. Figure 5.13 shows the differences between calculated and measured total mass flow rate as a function of the total measured mass rate. The standard deviation is 0.31 lbm/s in the range of 1.2 to 11.1 lbm/s mass rate. From the characterization results, the slotted orifice plate can be applied for the multiphase mass flow rate measurement.

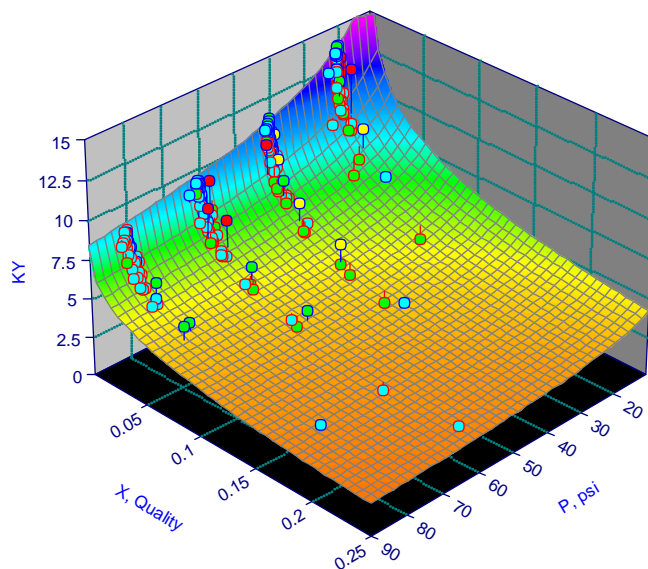


Figure 5.12 Calibration surface fit

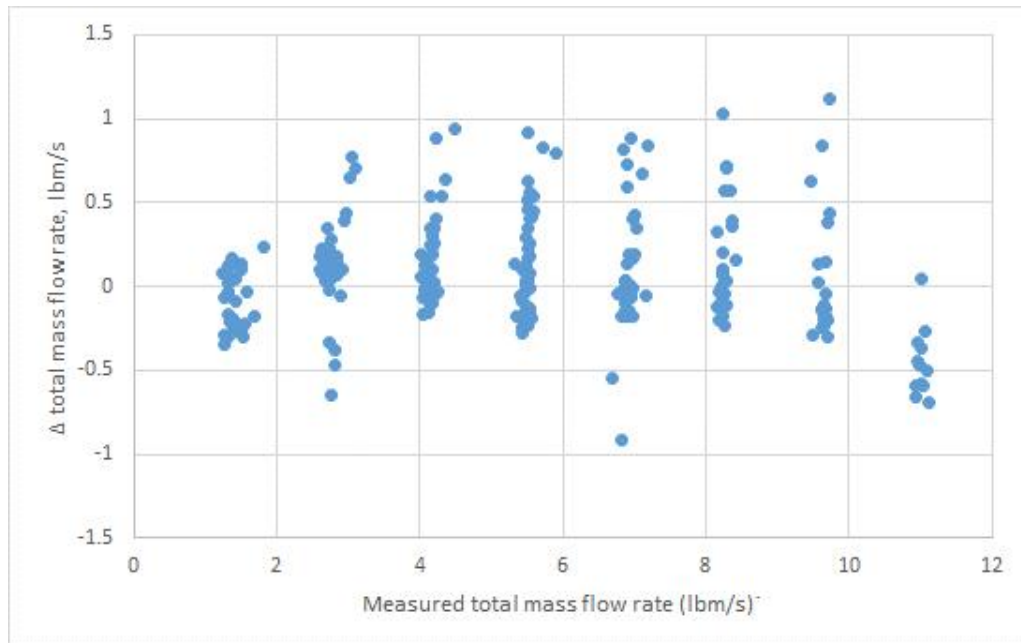


Figure 5.13 The differences between calculated and measured total mass flow rate as a function measured total mass flow rate

The E_u was evaluated with mixture superficial velocity and differential pressure in the surface fit as showed in Figure 5.14. The regression value of the surface curve is 0.957. The mixture density is redefined with using the calculated E_u which is obtained from the correlation. Figure 5.15 presents the differences of calculated and measured mixture density as a function of the measured mixture density. The standard deviation is 1.76 lbm/ft^3 in the range of 1.5 to 60.5 lbm/ft^3 density.

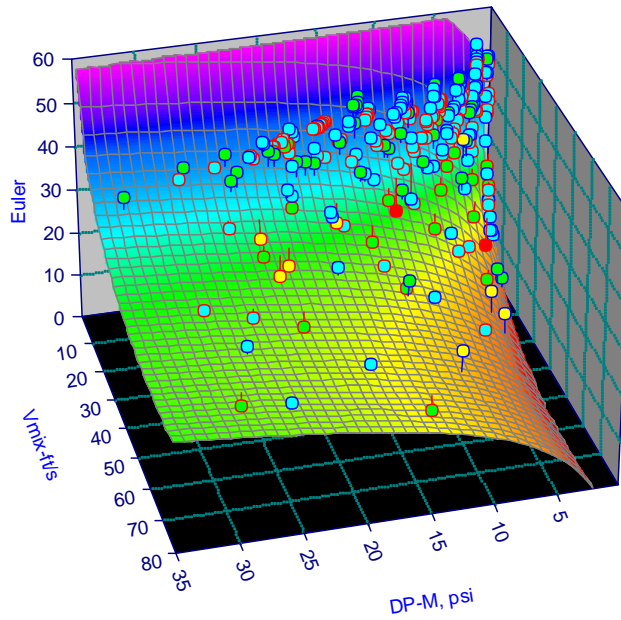


Figure 5.14 Surface fit the Euler number

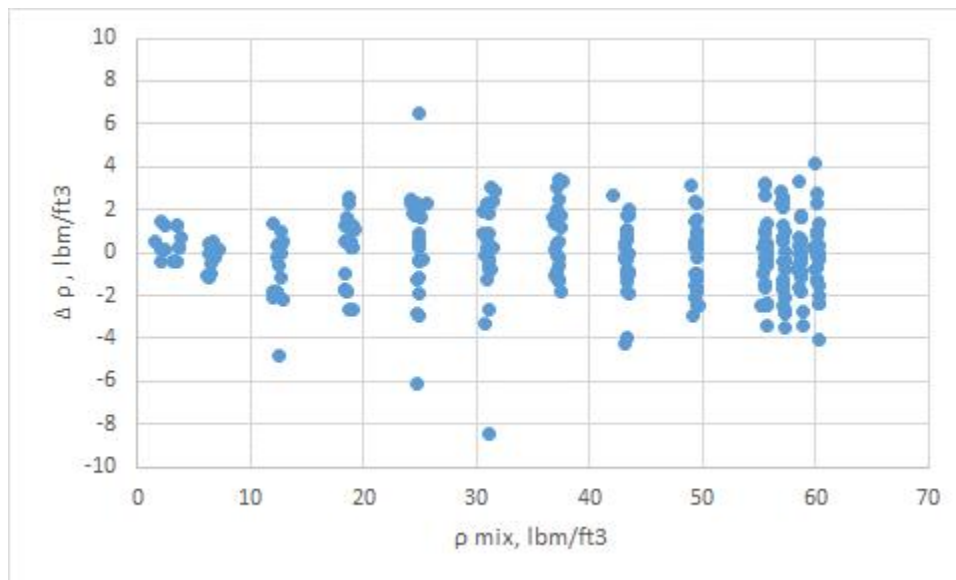


Figure 5.15 Differences between calculated and measured mixture density as a function of measured mixture density

Similar process is applied to evaluate M_o . Using surface fit method, the M_o is redefined with the new GVF and differential pressure as presented in Figure 5.16. The regression value of the surface curve is 0.991. The mixture dynamic viscosity is determined by using the calculated M_o which is obtained from the curve fit correlation. Figure 5.17 shows the differences of calculated dynamic viscosity and measured dynamic viscosity as the function of the measured dynamic viscosity. The standard deviation is $1.375E-06$ lbf s/ft² in the range of $1.438E-05$ to $1.1E-05$ lbf s/ft² dynamic viscosity.

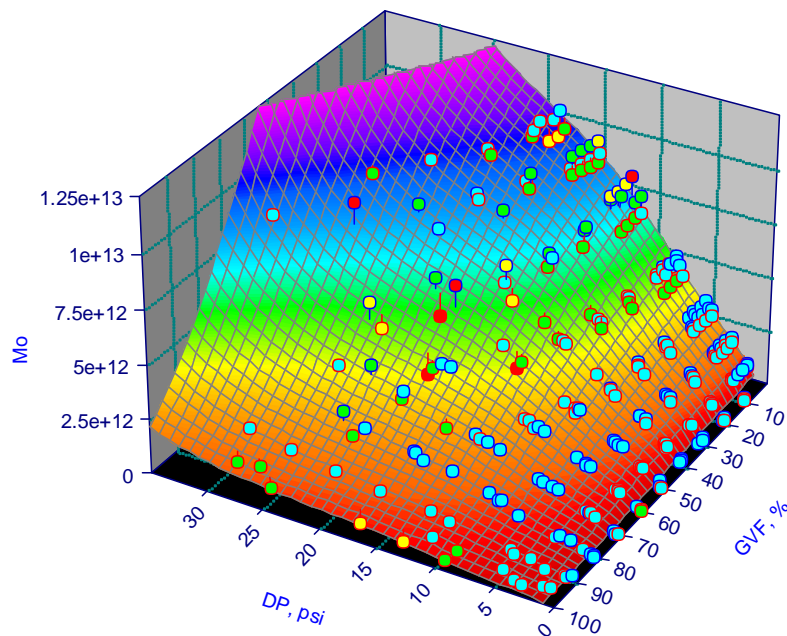


Figure 5.16 Surface fit the Morrison number

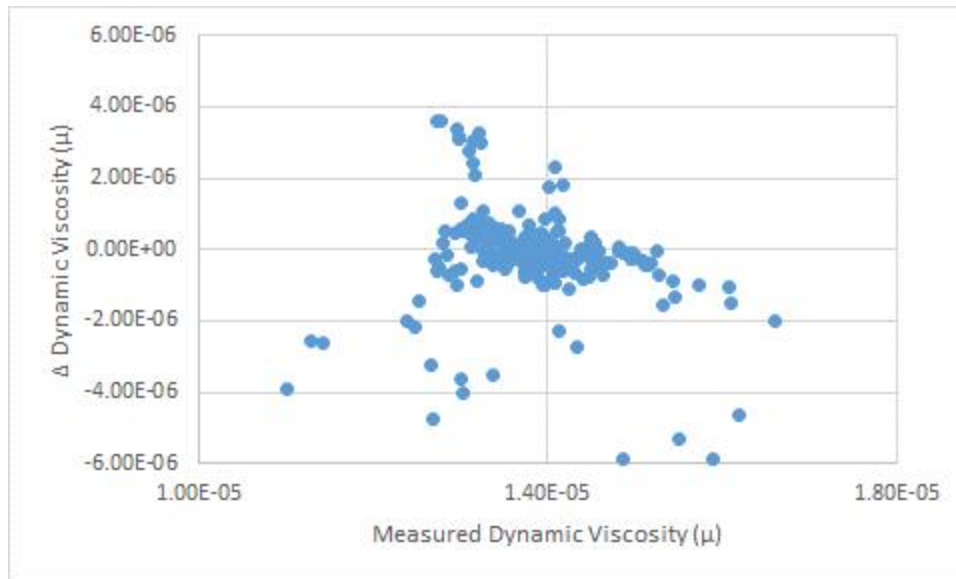


Figure 5.17 Differences between calculated and measured dynamic viscosity as a function of measured dynamic viscosity

The next possible way to characterize the slotted orifice plate would be to investigate the correlation between the Euler number and the Morrison number. Figure 5.18 shows that the correlation is dependant upon the liquid volumetric flow rate. Higher liquid volumetric flow rate produced more spread in the correlation.

In order to accommodate the liquid volumetric flow rate effect in this correlation, a modify Euler number is introduced. Figure 5.19 presents the correlation between the modify Euler number and Morrison number which is more linear. Further research is needed to investigate the other factor which could be affecting this correlation for more accurate results.

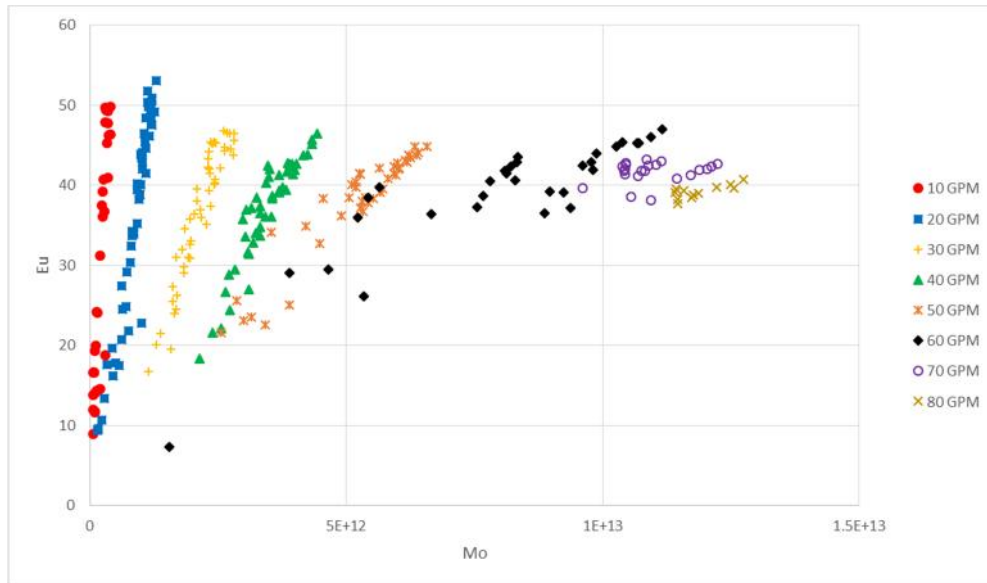


Figure 5.18 Euler number as a function of Morrison number at various liquid volumetric flow rate

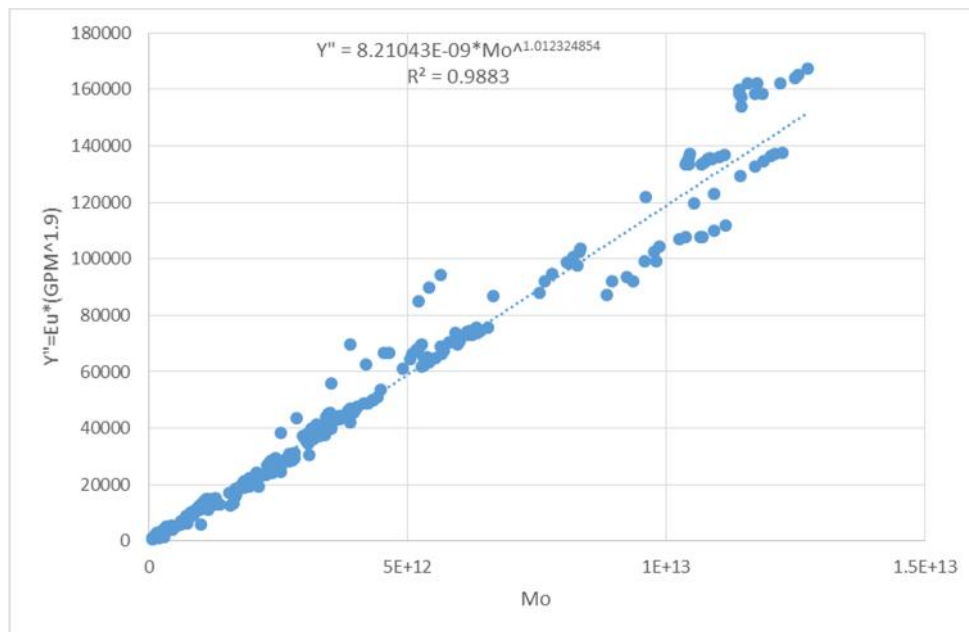


Figure 5.19 Modify Euler number to liquid volumetric flow rate as a function of Morrison number

6. CONCLUSION AND RECOMMENDATIONS

6.1 Conclusion

The experiment was conducted in order to evaluate the performance of the slotted orifice plate as a two-phase flow meter based upon examination of flow visualization, study the effect of the temperature to the measurement results, and analyze the characteristics of the plate. Water and air were used as the working fluids and the measurement applied for many operation variation in the range of 2.5% to 97.5% GVF.

The air and water flow visualization studied showed that the slotted orifice plate has capabilities to be a flow conditioner for two-phase flow in the pipe in all of the patterns flow. At the low rate, the mixture flow is mostly in the wavy flow in the upstream. The slotted orifice plate promotes turbulent flow and causes the flow to be well-mixed in the downstream. Similar condition occurs in medium and high flow rates where the slotted orifice plate creates well-homogenized flow in the downstream.

According to the flow pattern map in the horizontal pipe, the mixture flow is located in the bubbly flow, plug flow, and slug flow area. The flow pattern is dependent of volumetric flow rate and GVF. The higher of volumetric flow rate in the pipe, the lower GVF is needed to form the slug flow.

Temperature variation is found to affect the GVF measurement results due to the mixture conductivity behavior. Temperatures varied from 91°F to 131°F in this study. Using linearization and curve fitting methods to evaluate the relation between the gain magnitude and the mixture temperature, a new parameter is introduced to isolate the effect of the temperature to the measurement results. These methods can be applied for frequencies in the range within 0.2 MHz to 5.64 MHz. For the higher frequency (from 6.73 MHz to 10 MHz), the measurement accuracy is not acceptable, thus these approaches should not be applied.

Using this technique, the calculated GVF is then determined with a standard deviation of 1.47% and uncertainty is in the range of $\pm 5.5\%$ for 2.5% to 97.5% GVF at 1 MHz frequency. The results showed that the slotted orifice plate can be configured to measure multiphase flow for reservoir management and production application in the oil and gas industry.

The measured GVF, within the range 2.5% to 97.5% GVF, is applied to determine slotted orifice characteristics with using KY, Eu, and Mo based on differential pressure and pressure. For total mass flow rate calculated, the standard deviation is 0.31 lbm/s in the range of 1.2 to 11.1 lbm/s. For mixture density calculated, the standard deviation is 1.76 lbm/ft³ in the range of 1.5 to 60.5 lbm/ft³ density and for the calculated dynamic viscosity, the standard deviation is 1.245E-06 lbf s/ft² in the range of 1.438E-05 to 1.1E-05 lbf s/ft². From the characterization results, the slotted orifice plate can be applied for multiphase mass flow rate measurement.

6.2 Recommendations

The studied showed that the slotted orifice plate can be applied as a flow conditioner and for multiphase flow measurement. Further research is needed in order to obtain better reliability and accuracy.

- For more detail flow visualization, high speed video can be utilized to capture the clear border of the each pattern of the flow regime.
- Wider range of the mixture temperature can be applied to verify the method of the temperature effect isolation.
- Different mixture components can be used to satisfy the function of the slotted orifice plate as a multiphase flow meter.
- Wider range of operation condition such as higher volumetric rate and higher working pressure can be conducted to investigate the slotted orifice flowmeter in the harsh condition.
- Combined with the other multiphase meter can be promoted to produce higher accuracy and better reliability in the measurement results.

REFERENCES

- [1] Thorn, R., Johansen, G. A., & Hjertaker, B. T. (2013). Three-phase flow measurement in the petroleum industry. *Measurement Science and Technology*, 24(1), 1-17. doi:10.1088/0957-0233/24/1/012003

- [2] Falcone, G., Hewitt, G. F., Alimonti, C., & Harrison, B. (2002). Multiphase flow metering: Current trends and future developments. *Society of Petroleum Engineers 74689*, 77-84.

- [3] Morrison, G. L., Pirouzpanah, S., Cevik, M., & Patil, A. (2013, July 7-11). *Evaluation of a close coupled slotted orifice, electrical impedance, and swirl flow meters for multiphase flow*. Proceedings of the ASME 2013 Fluids Engineering Division Summer Meeting, Incline Village, NV. Retrieved August 11, 2014, from <http://proceedings.asmedigitalcollection.asme.org>

- [4] Pirouzpanah, S., Cevik, M., & Morrison, G. L. (2014). Multiphase flow measurements using coupled slotted orifice plate and swirl flow meter. *Flow Measurement and Instrumentation*, 40, 157-161.

- [5] Baker, R. C. (2000). *Flow Measurement Handbook: Industrial Designs, Operating Principles, and Applications*. Cambridge, UK: Cambridge University Press.

- [6] Morrison, G. L., Hall K. R., Holste, J. C., Macek, M. L., Ihfe, L. M., DeOtte, R. E., Jr., & Terracina, D. P. (1994). Comparison of Orifice and Slotted Plate Flowmeters. *Flow Measurement and Instrumentation*, 5(2), 71-74.
- [7] Ruiz, J. H. (2004). *Low differential pressure and multiphase flow measurements by means of differential pressure devices* (Doctoral dissertation). Texas A&M University, College Station, TX.
- [8] Ihfe, L. M. (1994). *Development of the slotted orifice flow conditioner* (Master's thesis). Texas A&M University, College Station, TX.
- [9] Macek, M. L. (1993). *A Slotted Orifice Plate Used as a Flow Measurement Device* (Master's thesis). Texas A&M University, College Station, TX.
- [10] Terracina, D. P. (1996). *The experimental and numerical development of the slotted plate, and its design parameter* (Master's thesis). Texas A&M University, College Station, TX.
- [11] Morrison, G. L., Terracina, D. P., & Brewer, C. (2001). Response of a slotted orifice flow meter to an air/water mixture. *Flow Measurement and Instrumentation*, 12, 175-180.

- [12] Geng, Y., Zheng, J., & Shi, T. (2006). Study on the metering characteristics of a slotted orifice for wet gas flow. *Flow Measurement and Instrumentation*, 17, 123-128.
- [13] Brewer, C. V. (1999). *Evaluation of the slotted orifice plate as a two phase flow meter* (Master's thesis). Texas A&M University, College Station, TX.
- [14] Flores, A. E. (2000). *Evaluation of a slotted orifice plate flow meter using horizontal two phase flow* (Master's thesis). Texas A&M University, College Station, TX.
- [15] Sparks, S. A. (2004). *Two phase mixing comparison, oil contamination comparison, and manufacturing accuracy effect on calibration of slotted orifice flow meters* (Master's thesis). Texas A&M University, College Station, TX.
- [16] Cevik, M. (2013). *Evaluation of a close coupled slotted orifice, electrical impedance, and swirl flow meters for multiphase flow* (Master's thesis). Texas A&M University, College Station, TX.
- [17] Da Silva, M. J. (2008). *Impedance sensors for fast multiphase flow measurement and imaging* (Doctoral dissertation). Technische Universtaat Dresden, Dresden, Germany.

- [18] Fossa, M. (1998). Design and performance of a conductance probe for measuring the liquid fraction in two-phase gas-liquid flows. *Flow Measurement and Instrumentation*, 9, 103-109.
- [19] Andreussi, P., Di Donfrancesco, A. D., & Messi, M. (1988). An impedance method for the measurement of liquid hold-up in two-phase flow. *International Journal Multiphase Flow*, 14(6), 777-785.
- [20] Bratland, O. (2013). *Pipe Flow 2: Multi-phase flow assurance*. Retrieved October 4, 2014, from <http://www.drbratland.com>
- [21] Corneliussen, S., Couput, J. P., Dahl, E., Dykesteen, E., Froyso, K. E., Malde, E., ... Tunheim, H. (2005). *Handbook of the multiphase flow metering* (Rev. 2). The Norwegian Society for Oil and Gas Measurement and The Norwegian Society of Chartered Technical and Scientific Professionals. Retrieved November 6, 2014, from <http://www.nfogm.no>
- [22] Mandhane, J. M., Gregory, G. A., & Aziz, K. (1974). A flow pattern map for gas-liquid flow in horizontal pipes. *International Journal Multiphase Flow*, 1, 537-553.

- [23] Coleman, J. W., & Garimella, S. (1999). Characterization of two-phase flow patterns in small diameter round and rectangular tubes. *International of Heat and Mass Transfer*, 42, 2869-2881.
- [24] Office of the State Climatologist. *College Station Monthly Summary June-August 2014*. Retrieved January 20, 2015, from <http://climatexas.tamu.edu/index.php/monthly-reports/college-station-monthly-summaries>
- [25] Girdhar, P., & Moniz, O. (2004). *Practical Centrifugal Pumps*. Burlington, MA: Elsevier.

APPENDIX A

FIGURES

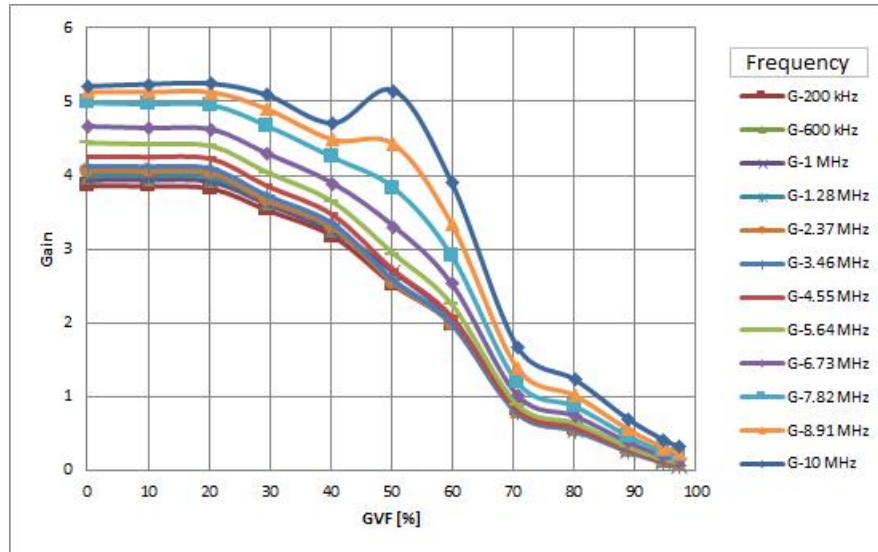


Figure A.1 Gain variation with GVF for different frequencies @10GPM & 40psi

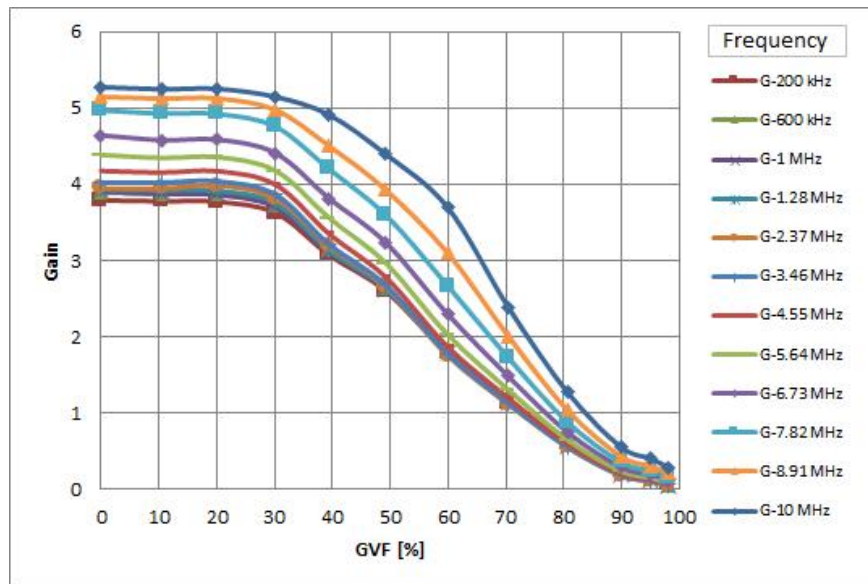


Figure A.2 Gain variation with GVF for different frequencies @10GPM & 60psi

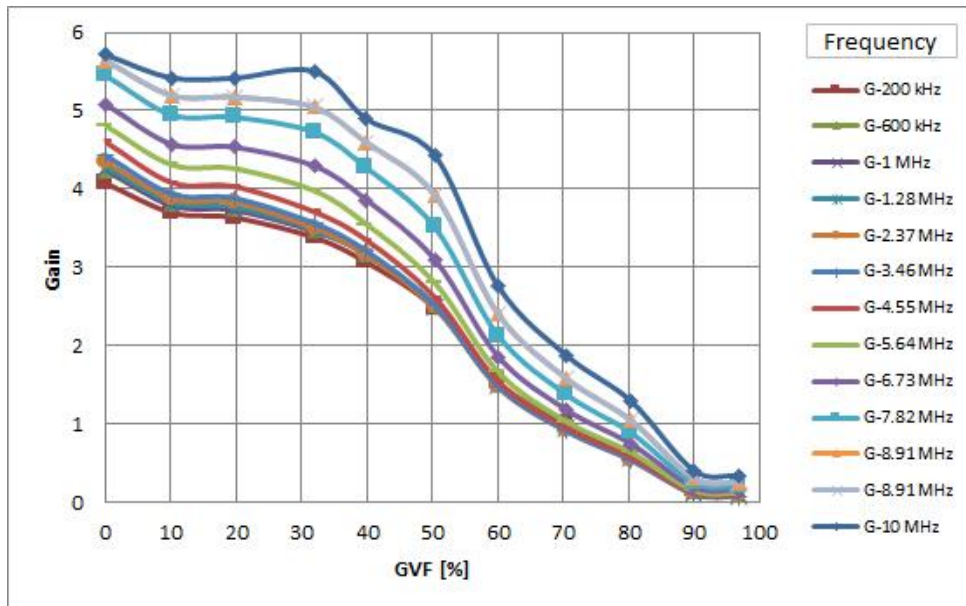


Figure A.3 Gain variation with GVF for different frequencies @10GPM & 80psi

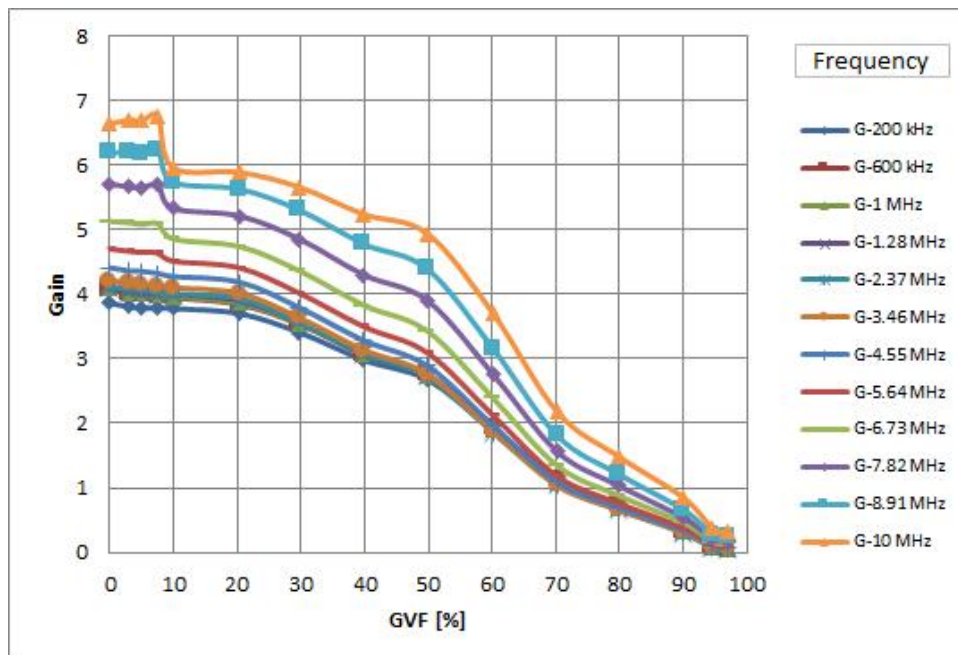


Figure A.4 Gain variation with GVF for different frequencies @20GPM & 20psi

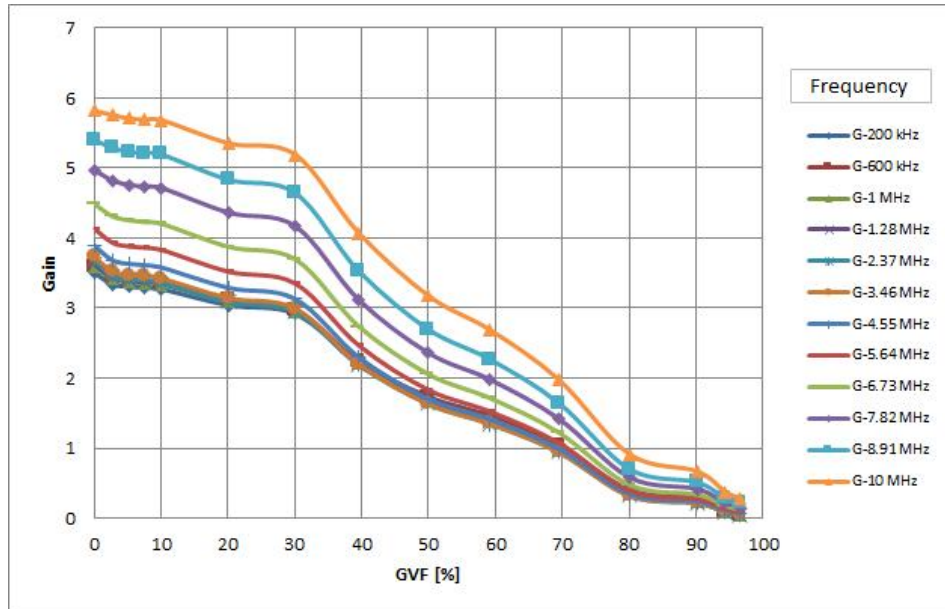


Figure A.5 Gain variation with GVF for different frequencies @20GPM & 40psi

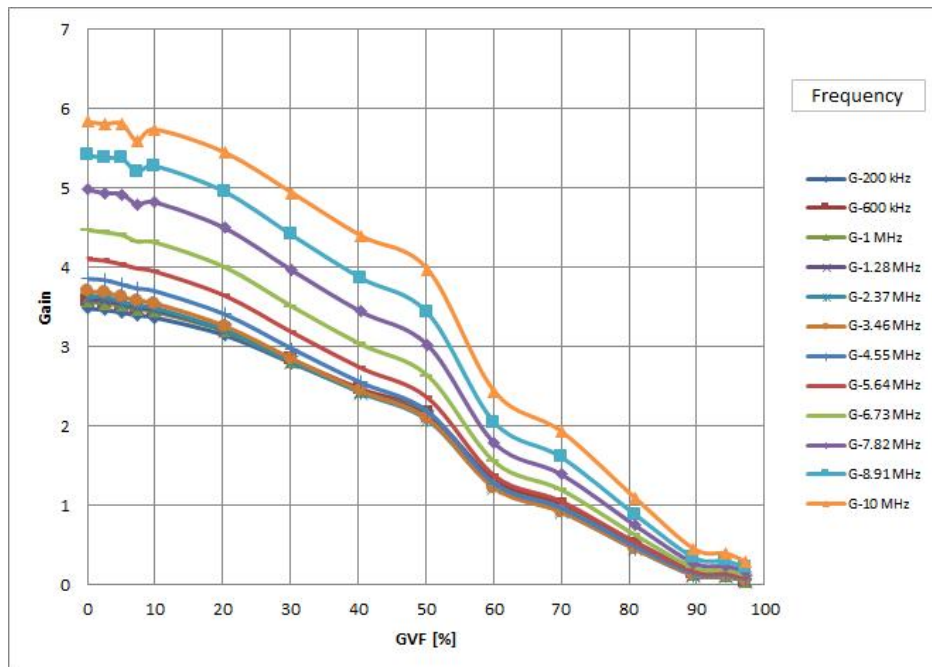


Figure A.6 Gain variation with GVF for different frequencies @20GPM & 60psi

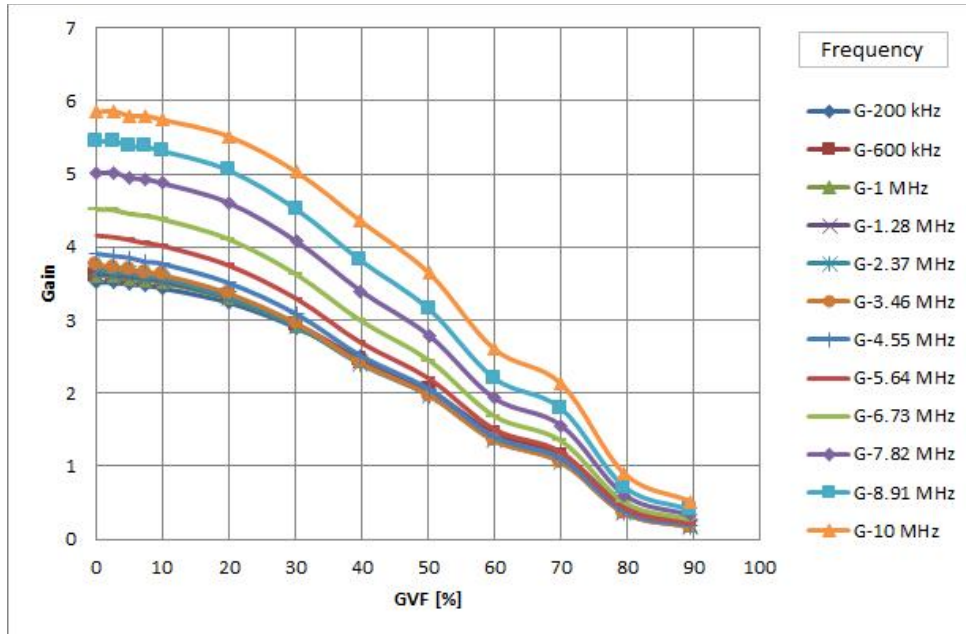


Figure A.7 Gain variation with GVF for different frequencies @20GPM & 80psi

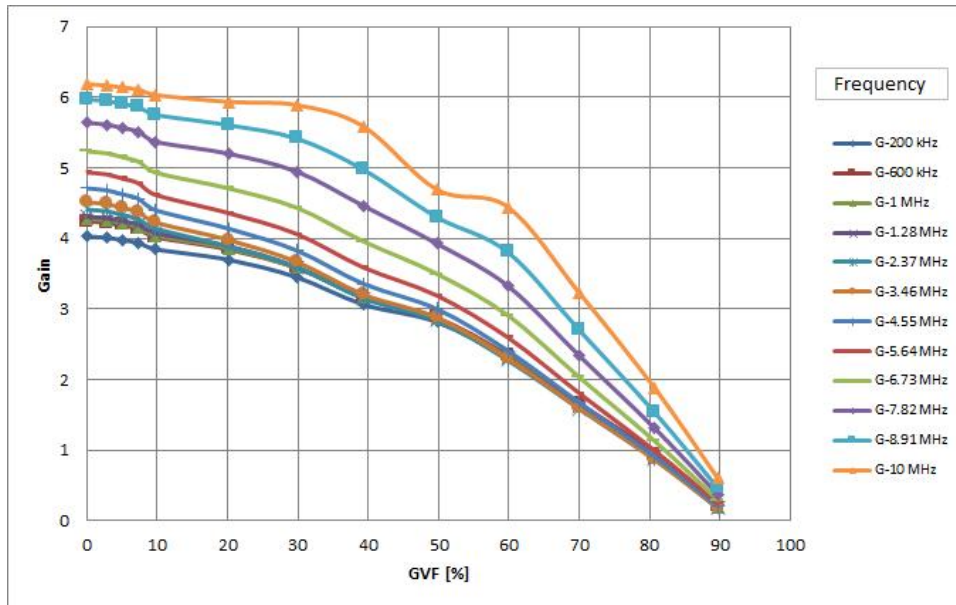


Figure A.8 Gain variation with GVF for different frequencies @30GPM & 20psi

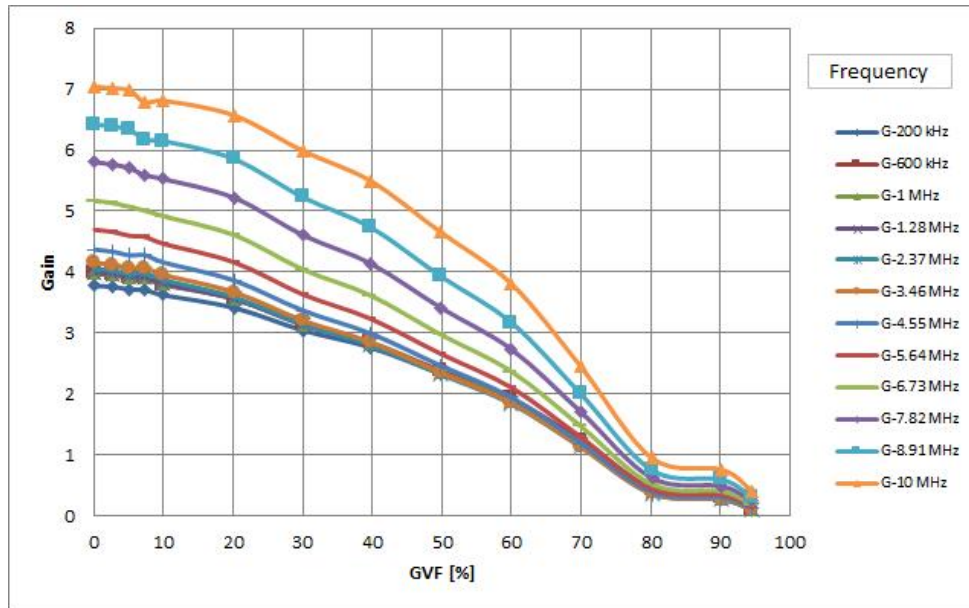


Figure A.9 Gain variation with GVF for different frequencies @30GPM & 60psi

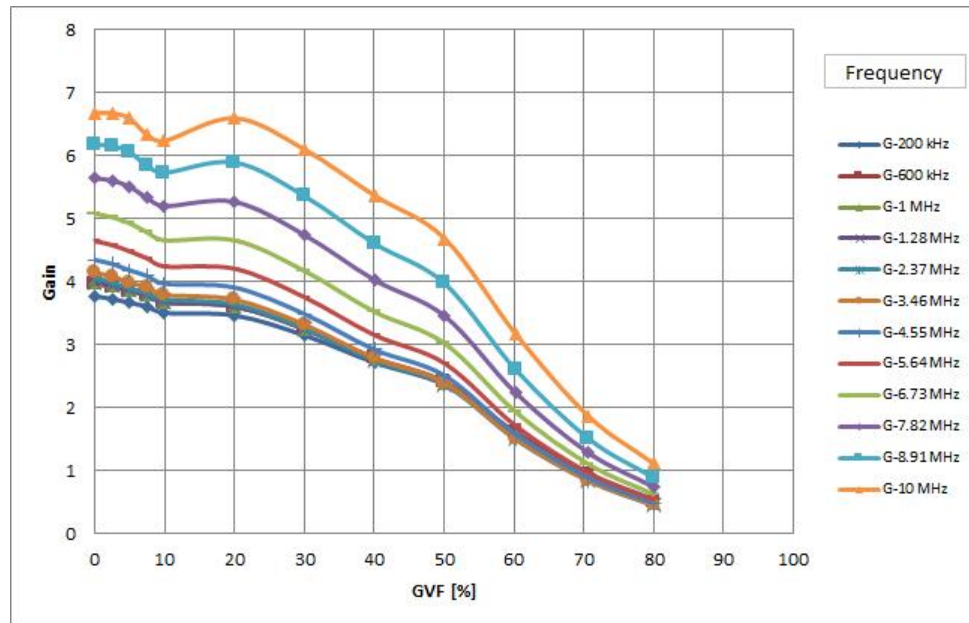


Figure A.10 Gain variation with GVF for different frequencies @30GPM & 80 psi

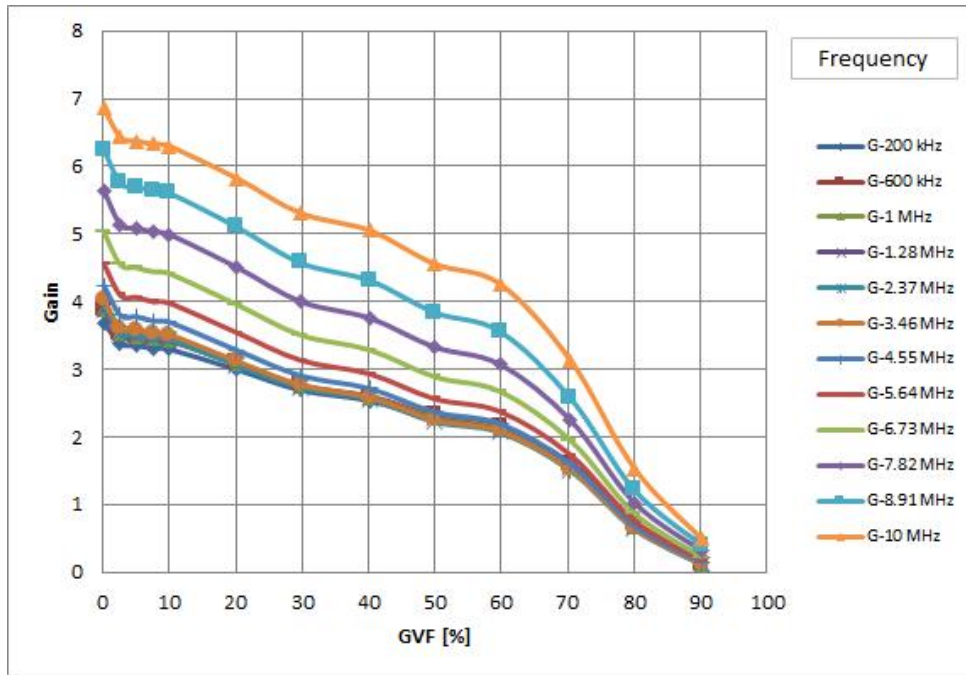


Figure A.11 Gain variation with GVF for different frequencies @40GPM & 20psi

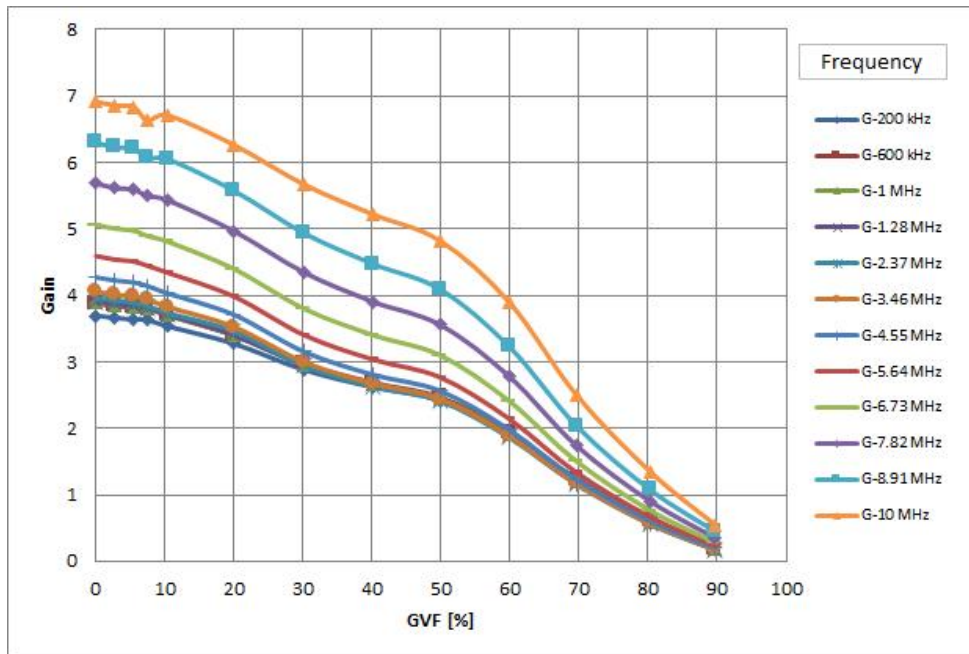


Figure A.12 Gain variation with GVF for different frequencies @40GPM & 40psi

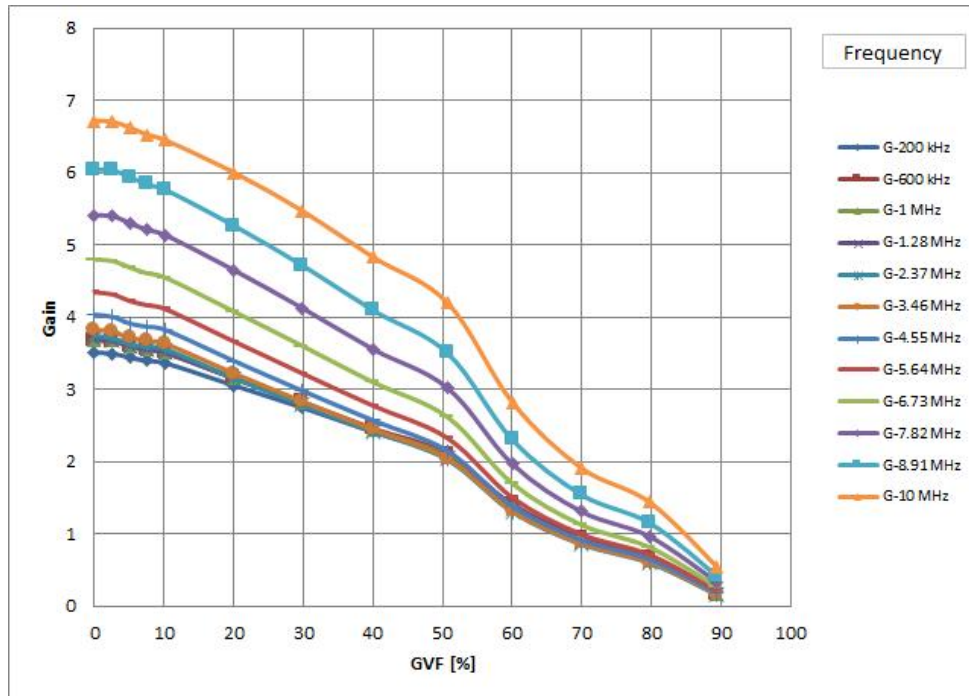


Figure A.13 Gain variation with GVF for different frequencies @40GPM & 60 psi

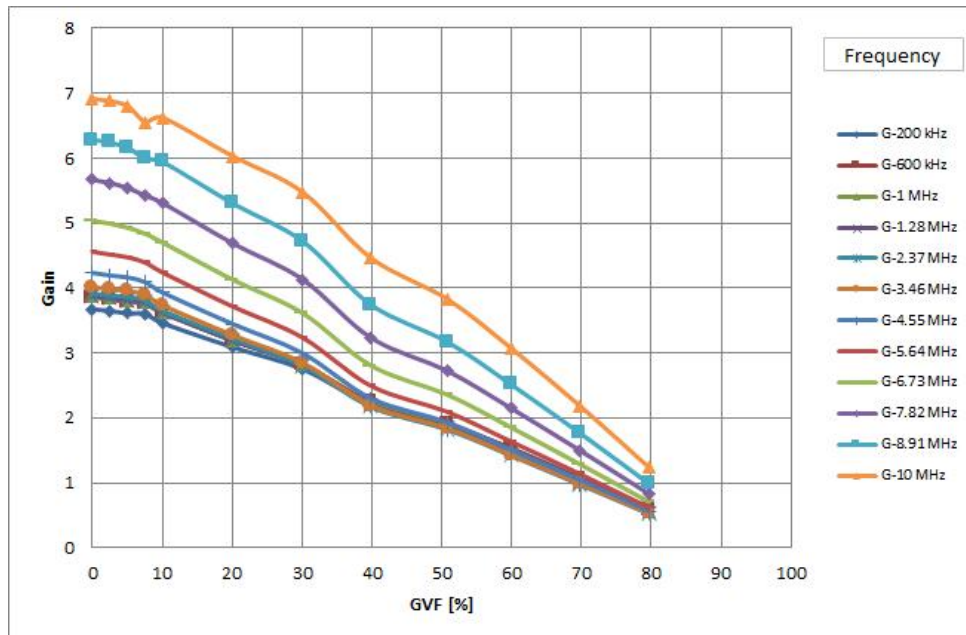


Figure A.14 Gain variation with GVF for different frequencies @40GPM & 80psi

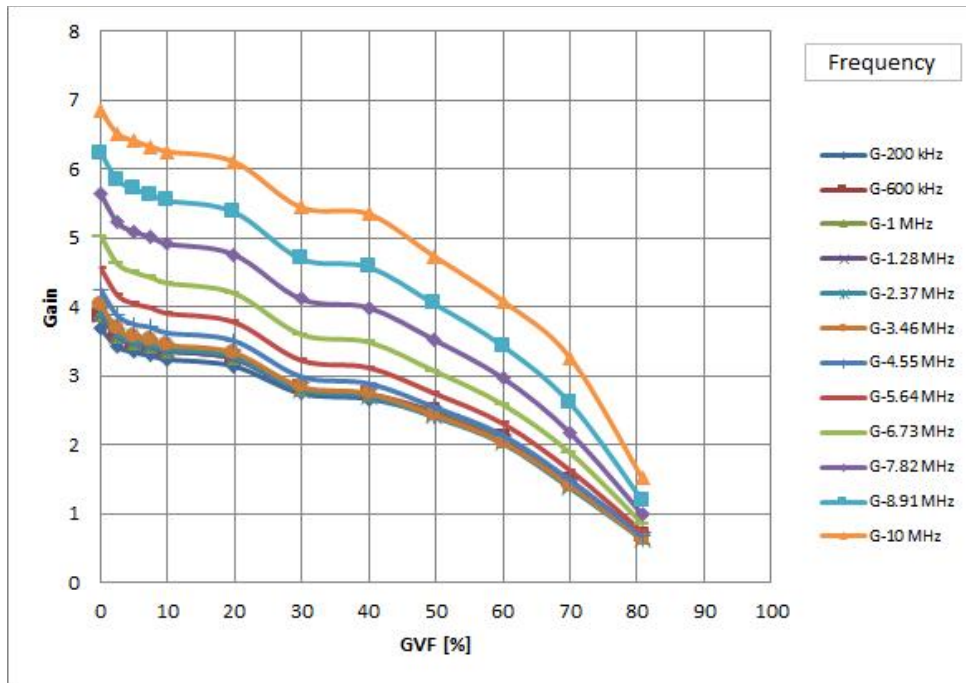


Figure A.15 Gain variation with GVF for different frequencies @50GPM & 20psi

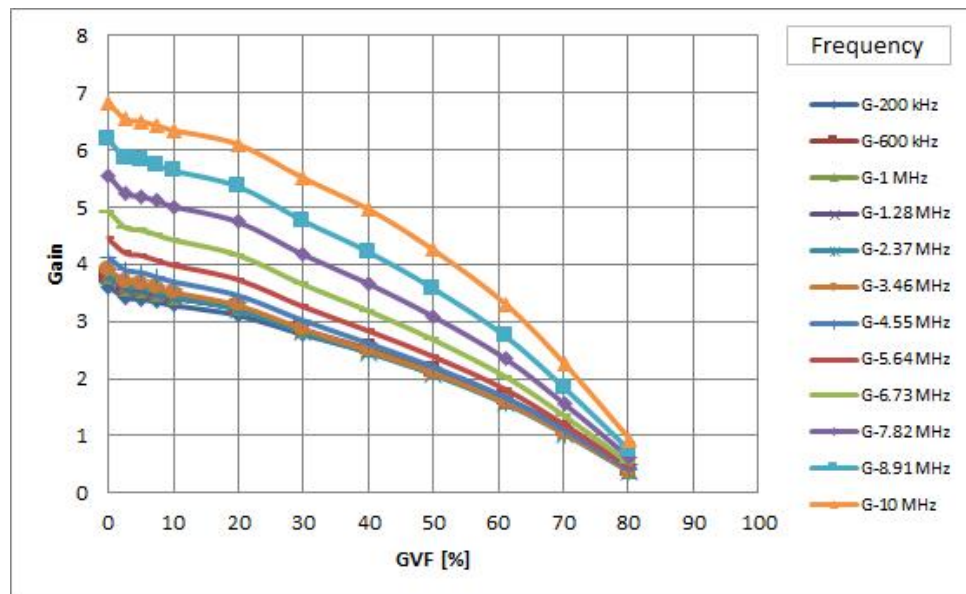


Figure A.16 Gain variation with GVF for different frequencies @50GPM & 40psi

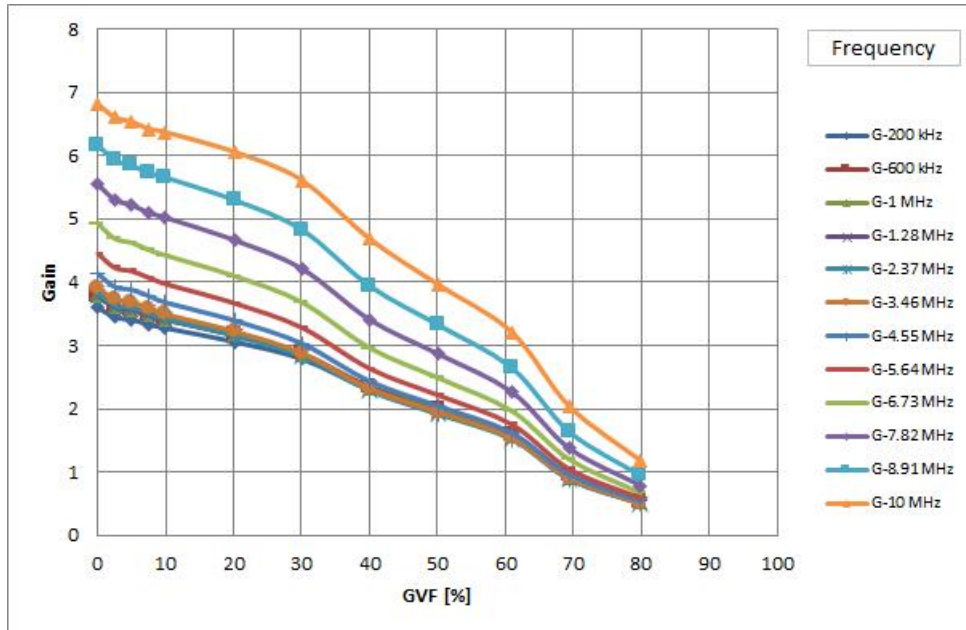


Figure A.17 Gain variation with GVF for different frequencies @50GPM & 60psi

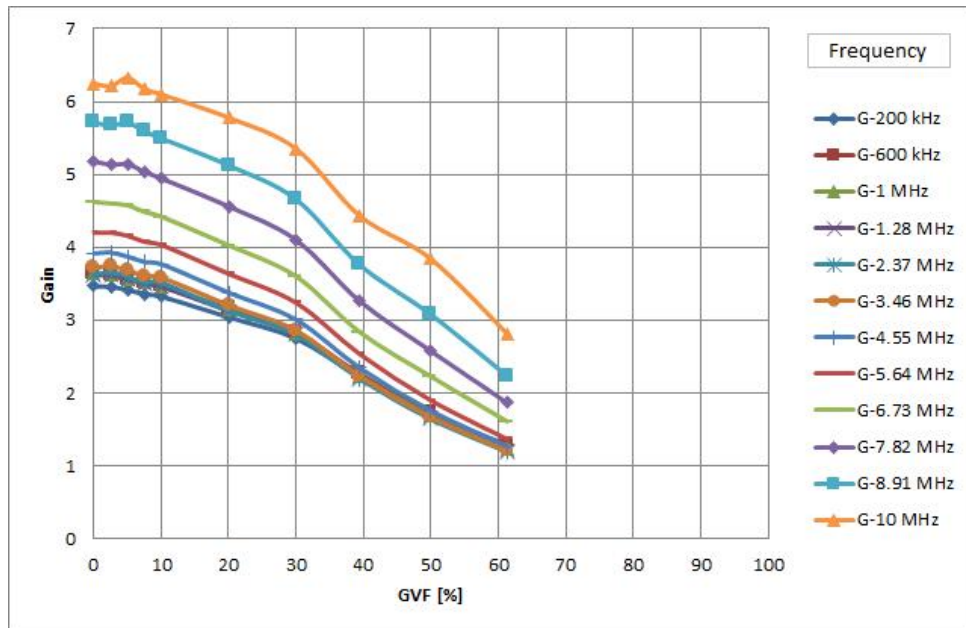


Figure A.18 Gain variation with GVF for different frequencies @50GPM & 80psi

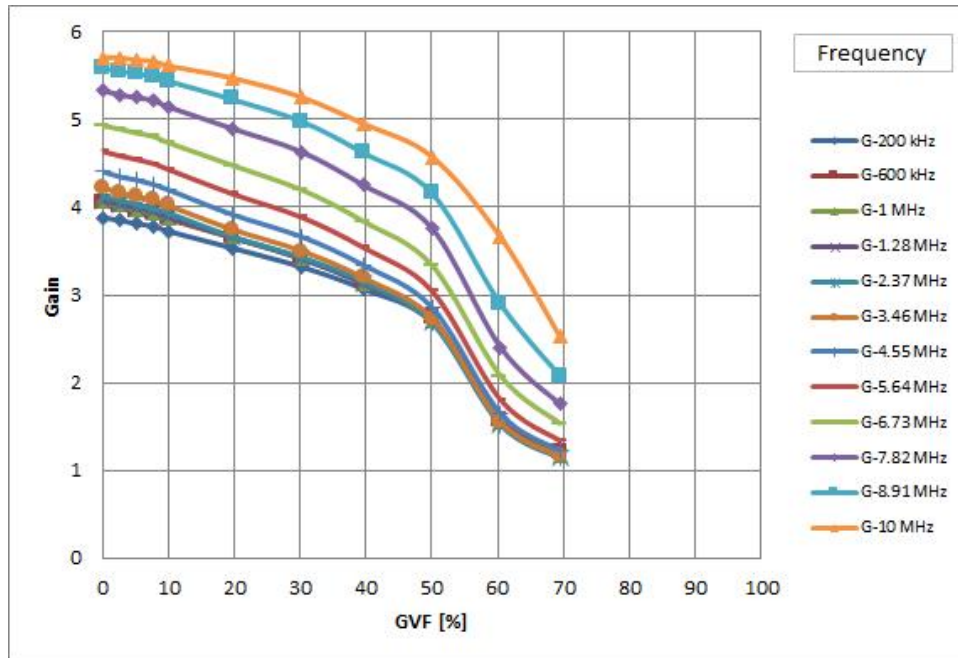


Figure A.19 Gain variation with GVF for different frequencies @60GPM & 20psi

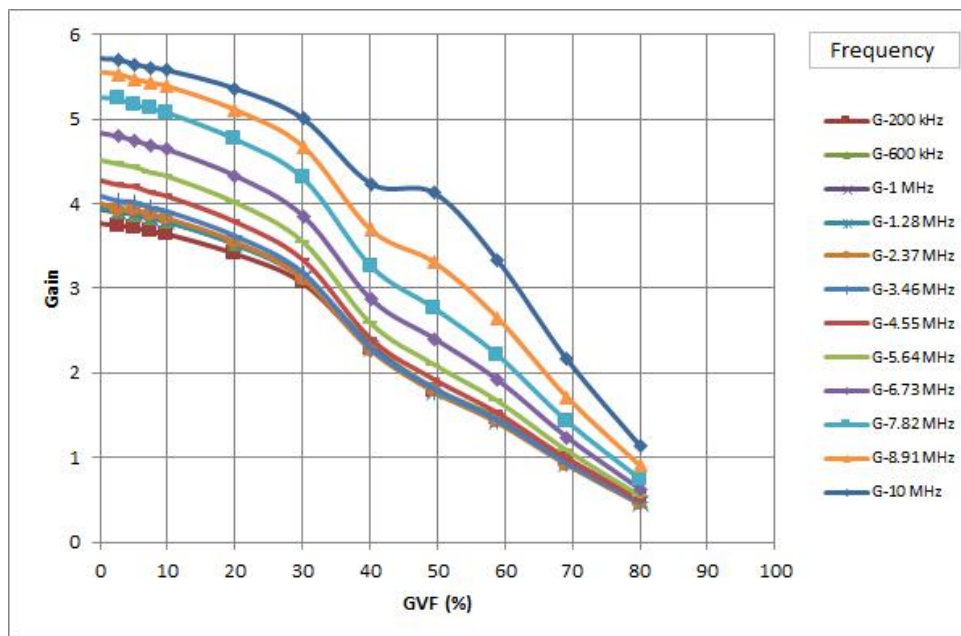


Figure A.20 Gain variation with GVF for different frequencies @60GPM & 40psi

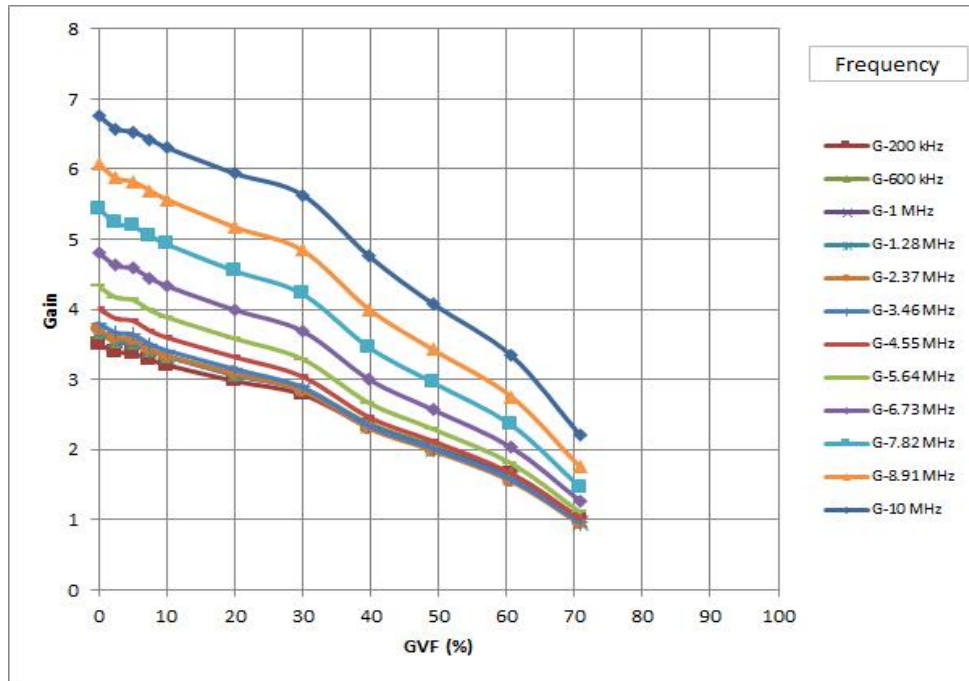


Figure A.21 Gain variation with GVF for different frequencies @60GPM & 60psi

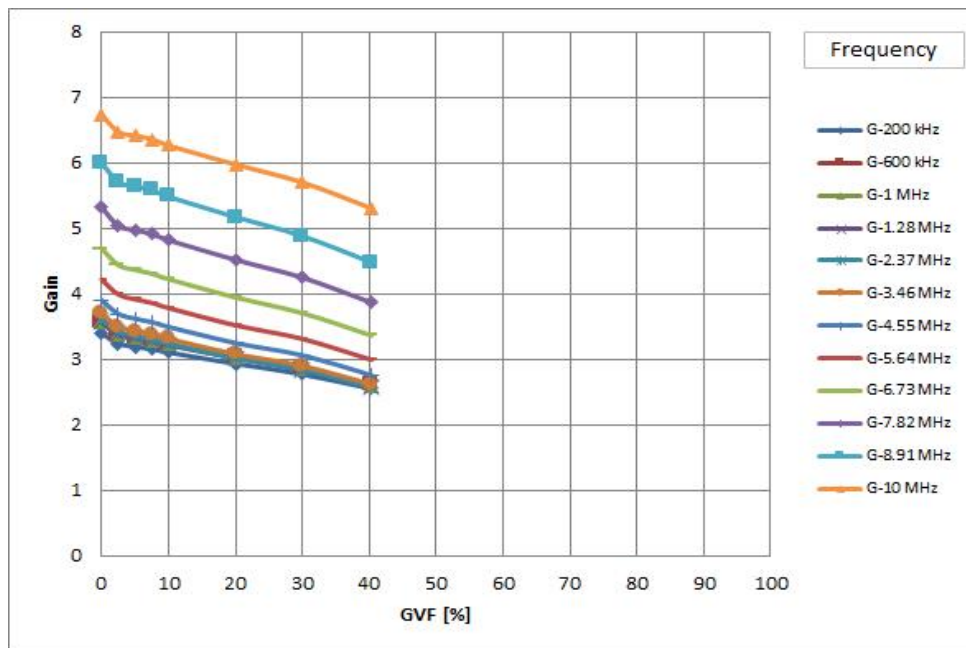


Figure A.22 Gain variation with GVF for different frequencies @70GPM & 20psi

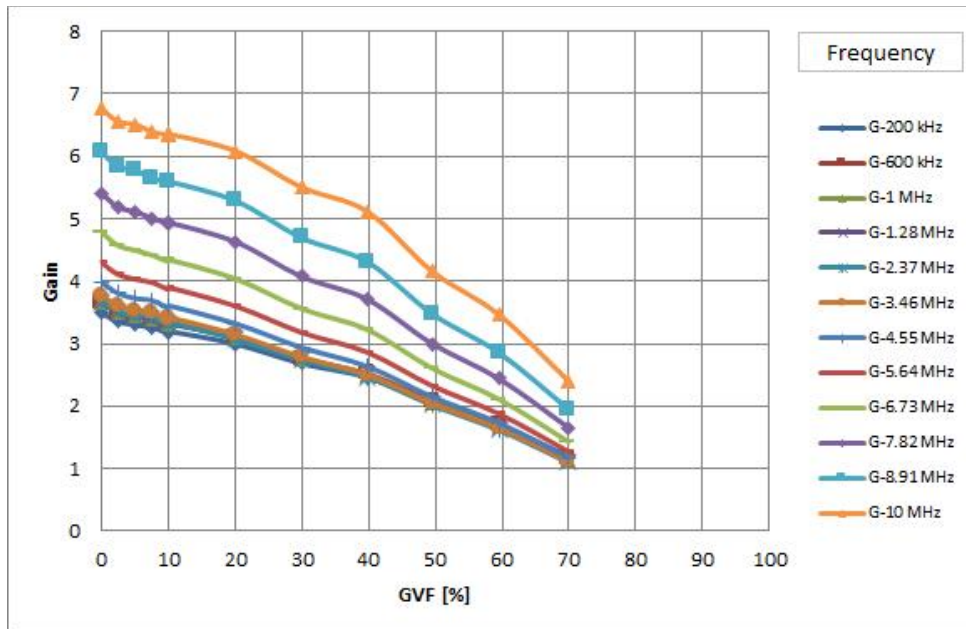


Figure A.23 Gain variation with GVF for different frequencies @70GPM & 40psi

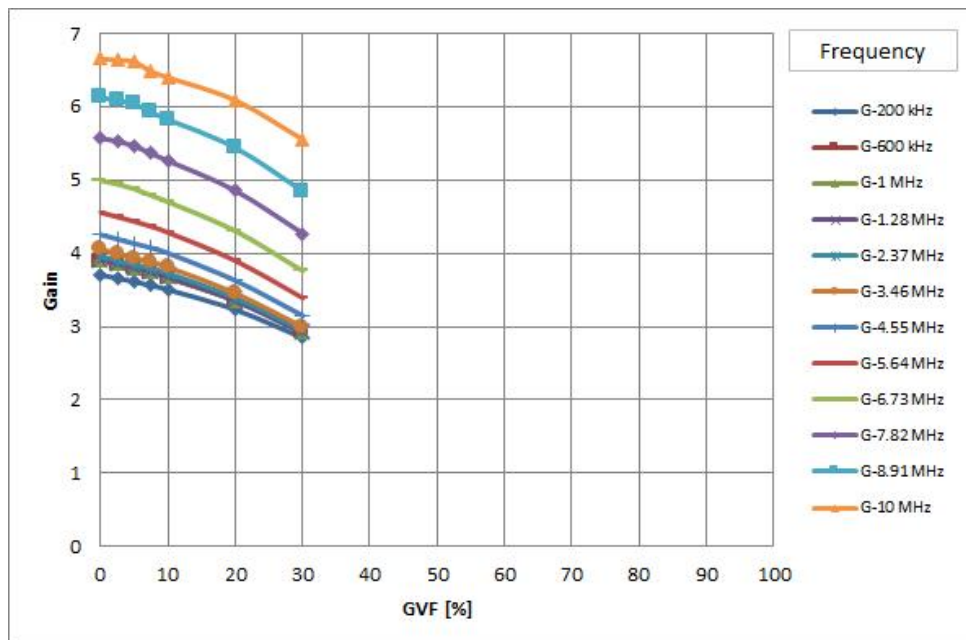


Figure A.24 Gain variation with GVF for different frequencies @70GPM & 60psi

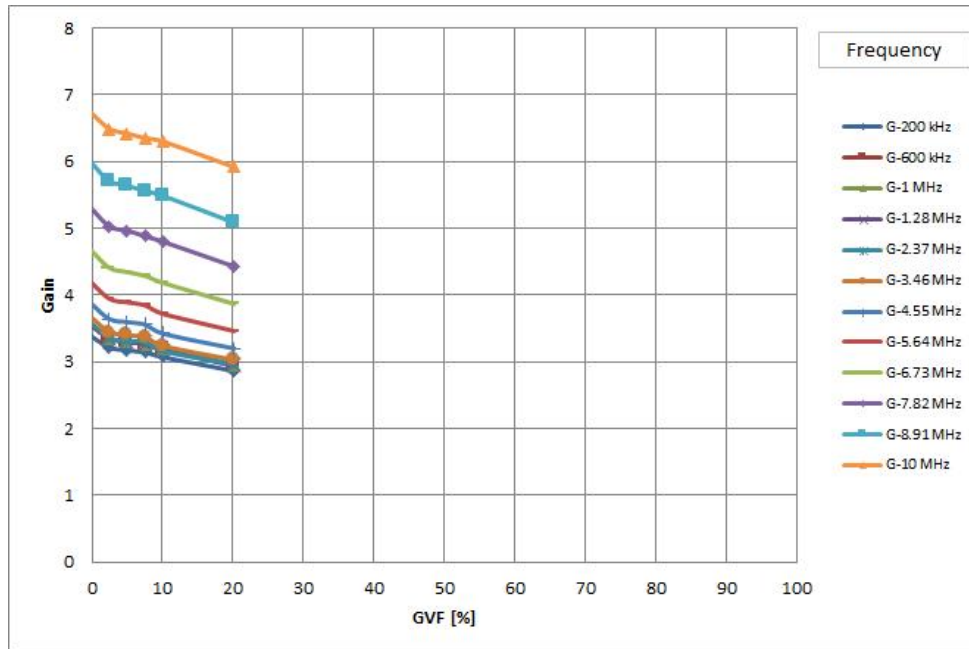


Figure A.25 Gain variation with GVF for different frequencies @80GPM & 20psi

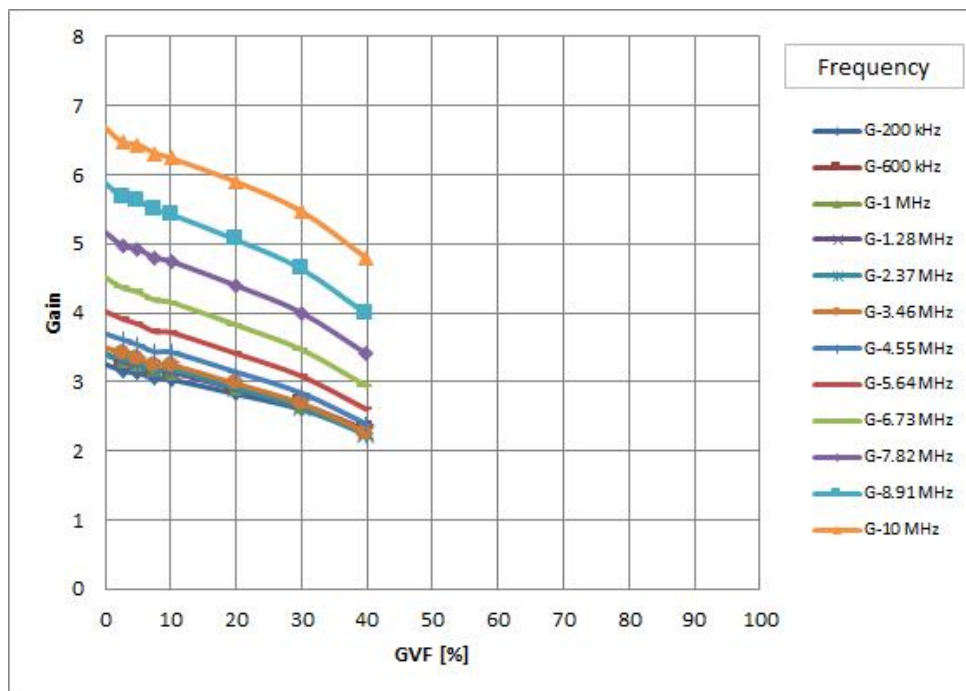


Figure A.26 Gain variation with GVF for different frequencies @80GPM & 40 psi

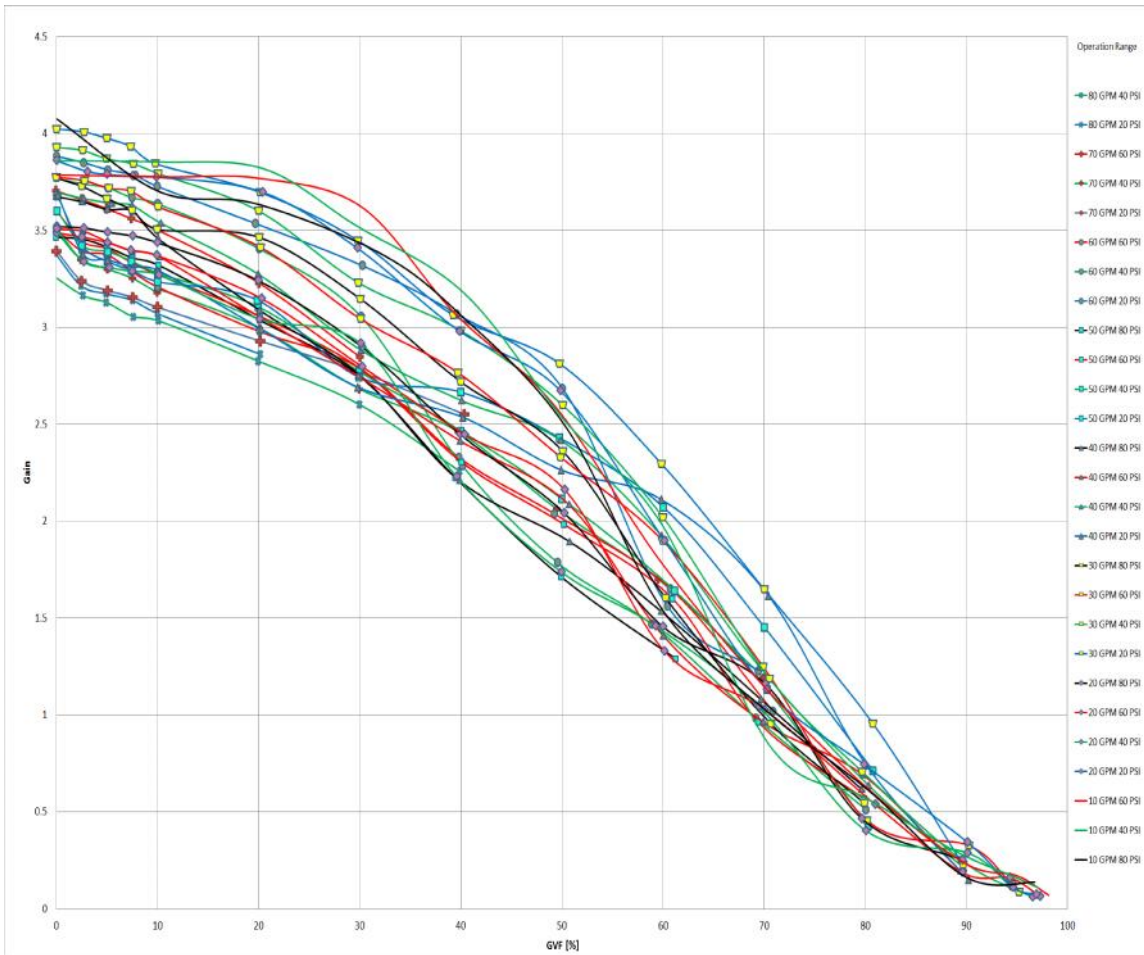


Figure A.27 Gain vs GVF for different operation range @ Freq. 200 kHz

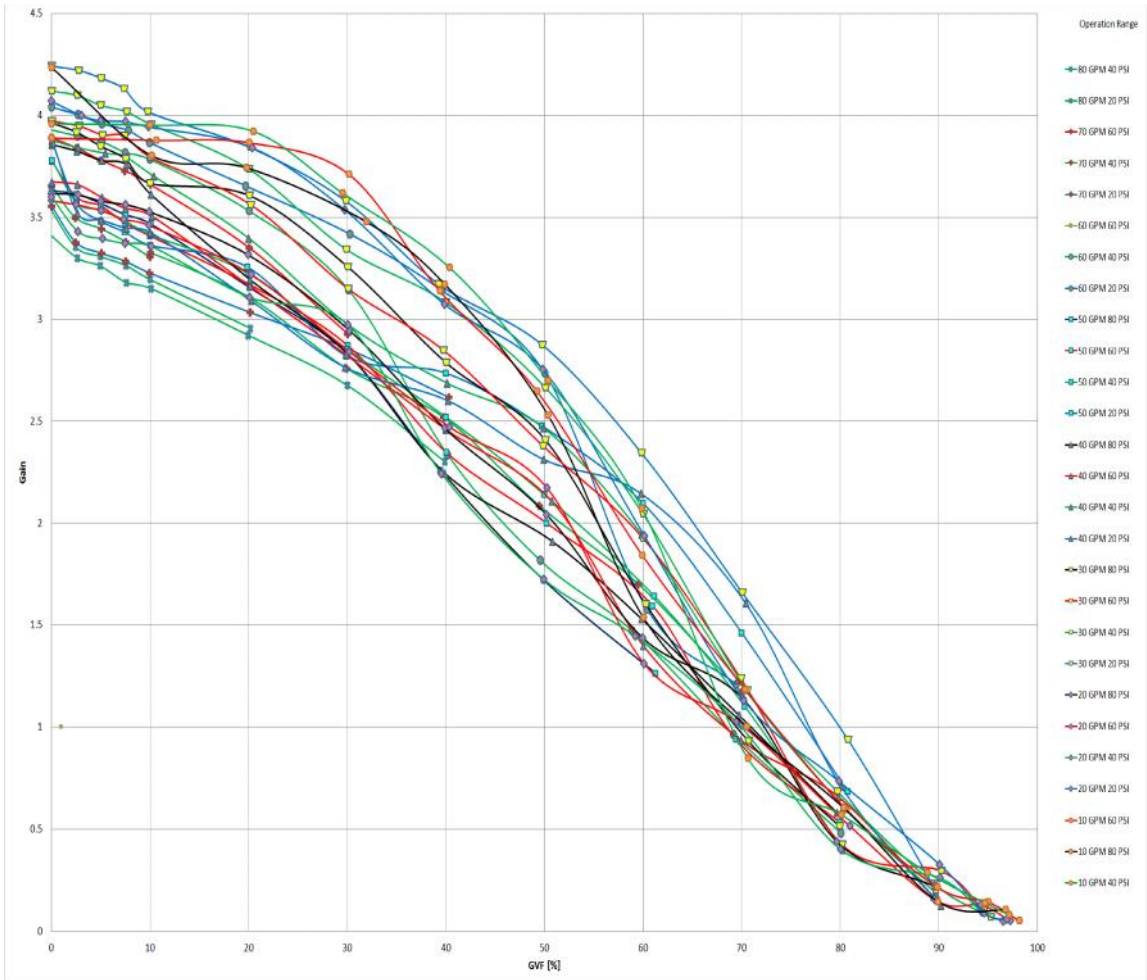


Figure A.28 Gain vs GVF for different operation range @ Freq. 600 kHz

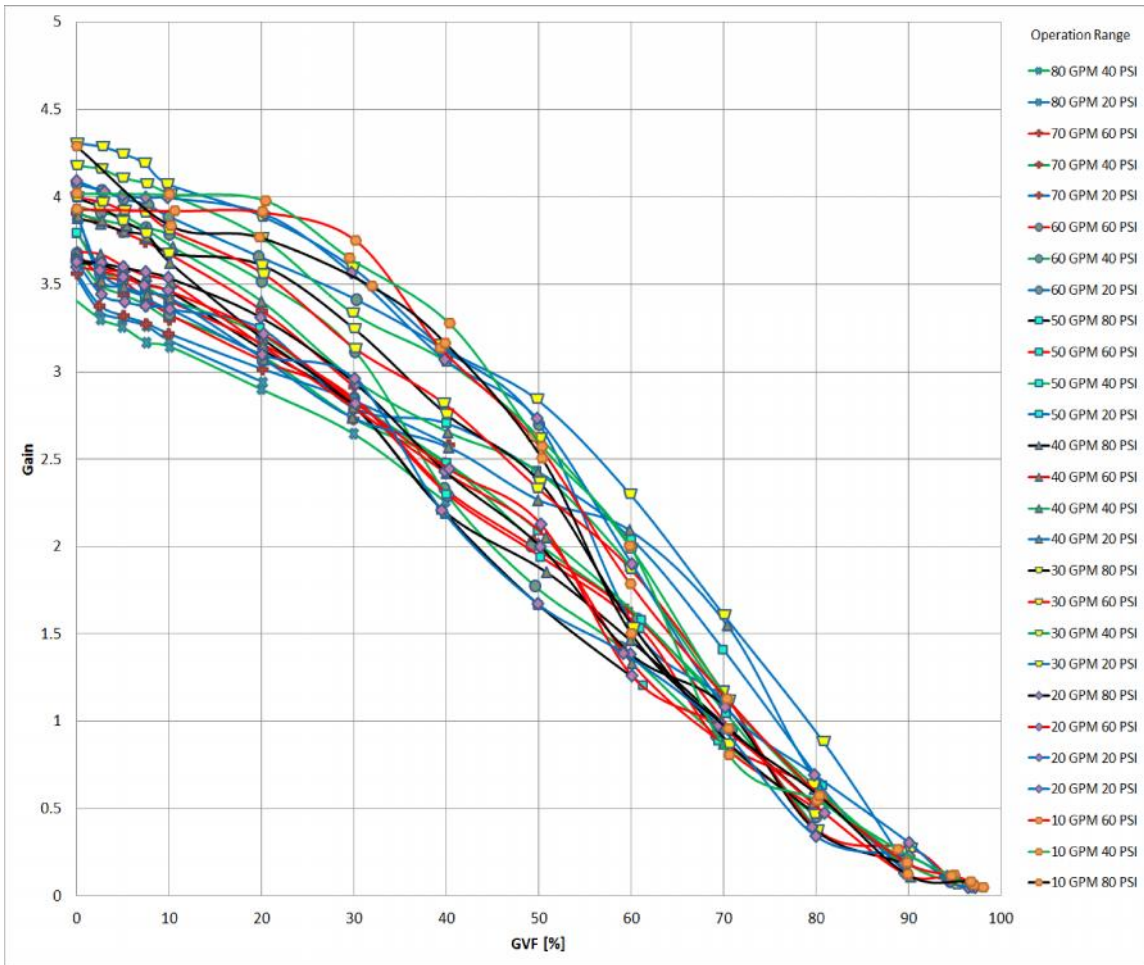


Figure A.29 Gain vs GVF for different operation range @ Freq. 1.28 MHz

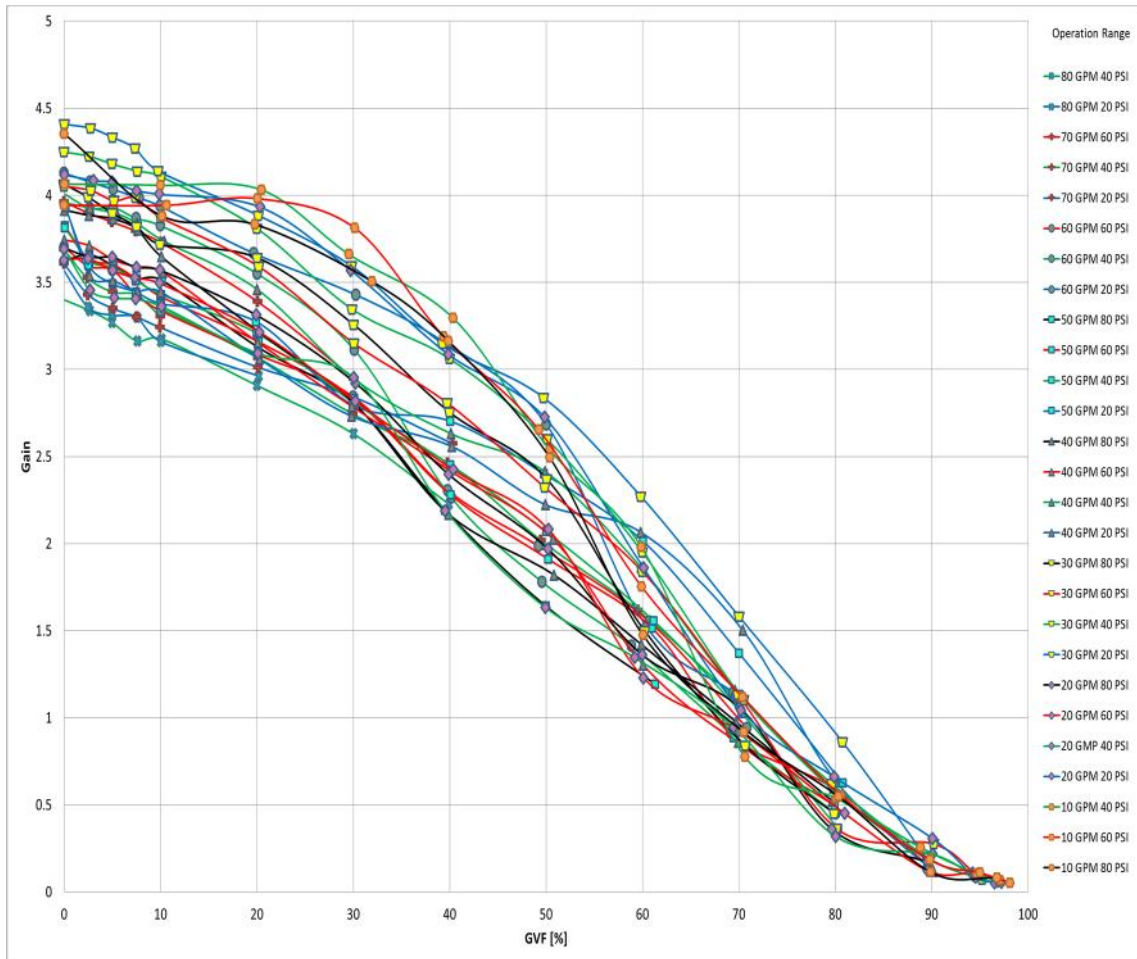


Figure A.30 Gain vs GVF for different operation range @ Freq. 2.37MHz

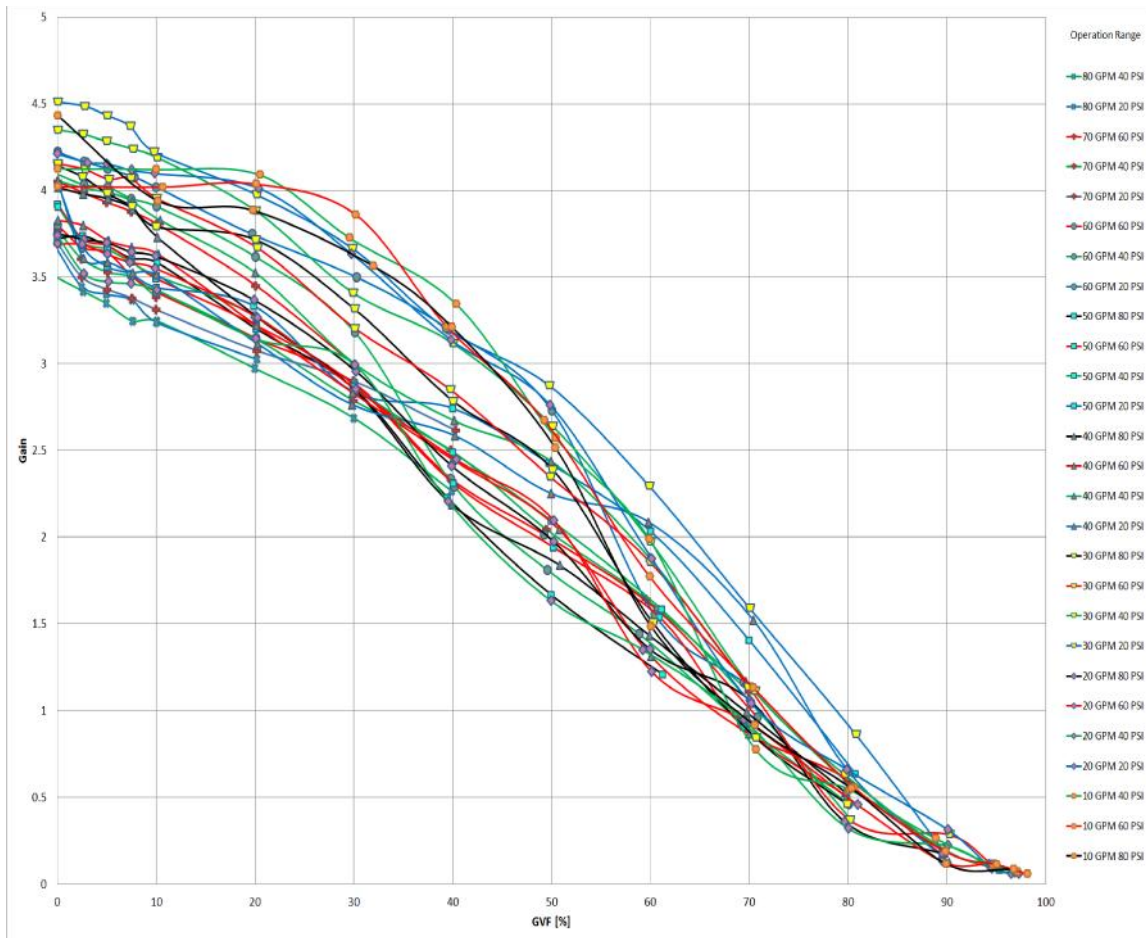


Figure A.31 Gain vs GVF for different operation range @ Freq. 3.46 MHz

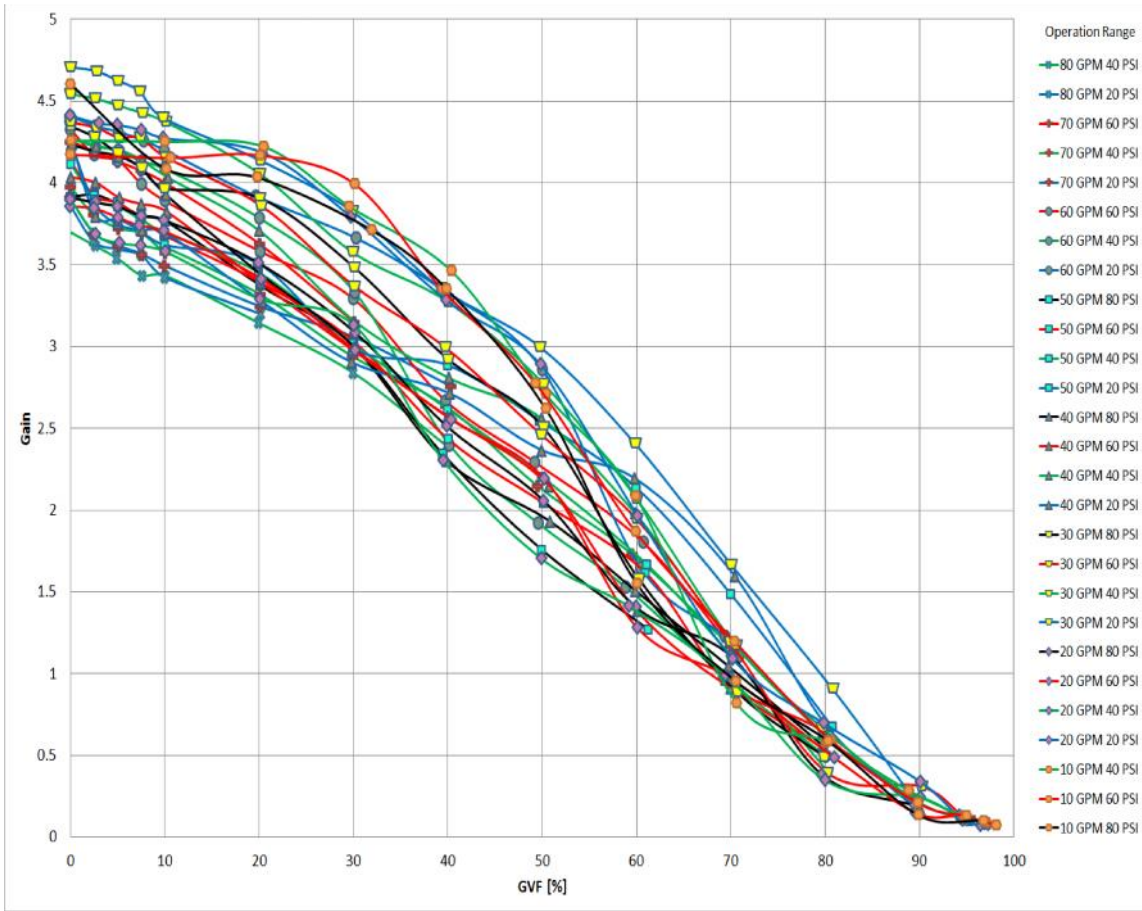


Figure A.32 Gain vs GVF for different operation range @ Freq. 4.55 MHz

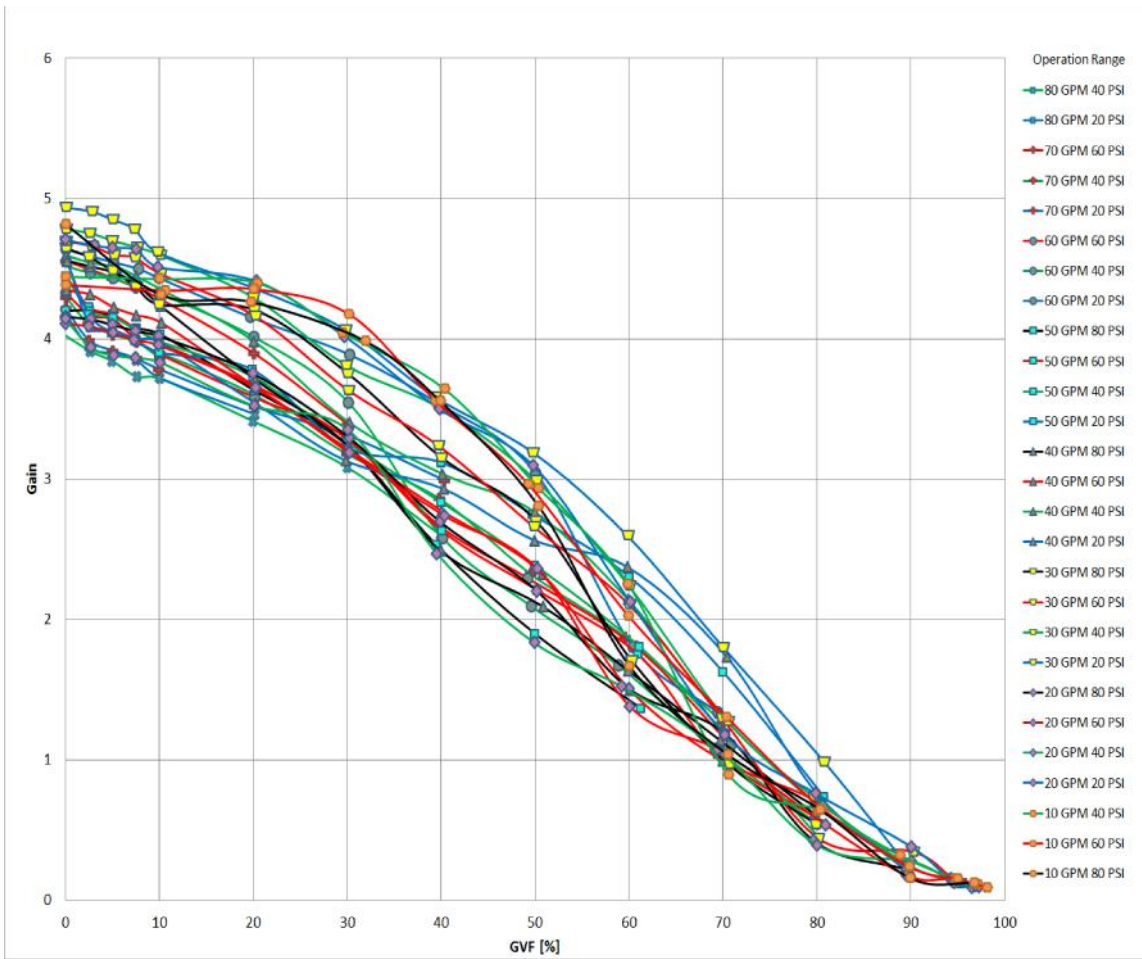


Figure A.33 Gain vs GVF for different operation range @ Freq. 5.64 MHz

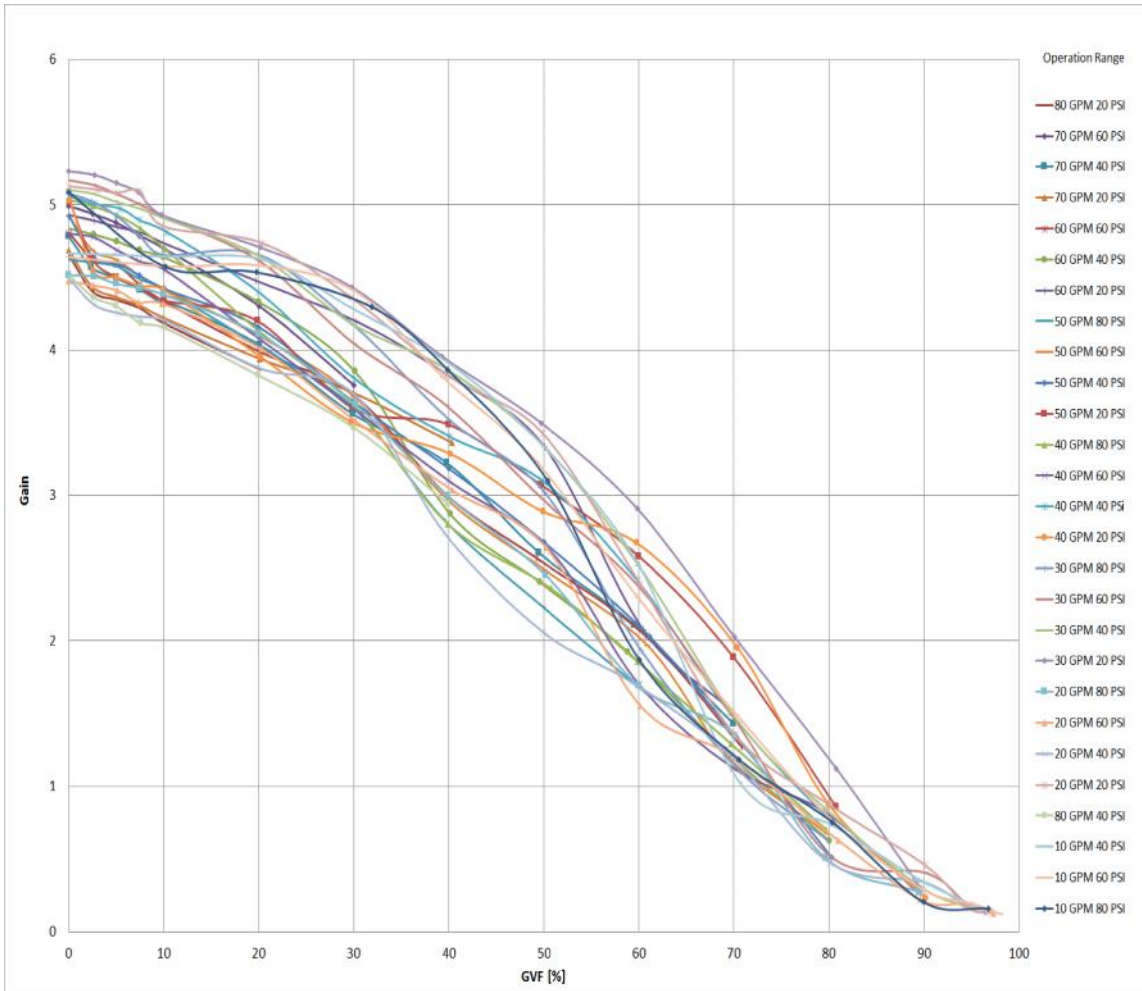


Figure A.34 Gain vs GVF for different operation range @ Freq. 6.73 MHz

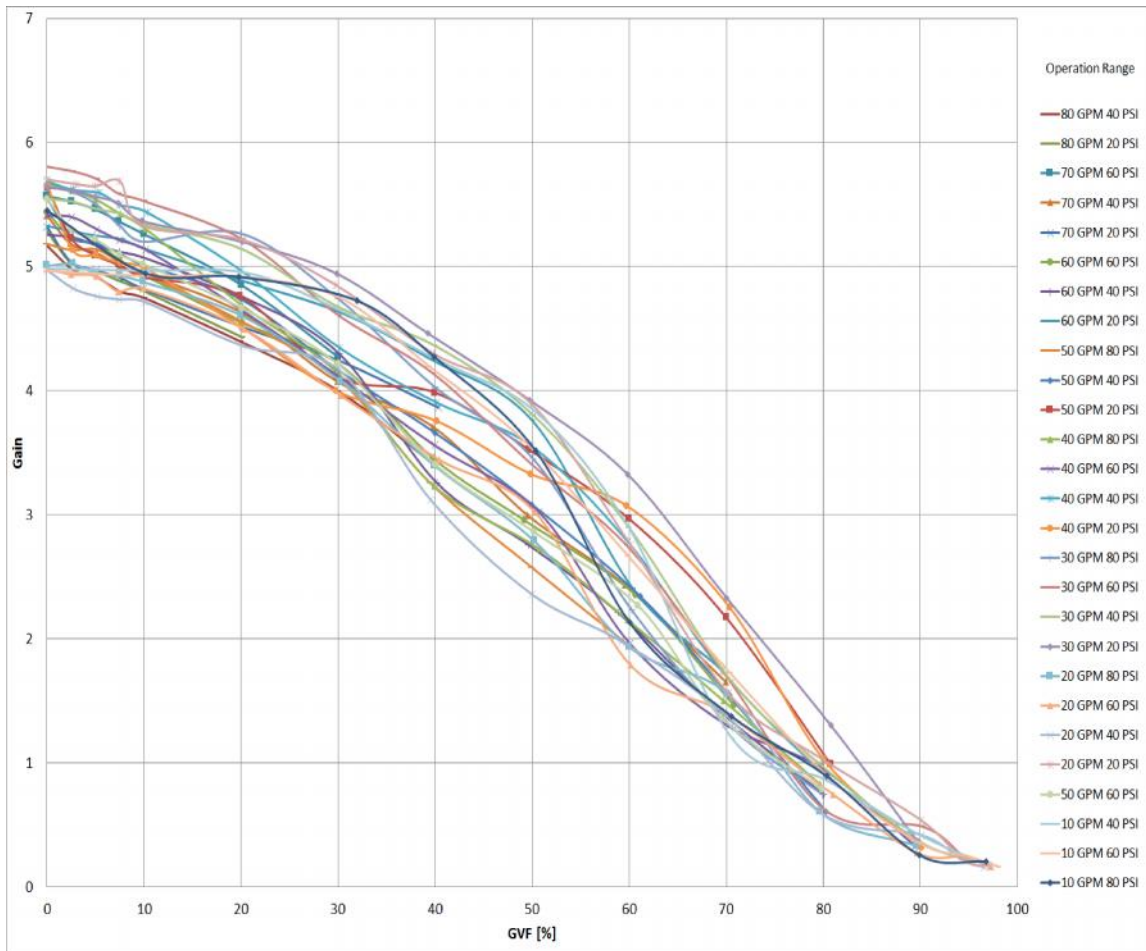


Figure A.35 Gain vs GVF for different operation range @ Freq. 7.81 MHz

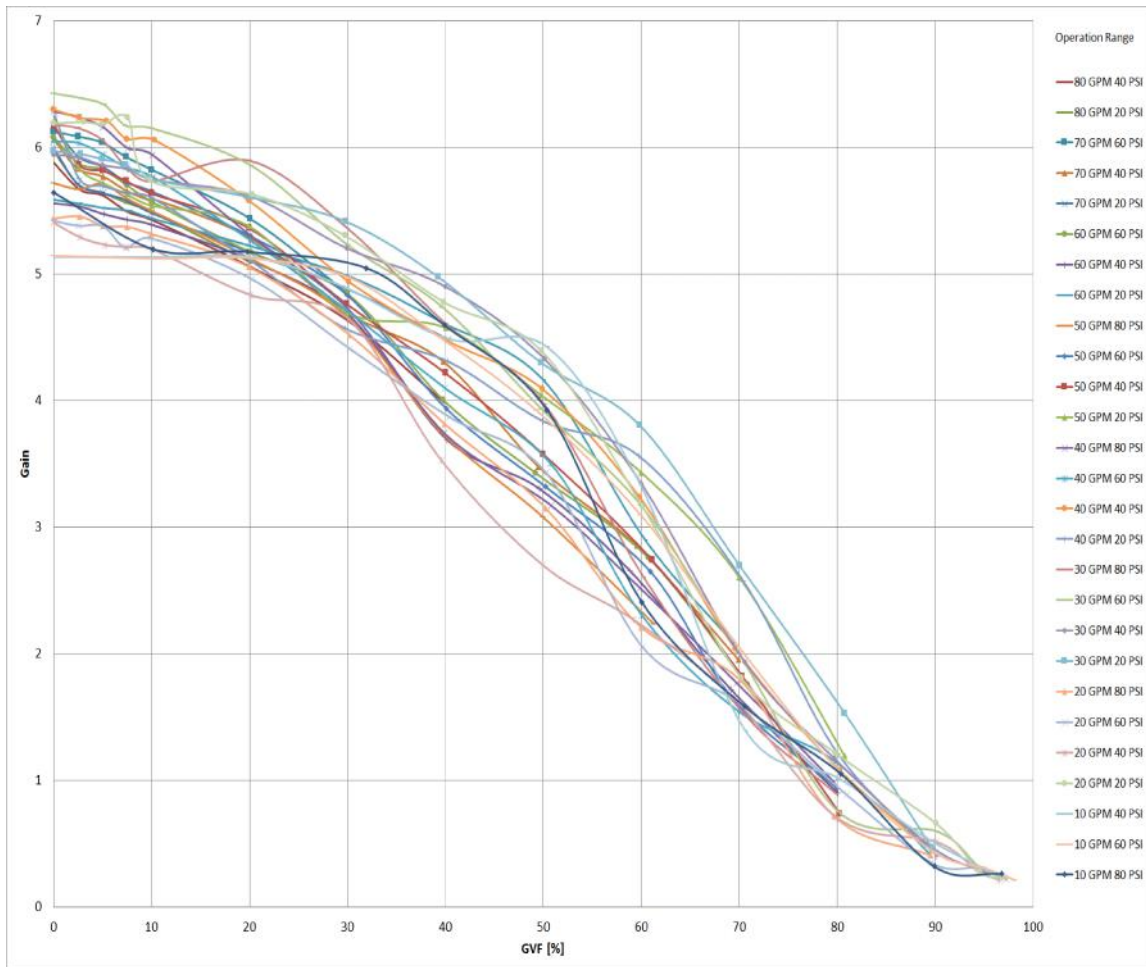


Figure A.36 Gain vs GVF for different operation range @ Freq. 8.91 MHz

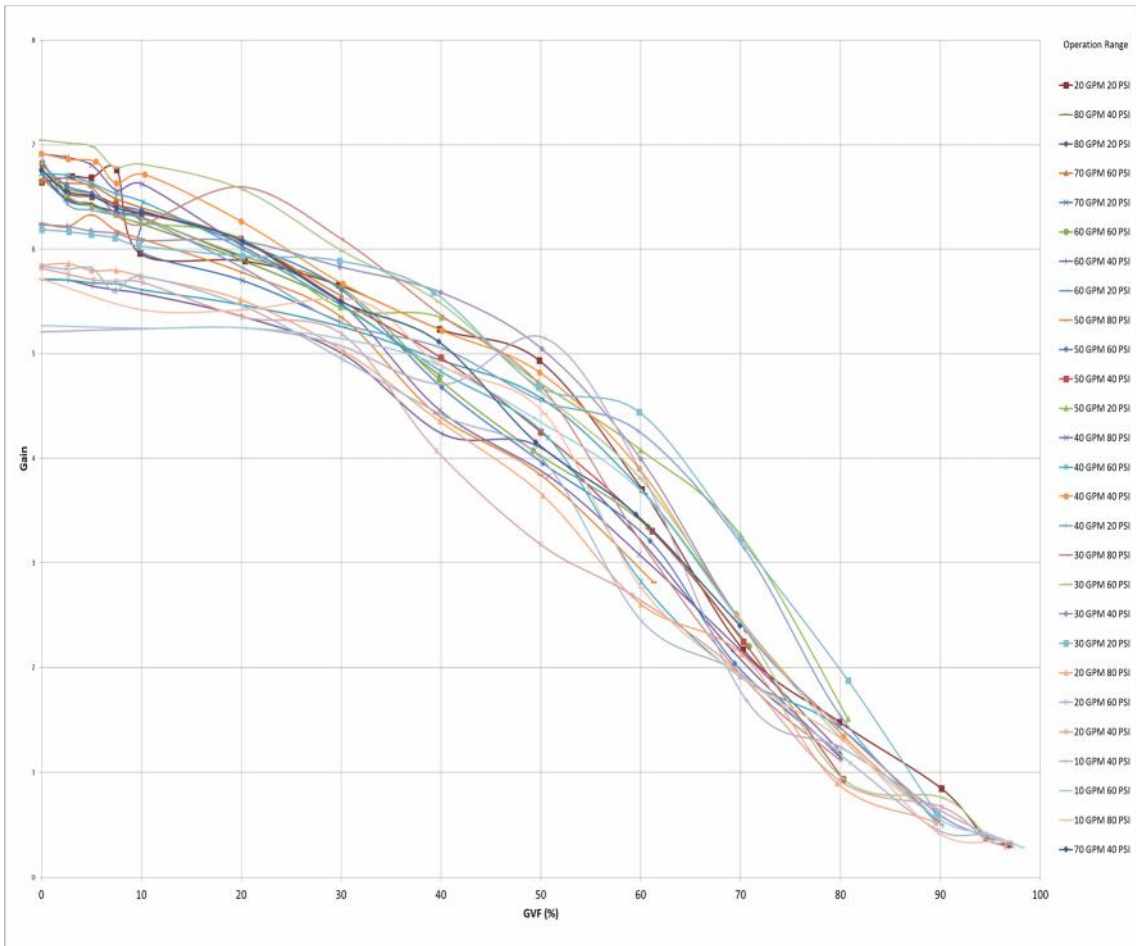


Figure A.37 Gain vs GVF for different operation range @ Freq. 10 MHz

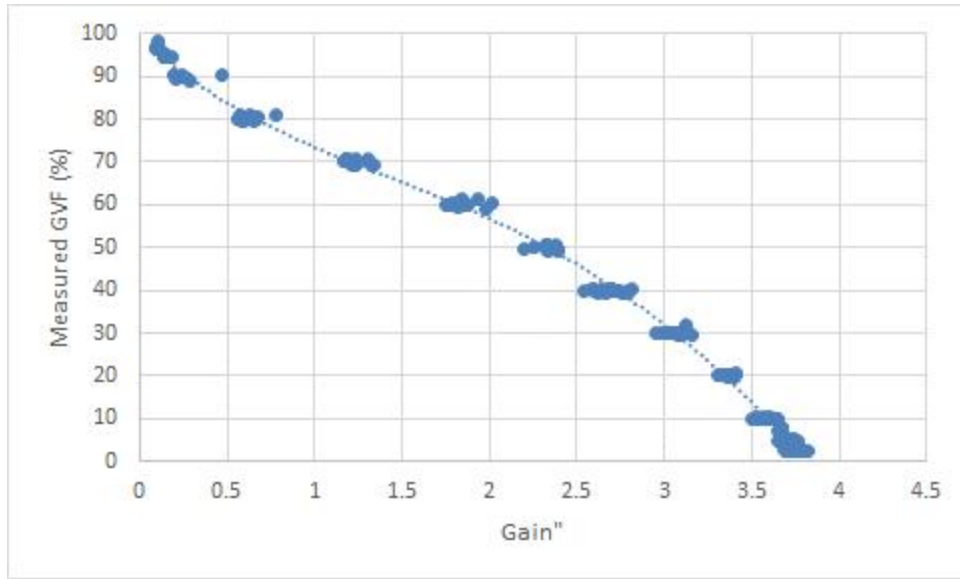


Figure A.38 Measured GVF vs Gain'' @ 200 kHz

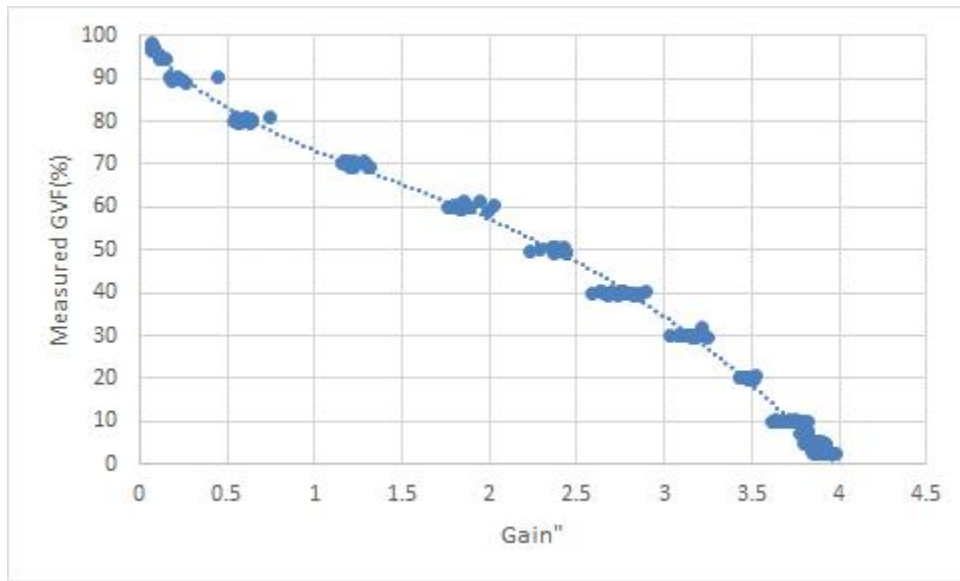


Figure A.39 Measured GVF vs Gain'' @ 600 kHz

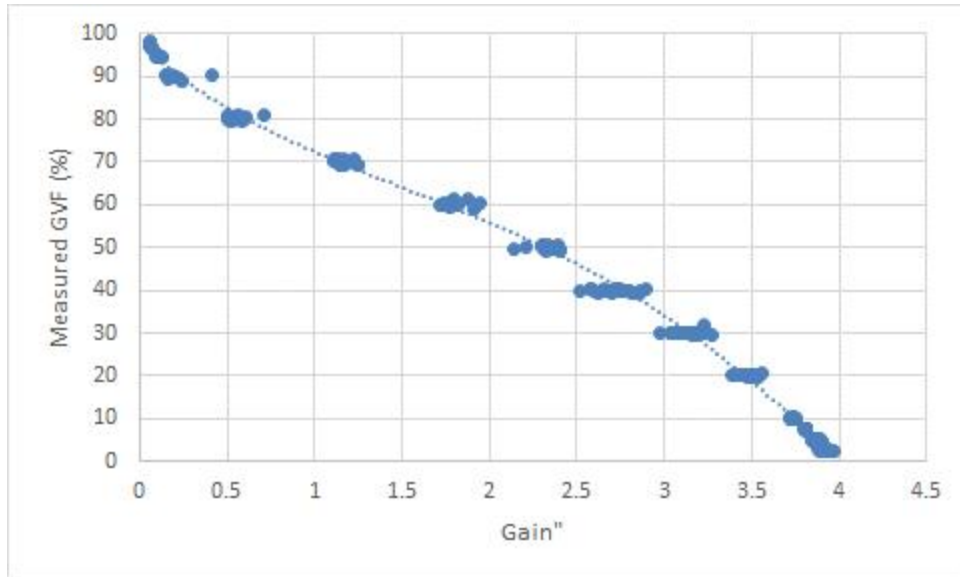


Figure A.40 Measured GVF vs Gain'' @ 1.28 MHz

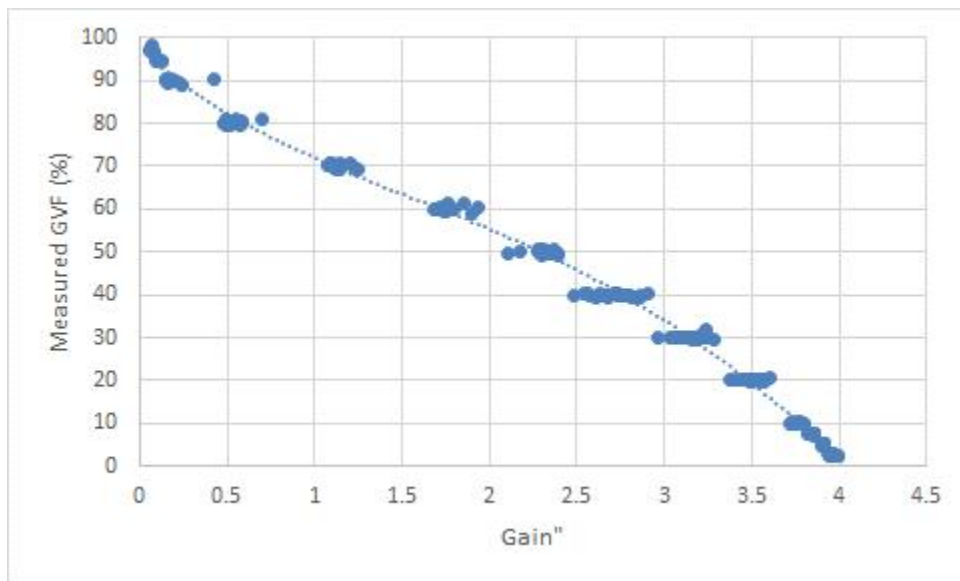


Figure A.41 Measured GVF vs Gain'' @ 2.37 MHz

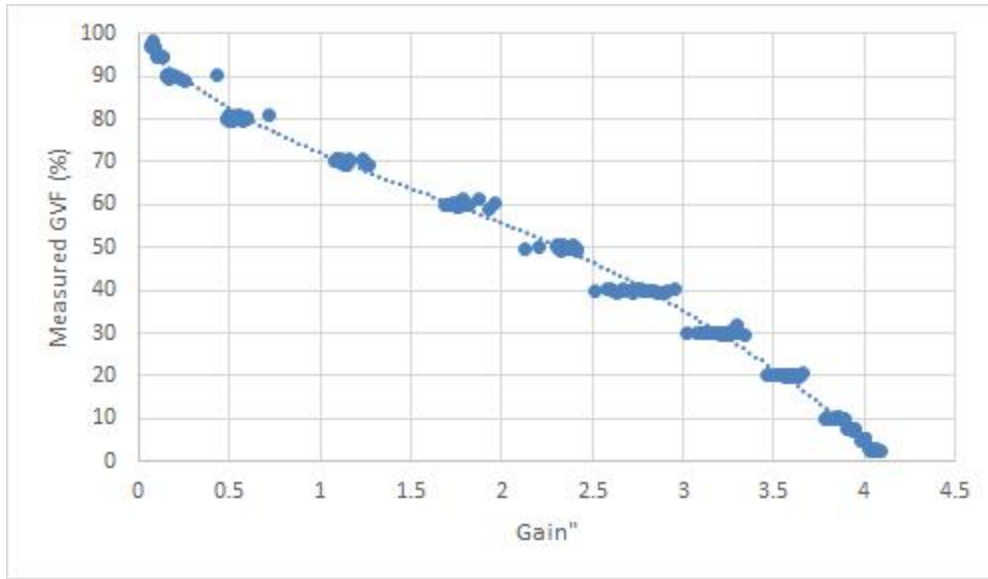


Figure A.42 Measured GVF vs Gain'' @ 3.46 MHz

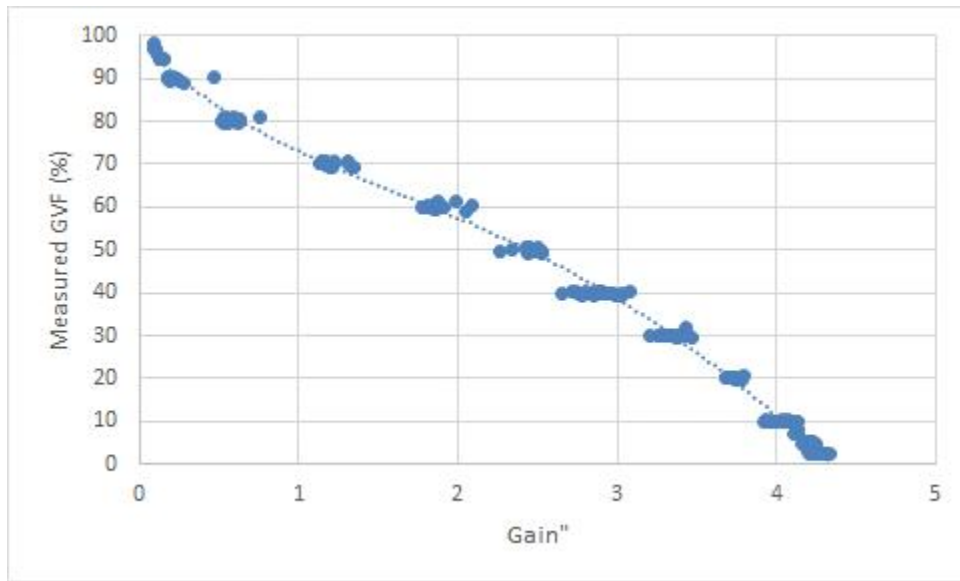


Figure A.43 Measured GVF vs Gain'' @ 4.55 MHz

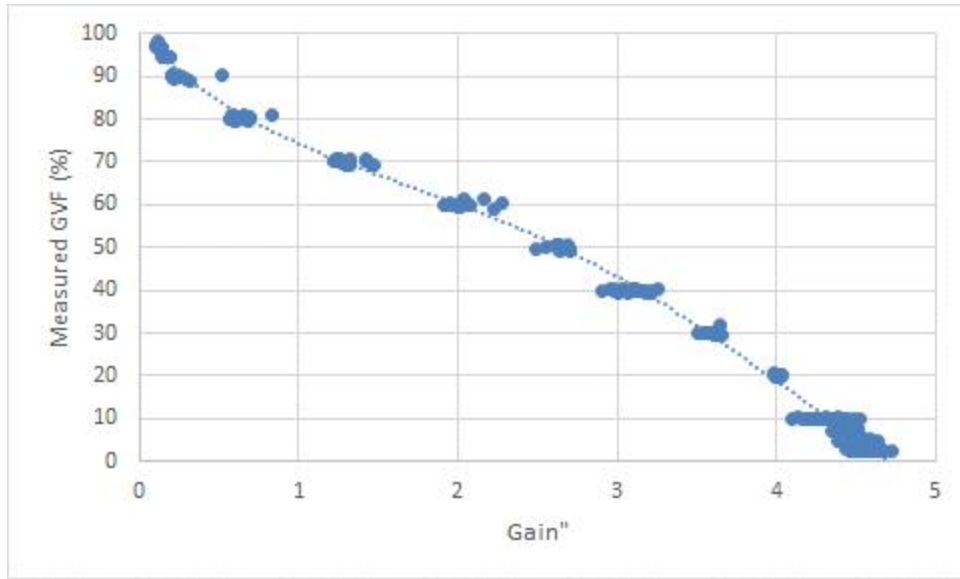


Figure A.44 Measured GVF vs Gain'' @ 5.64 MHz

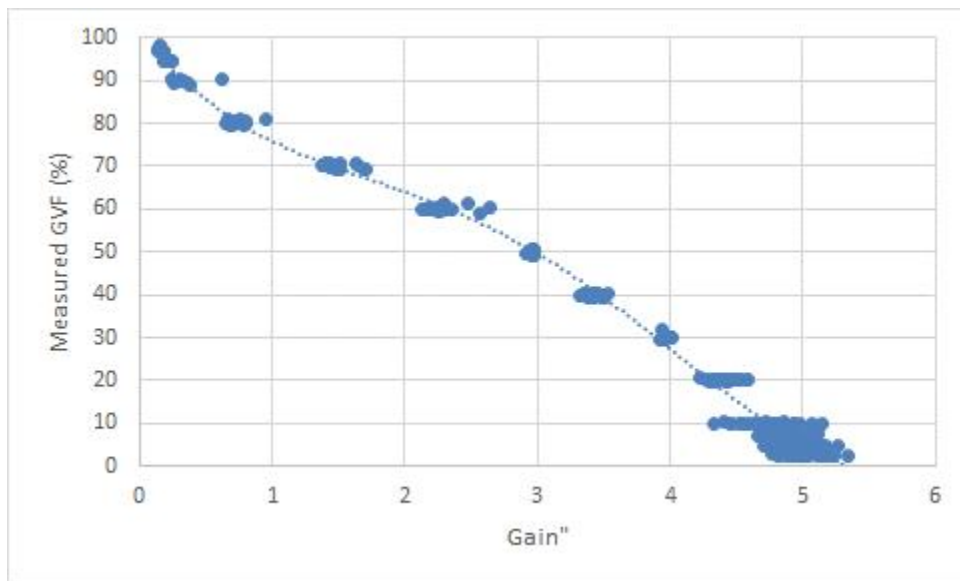


Figure A.45 Measured GVF vs Gain'' @ 6.73 MHz

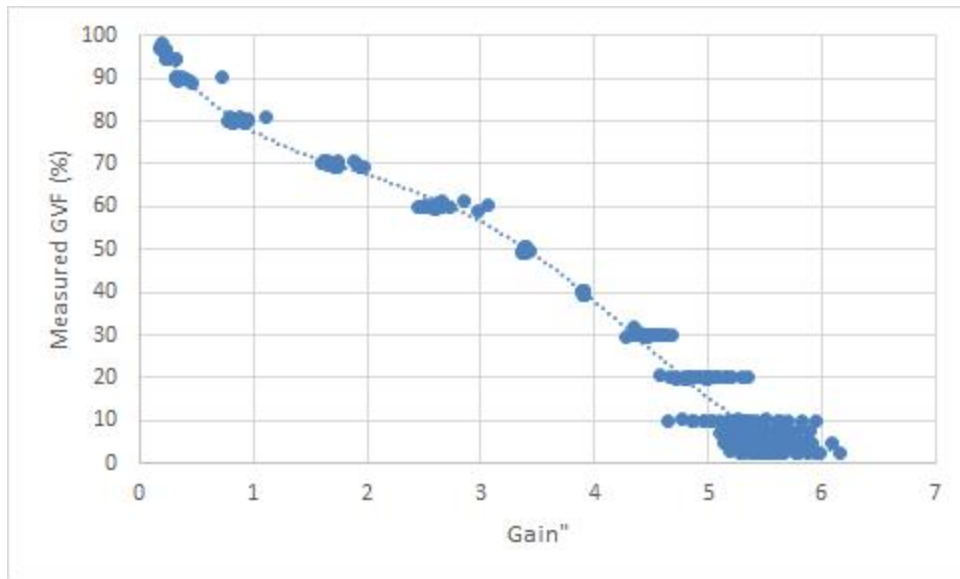


Figure A.46 Measured GVF vs Gain'' @ 7.82 MHz

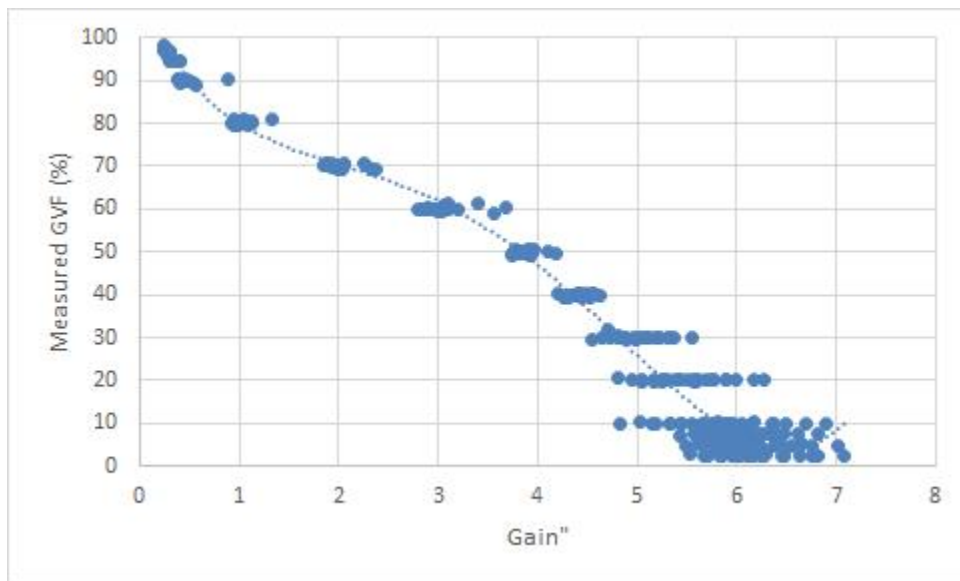


Figure A.47 Measured GVF vs Gain'' @ 8.91 MHz

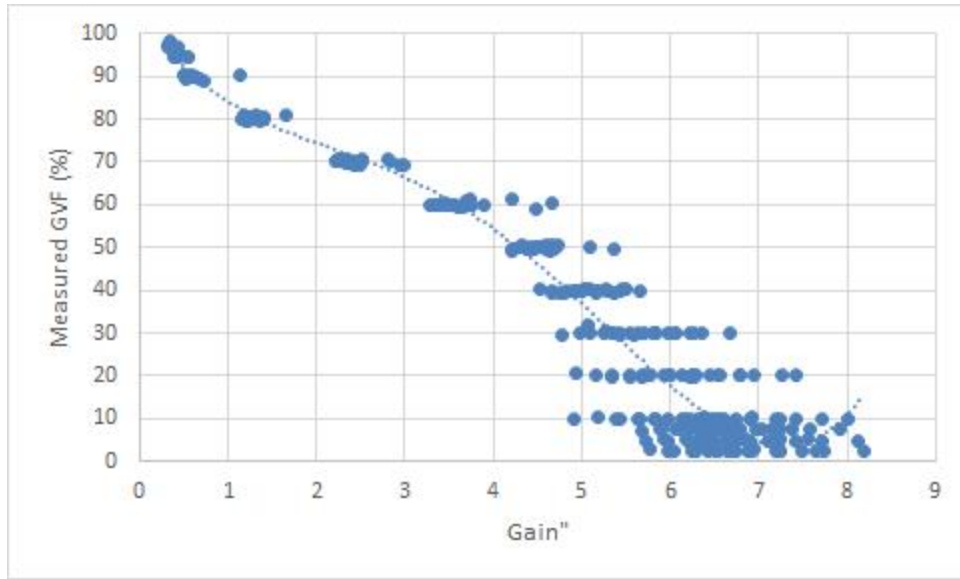
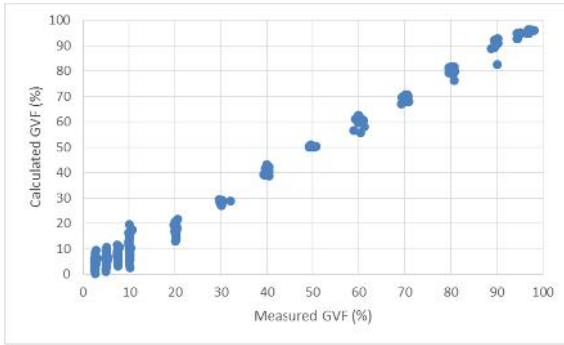
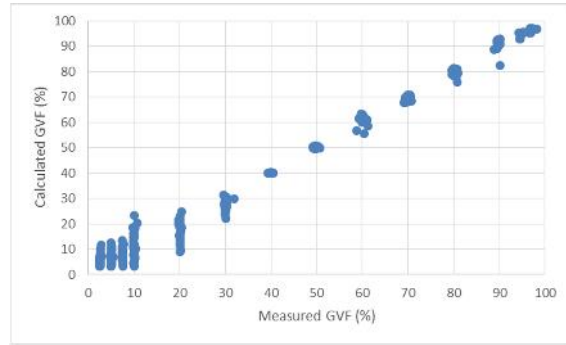


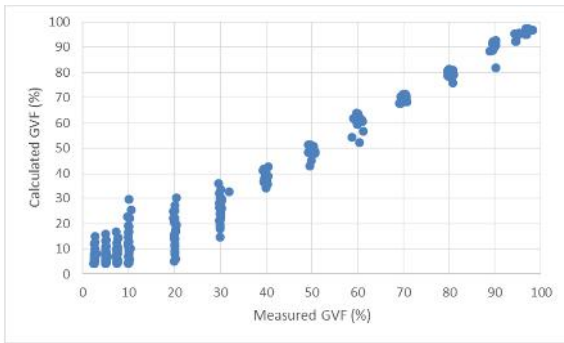
Figure A.48 Measured GVF vs Gain'' @ 10 MHz



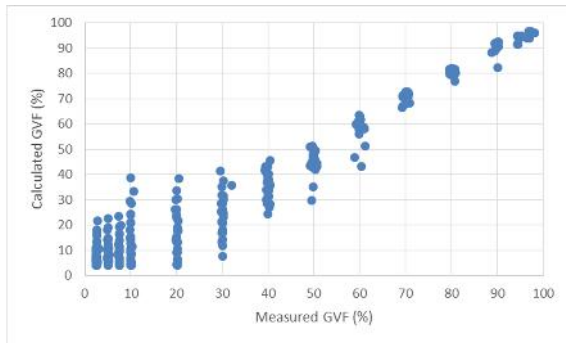
(a) 6.73 MHz



(b) 7.82 MHz

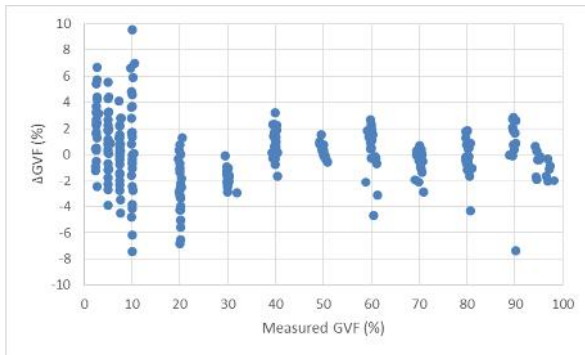


(c) 8.91 MHz

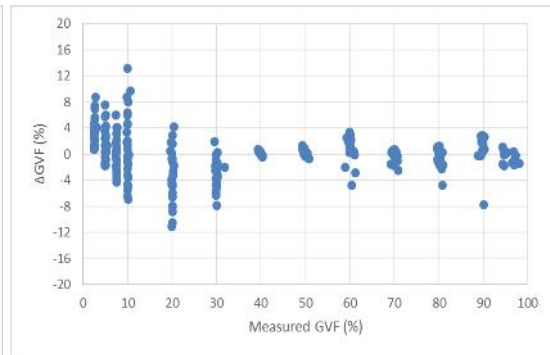


(d) 10 MHz

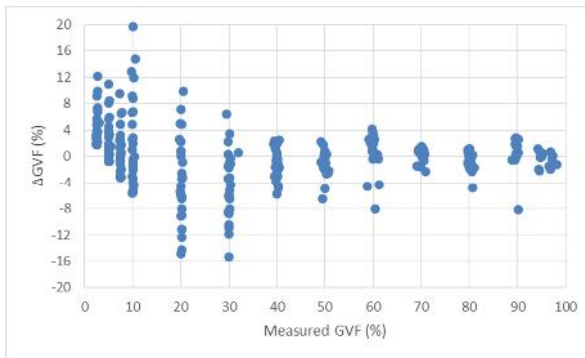
Figure A.49 Calculated GVF as the function of Measured GVF for high frequencies



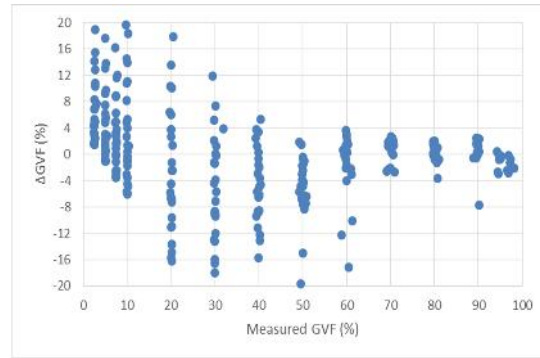
(a) 6.73 MHz



(b) 7.82 MHz



(c) 8.91 MHz



(d) 10 MHz

Figure A.50 The differences of the calculated GVF and measured GVF as the function of measured GVF at high frequencies

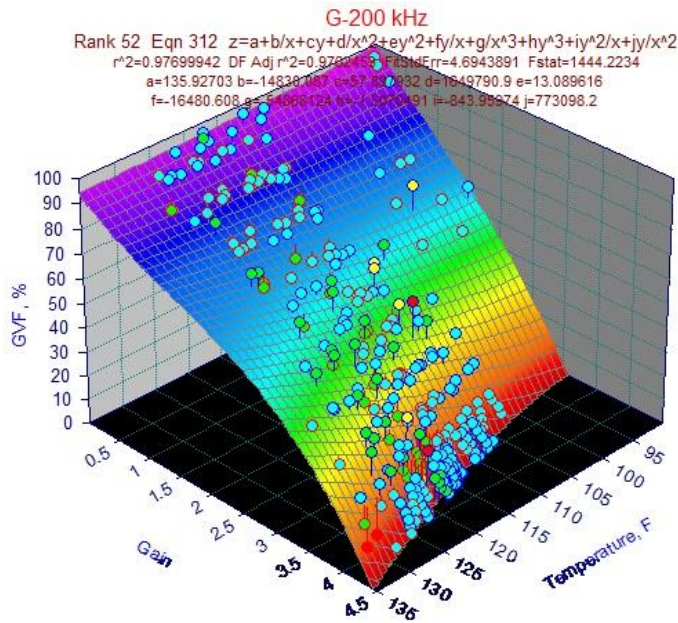


Figure A.51 Surface curve GVF @ 200 kHz

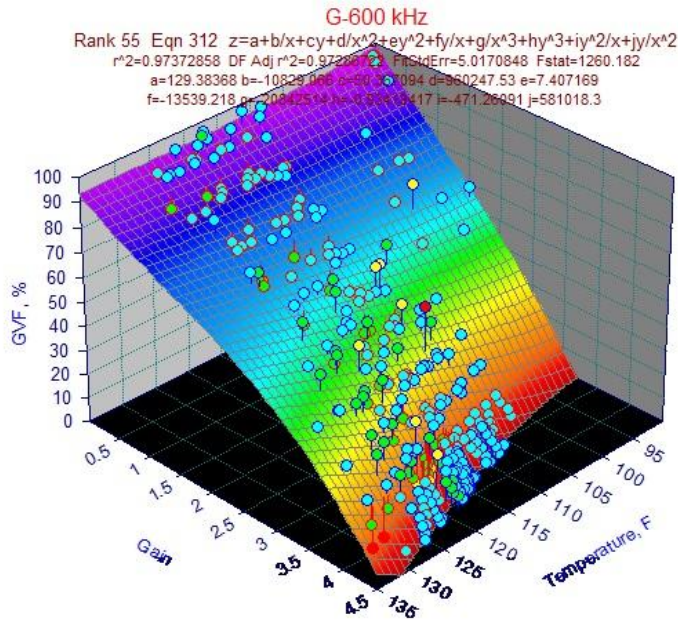


Figure A.52 Surface curve GVF @ 600 kHz

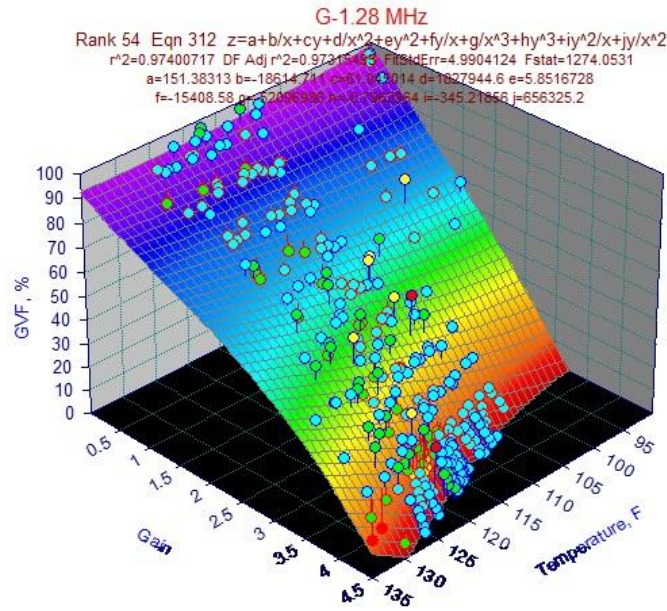


Figure A.53 Surface curve GVF @ 1.28 MHz

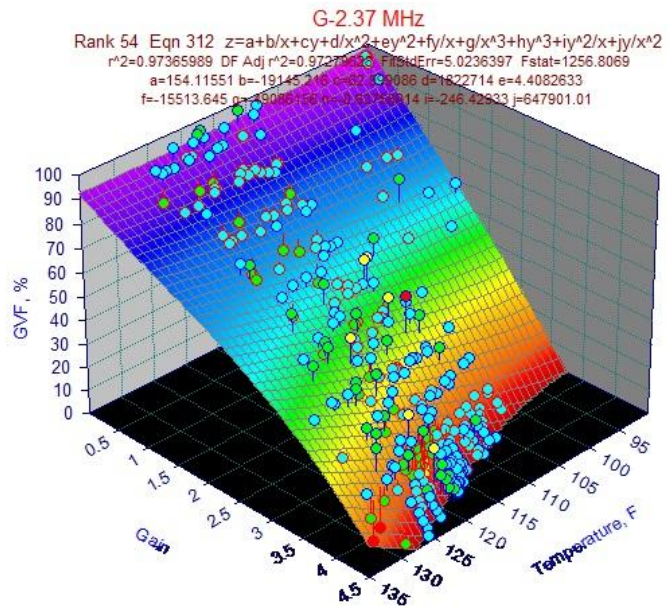


Figure A.54 Surface curve GVF @ 2.37 MHz

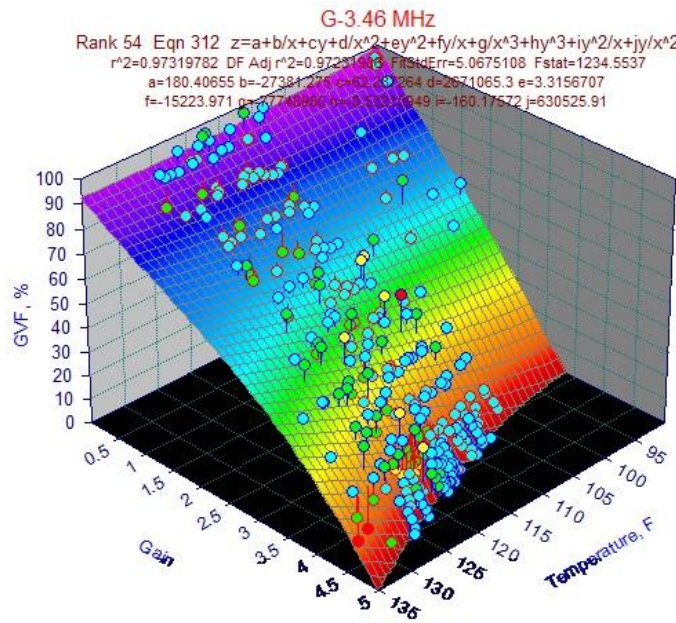


Figure A.55 Surface curve GVF @ 3.46 MHz

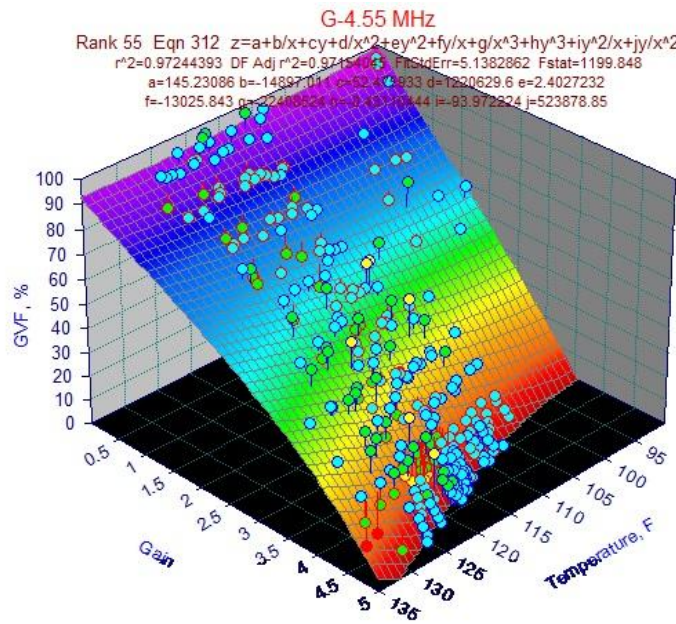


Figure A.56 Surface curve GVF @ 4.55 MHz

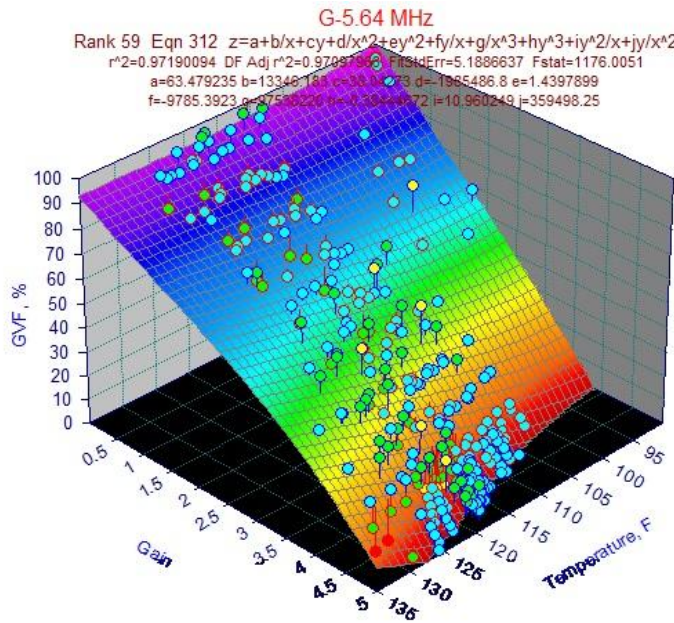


Figure A.57 Surface curve GVF @ 5.64 MHz

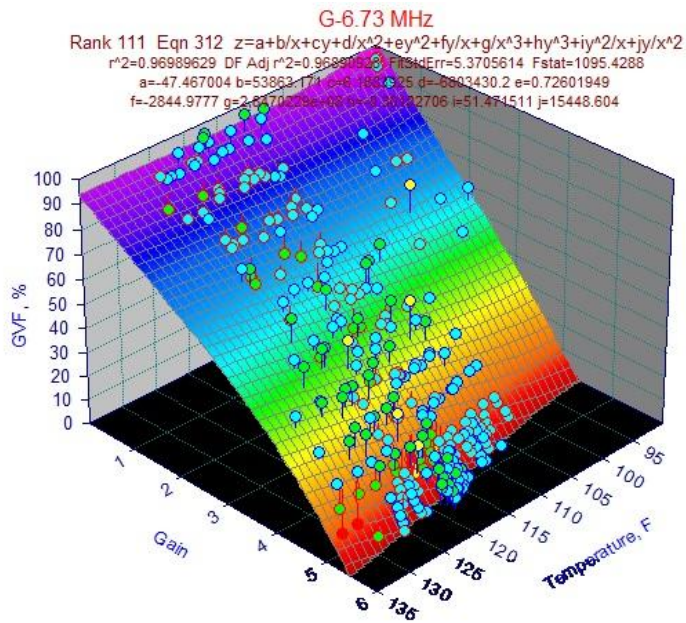


Figure A.58 Surface curve GVF @ 6.73 MHz

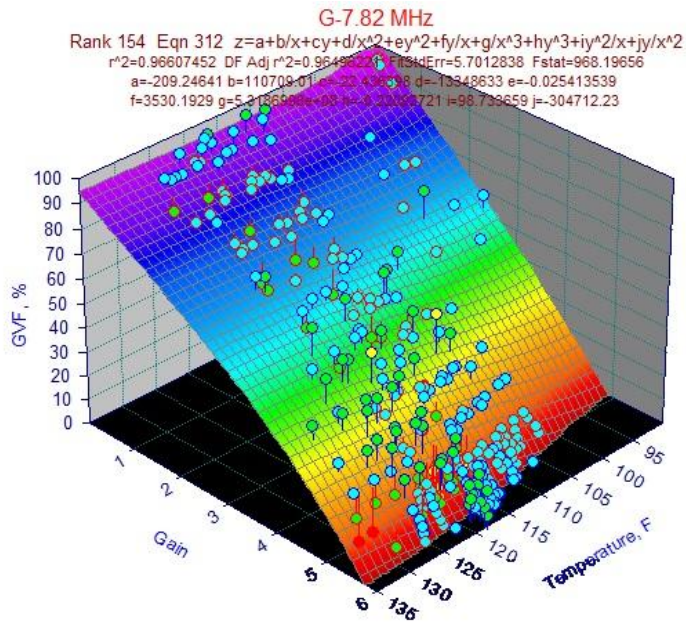


Figure A.59 Surface curve GVF @ 7.82 MHz

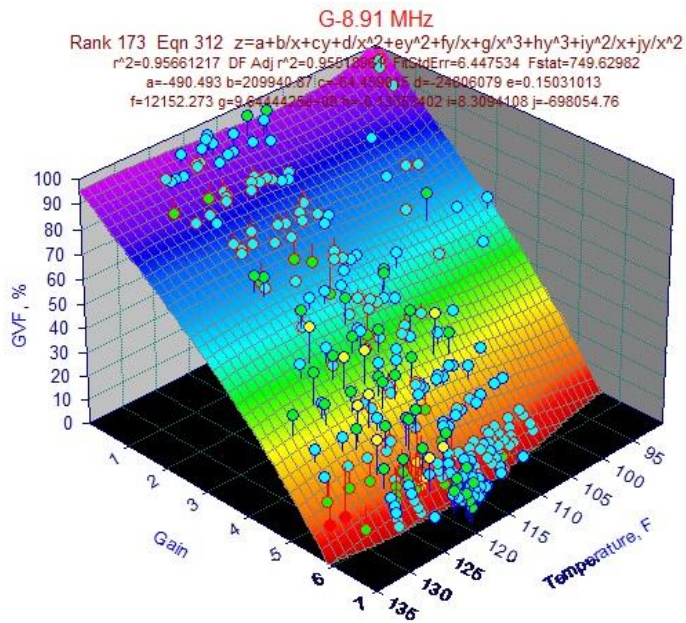


Figure A.60 Surface curve GVF @ 8.91 MHz

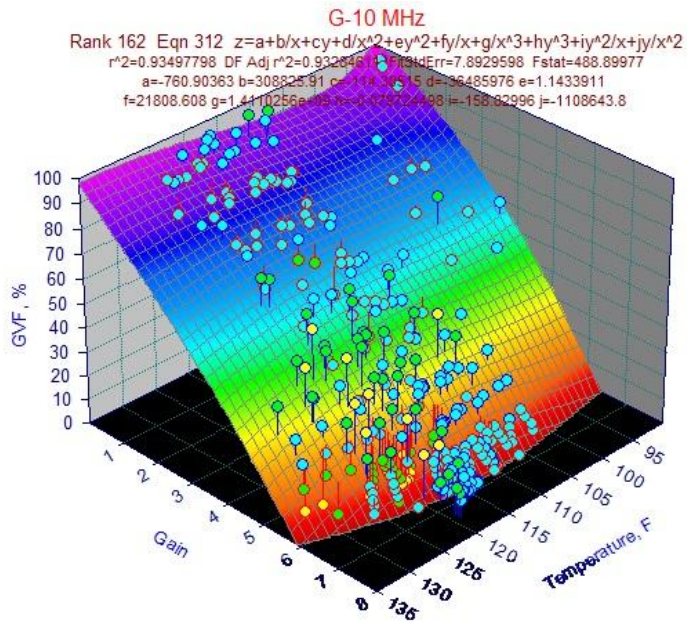


Figure A.61 Surface curve GVF @ 10 MHz

APPENDIX B

TABLES

GVF	Linear Equation			
	y = Gain'		x = Mixture Temperature	
	200 kHz	600 kHz	1MHz	1.28 MHz
2.5%	y = 0.0344483x - 0.3903790	y = 0.0361989x - 0.4346127	y = 0.0371644x - 0.5373462	y = 0.0385847x - 0.6916115
5.0%	y = 0.0349954x - 0.4943328	y = 0.0366581x - 0.5348175	y = 0.0376648x - 0.6436697	y = 0.0392711x - 0.8200229
7.5%	y = 0.0369294x - 0.7615550	y = 0.0389194x - 0.8441601	y = 0.0399190x - 0.9547646	y = 0.0413949x - 1.1186215
10.0%	y = 0.0334906x - 0.4286952	y = 0.0333036x - 0.2735398	y = 0.0335012x - 0.2954764	y = 0.0392395x - 0.9384200
20.0%	y = 0.0402819x - 1.4135107	y = 0.0409550x - 1.3799904	y = 0.0414241x - 1.4395658	y = 0.0436931x - 1.6973313
30.0%	y = 0.0406283x - 1.7512047	y = 0.0418101x - 1.8026064	y = 0.0423107x - 1.8737800	y = 0.0447562x - 2.1576112
40.0%	y = 0.0389598x - 1.9196494	y = 0.0409069x - 2.0857611	y = 0.0415326x - 2.1794396	y = 0.0430412x - 2.3632565
50.0%	y = 0.0299412x - 1.2006524	y = 0.0305557x - 1.2306200	y = 0.0308517x - 1.2917974	y = 0.0317076x - 1.4100567
60.0%	y = 0.0128798x + 0.2499353	y = 0.0131708x + 0.2297171	y = 0.0132532x + 0.1871218	y = 0.0133371x + 0.1558857
70.0%	y = 0.0083359x + 0.2014025	y = 0.0085496x + 0.1677338	y = 0.0084202x + 0.1489764	y = 0.0082823x + 0.1448787
80.0%	y = 0.0001625x + 0.6242607	y = 0.0000039x + 0.5822306	y = -0.0001423x + 0.5720773	y = -0.0006301x + 0.6140767
90.0%	y = -0.0035037x + 0.6502091	y = -0.0038120x + 0.6621042	y = -0.0039175x + 0.6580840	y = -0.0039978x + 0.6602691
95.0%	y = 0.0004710x + 0.0836515	y = 0.0004501x + 0.0613424	y = 0.0003713x + 0.0587519	y = 0.0003424x + 0.0582832
97.5%	y = 0.0012000x - 0.0403824	y = 0.0008453x - 0.0241301	y = 0.0005856x - 0.0039448	y = 0.0004883x + 0.0045028
GVF	2.37 MHz	3.46 MHz	4.55 MHz	5.64 MHz
2.5%	y = 0.0400053x - 0.8130864	y = 0.0407175x - 0.8105305	y = 0.0401797x - 0.5556857	y = 0.0372019x + 0.0695234
5.0%	y = 0.0416491x - 1.0529568	y = 0.0421697x - 1.0305690	y = 0.0416953x - 0.7854474	y = 0.0381927x - 0.1027277
7.5%	y = 0.0429700x - 1.2652823	y = 0.0437019x - 1.2678173	y = 0.0433054x - 1.0358628	y = 0.0404175x - 0.4283524
10.0%	y = 0.0376524x - 0.7330101	y = 0.0376009x - 0.6522569	y = 0.0358553x - 0.2733212	y = 0.0315259x + 0.4915606
20.0%	y = 0.0456437x - 1.9028994	y = 0.0457302x - 1.8468542	y = 0.0446498x - 1.5554398	y = 0.0416339x - 0.9535685
30.0%	y = 0.0453319x - 2.2214351	y = 0.0460668x - 2.2543452	y = 0.0457371x - 2.0664763	y = 0.0442161x - 1.6552719
40.0%	y = 0.0448067x - 2.5773994	y = 0.0454292x - 2.6139983	y = 0.0460744x - 2.5602109	y = 0.0460082x - 2.3447544
50.0%	y = 0.0321180x - 1.4769602	y = 0.0322547x - 1.4672069	y = 0.0326719x - 1.4063154	y = 0.0334757x - 1.3171480
60.0%	y = 0.0125580x + 0.2163832	y = 0.0121398x + 0.2793940	y = 0.0120806x + 0.3696859	y = 0.0123882x + 0.4774857
70.0%	y = 0.0074331x + 0.2168176	y = 0.0068159x + 0.2962252	y = 0.0067x + 0.3659	y = 0.0069x + 0.4374
80.0%	y = -0.0013222x + 0.6780734	y = -0.0014729x + 0.7024746	y = -0.0015486x + 0.7448510	y = -0.0015323x + 0.8001024
90.0%	y = -0.0041936x + 0.6803553	y = -0.0041721x + 0.6849920	y = -0.0043155x + 0.7218724	y = -0.0045793x + 0.7851978
95.0%	y = 0.0002748x + 0.0663576	y = 0.0002919x + 0.0716020	y = 0.0003610x + 0.0793980	y = 0.0003910x + 0.0991569
97.5%	y = 0.0002999x + 0.0281900	y = 0.0002743x + 0.0385013	y = 0.0003111x + 0.0484630	y = 0.0003796x + 0.0617747
GVF	6.73 MHz	7.82 MHz	8.91 MHz	10 MHz
2.5%	y = 0.0305487x + 1.2487747	y = 0.0215432x + 2.8355897	y = 0.0043747x + 5.3432793	y = -0.0233269x + 9.0626330
5.0%	y = 0.0310322x + 1.1330227	y = 0.0216543x + 2.7628323	y = 0.0040824x + 5.3217302	y = -0.0242521x + 9.1280819
7.5%	y = 0.0340402x + 0.7103819	y = 0.0256654x + 2.2185135	y = 0.0083746x + 4.7384656	y = -0.0202021x + 8.5703432
10.0%	y = 0.0223806x + 1.9380946	y = 0.0111729x + 3.7601140	y = -0.0094798x + 6.6616422	y = -0.0402137x + 10.7463914
20.0%	y = 0.0349523x + 0.1996218	y = 0.0264139x + 1.7067718	y = 0.0081682x + 4.3404930	y = -0.0212901x + 8.3283817
30.0%	y = 0.0395497x - 0.7529980	y = 0.0340072x + 0.3861695	y = 0.0183508x + 2.7225258	y = -0.0073053x + 6.3247223
40.0%	y = 0.0444042x - 1.8297090	y = 0.0425957x - 1.1692436	y = 0.0330689x + 0.4307122	y = 0.0150649x + 3.1573909
50.0%	y = 0.0329336x - 0.9546171	y = 0.0344308x - 0.7197509	y = 0.0296102x + 0.3006405	y = 0.0186449x + 2.1936917
60.0%	y = 0.0120647x + 0.7553320	y = 0.0133195x + 0.9375498	y = 0.0111109x + 1.5814730	y = 0.0060306x + 2.7302552
70.0%	y = 0.0069x + 0.6085	y = 0.0082445x + 0.6745859	y = 0.0069837x + 1.0908237	y = 0.0049773x + 1.7336376
80.0%	y = -0.0016299x + 0.9077084	y = -0.0012516x + 0.9938253	y = -0.0019615x + 1.2346707	y = -0.0021934x + 1.5117946
90.0%	y = -0.0052782x + 0.9208453	y = -0.0053884x + 1.0056593	y = -0.0063196x + 1.2019466	y = -0.0080179x + 1.5308445
95.0%	y = 0.0002576x + 0.1529513	y = 0.0005540x + 0.1707195	y = 0.0005562x + 0.2330486	y = 0.0006299x + 0.3212452
97.0%	y = 0.0003304x + 0.1004868	y = 0.0005939x + 0.1144485	y = 0.0005390x + 0.1715948	y = 0.0006309x + 0.2417637

Table B.1 Linearization equation for each GVF and all frequencies

APPENDIX C

LIST OF SUPPLEMENTAL VIDEO FILES

Videos available at the supplemental video files. The files contain:

- A. Low Liquid Flow Rate
- B. Medium Liquid Flow Rate
- C. High Liquid Flow Rate
- D. Additional Videos